Numerical Modeling for Optimization of Invert Trap in an Open Rectangular Combined Drainage and Sewer Channel

MALI SHIVASHANKAR
(Roll No: 717103)

DEPARTMENT OF CIVIL ENGINEERING
NATIONAL INSTITUTE OF TECHNOLOGY
WARANGAL, TELANGANA – 506004, INDIA

MARCH – 2023

Numerical Modeling for Optimization of Invert Trap in an Open Rectangular Combined Drainage and Sewer Channel

Submitted in partial fulfilment of the requirements
for the award of the degree of

DOCTOR OF PHILOSOPHY

in

CIVIL ENGINEERING

by

MALI SHIVASHANKAR

(Roll No: 717103)

Supervisor

Dr. MANISH PANDEY

Assistant Professor

DEPARTMENT OF CIVIL ENGINEERING

NATIONAL INSTITUTE OF TECHNOLOGY

WARANGAL, TELANGANA – 506004, INDIA

MARCH – 2023

Dedicated to

Prof. E Venkata Rathnam (Late),

Beloved Parents, and Family

Members

NATIONAL INSTITUTE OF TECHNOLOGY

WARANGAL

CERTIFICATE

This is to certify that the thesis entitled **"NUMERICAL MODELING FOR OPTIMIZATION OF INVERT TRAP IN AN OPEN RECTANGULAR COMBINED DRAINAGE AND SEWER CHANNEL"** being submitted by **Mr. MALI SHIVASHANKAR** for the award of the degree of **DOCTOR OF PHILOSOPHY** in the Department of Civil Engineering, National Institute of Technology, Warangal, is a record of bonafide research work carried out by him under my supervision and it has not been submitted elsewhere for the award of any degree.

Dr. Manish Pandey
Thesis Supervisor
Assistant Professor
Department of Civil Engineering
National Institute of Technology
Warangal (T.S) – India

Dissertation Approval

This dissertation entitled **"NUMERICAL MODELING FOR OPTIMIZATION OF INVERT TRAP IN AN OPEN RECTANGULAR COMBINED DRAINAGE AND SEWER CHANNEL"** by **Mr. Mali Shivashankar** is approved for the degree of **Doctor of Philosophy.**

Examiners

_____

_____

_____

Supervisor(s)

_____

_____

_____

Chairman

_____

Date: _____

Place: _____

DECLARATION

This is to certify that the work presented in the thesis entitled **"NUMERICAL MODELING FOR OPTIMIZATION OF INVERT TRAP IN AN OPEN RECTANGULAR COMBINED DRAINAGE AND SEWER CHANNEL"** is a bonafide work done by me under the supervision of **Dr. Manish Pandey** and was not submitted elsewhere for the award of any degree. I declare that this written submission represents my ideas in my own words and where others' ideas or words have been included, I have adequately cited and referenced the original sources. I also declare that I have adhered to all principles of academic honesty and integrity and have not misrepresented or fabricated or falsified any idea /data / fact /source in my submission. I understand that any violation of the above will be a cause for disciplinary action by the Institute and can also evoke penal action from the sources which have thus not been properly cited or from whom proper permission has not been taken when needed.

_____

(MALI SHIVASHANKAR)

(Roll No: **717103**)

Date: _____

Acknowledgements

Since research requires ample resources, support and motivation, I would like to thank and extend my gratitude to the ***National Institute of Technology, Warangal (NITW),*** for allowing me to work with such wonderful people and their support to complete this thesis work.

First and foremost, I would like to express my deep sense of gratitude to my thesis supervisor ***Dr. Manish Pandey***, Assistant Professor, Department of Civil Engineering for his continuous monitoring, invaluable guidance, moral support, patience, encouragement, and timely inputs throughout my doctoral study and research work. The present research would not have been possible without his continuous support. His dedication to research work will always be a source of inspiration for the rest of my life.

"I would like to express my deepest gratitude to Late Prof. ***E Venkata Rathnam*** (Former supervisor) for his unwavering support and guidance throughout my academic journey. His invaluable insights and advice have been instrumental in shaping my research and personnel life, and I am truly grateful for his dedication to my education. His contributions to the academic community will be deeply missed. My sincere condolences go out to his family and friends during this difficult time.

I am thankful to my Doctoral Scrutiny Committee: Chairman ***Dr. P Rathish Kumar***, Professor, and Head, Department of Civil Engineering and members ***Dr. N V Umamahesh***, Professor, Department of Civil Engineering, ***Dr. Anandraj P***, Professor, Department of Civil Engineering, and ***Dr Anant Kumar Rai***, Assistant Professor, Department of Mechanical Engineering for their continuous monitoring, keen interest, insightful comments and encouragement during the active research period.

I am also thankful to ***Prof. KV Jayakumar*** (Emeritus Professor), ***Prof. M Heera Lal***, and ***Dr. S Shankar***, Associate Professor, Department of Civil Engineering and ***Dr P Muthu,*** Associate Professor, Department of Mathematics, NITW for the moral support given during the period of research work.

I am thankful to ***Dr. Hemant Mittal***, Department of Mechanical Engineering, NIT Andhra Pradesh, for his support and encouragement to complete my research work has been invaluable. Although his presence is remote, he is always willing to help at any time whenever I faced a problem in CFD model setup. I am grateful to ***Dr. Binit Kumar***, Post Doctoral Fellow, Department of Civil Engineering, NITW for his continuous support while writing thesis. I am also thankful to ***Dr. Anoop Kumar Shukla***, Assistant Professor, Manipal School of Architecture

and Planning and ***Dr. Mohammad Zakwan***, Assistant Professor (Polytechnic), MANUU for their support in research work.

I thank my fellow research scholars and friends ***Mr. Aravind, Mr. Lava Kumar, Mr. V Manikanta, Mr. Sai Guguloth, Mr. Harish, Mr. Prasantha Majhi, Mr. K Satish Kumar, Mr. K Kumar, Mrs. K Sreelatha, Mr. K Satish Kumar, Mr. S Ashok, Mr. Gaurav, Mr. Pattabhiram, Mr. Sagar Banavath, Mrs. M Sagarika, Mr. A Ashok, Mr. S Anil, Mr. Manohar Reddy, Mr. M Sagar, Dr. P Shruthi, Mr. Chandhru, Mrs. Sandhya, Ms. Manjari*** for their direct or indirect help throughout research work and creating an enjoyable and fun work environment. Last but not the least I extend my biggest and whole hearted thanks to my parents ***Mr. Mali Thulasiram*** and ***Mrs. Mali Rajeswai,*** family members ***Mr. Ramesh, Mrs. Shilparani, Mrs. Deepika, Ms. Geethanvitha, Mr. Tanishq Shiva Phanigrahi, Mr. Sriyansh*** for standing with me in testing times and offering good moral support all these years.

Mali Shivashankar
Roll No: 717003

Abstract

Uncontrolled municipal solid waste, construction waste and sediments from streams release fine sediments into the sewer and urban drainage systems. Sediment transportation and deposition in sewers and urban drainage channels is a major issue that is faced by the whole world. Sediments can accumulate in open drainage and sewer channels, reducing their cross-sectional area and hence their capacity to transport water. This can lead to flooding during heavy rainfall or high flow periods, as the channels are unable to handle the increased volume of water. It can cause blockages in open drainage and sewer channels, which can prevent water from flowing freely. This can result in backups and overflows, which can lead to property damage and health hazards. Due to blockage of channels, the frequency and cost of maintenance activities for open drainage and sewer channels also increases. Regular removal of sediments from its entire length is expensive and time-consuming. Investigators has been making consistent attempts to comprehend the dynamics of sediment movement in running water. Accurately measuring the settling velocity of sediment is critical when studying the interactions between sediment flow, deposition, and erosion in flowing water, particularly when suspension is the dominant process. Any miscalculation in predicting the settling velocity can result in an error of three or more times in estimating the transport of the suspended load in flowing water. Therefore, quantitative measurements of the settling velocity are crucial for reliable results. To address the sediment issue in a flowing channel, various methods have been devised, including sediment ejectors, excluders, and extractors, as well as several sediment trapping devices. These techniques are implemented at appropriate locations along the channel to decrease the amount of sediment present in the channel, ensuring the smooth and optimal functioning of the drainage system. One such sediment trapping device is the invert trap, which captures sediment flowing into a sewer and drainage channels. Earlier investigations on the invert-trap were mainly focused on varying the flow depth, particle size and slot opening. Kaushal et al. (2012) suggested that invert trap of a rectangular shape and a trapezoidal base is the most effective design for sediment trapping inside the drainage channel. However, there are limited studies available on different invert-trap geometries, which play an important role in sediment trapping. The present study focuses on invert-trap with varying the geometry set up with a base geometry (top width as 32cm, depth as 28cm) of rectangular chamber with a trapezoidal base (BG). The changes considered include an arc passing through three points (G1), an isosceles triangle (G2) and a right triangle (G3) for different slot openings and flow depths, for natural sewer solids (NSS1). In the current study, 2D-Computational Fluid Dynamics (CFD) modeling has been

performed using Volume of Fluid (VOF) and Discrete Phase Model (DPM) along with realizable k-ε turbulence model in fluent software for flow simulation and retention efficiency in the considered geometries. To optimise the invert trap design, numerical analysis was performed with proper prediction of particles settling velocity, different flow depths (2 cm, 3 cm, 4 cm, and 5 cm), slot openings (9 cm and 15 cm), different geometries (BG, G1, G2, G3), and trap depths (0.24 m, 0.28 m, 0.35 m, 0.45 m, 0.55 m, and 0.65 m) for a given sediment type. Application of Hybrid Generalized Reduced Gradient-Genetic Algorithm (Hybrid GRG-GA) reduces the sum of square of error in fall velocity by over 70% and 30% on an average as compared to previous equations during training and testing respectively. Therefore, Hybrid GRG-GA approach has been used efficiently for calculating the settling velocity. The CFD (coupled VOF and DPM) model has been validated with Mohsin and Kaushal's (2017b) experimental trap efficiencies for natural sewer sediments (NSS1). The investigation shows CFD (coupled VOF and DPM) model predicts better trap efficiency for natural sewer solids (NSS1) with particle size (diameter ranges 0.15 mm - 0.30 mm). Therefore, the validated model was used to optimize the invert trap geometry. In all the considered geometries the right triangle base geometry (G3) offers maximum trap efficiency out of the three trial geometries for both the slot openings and any given flow depth. There is also a competitive advantage in emptying the invert trap as all the particles settle on only one side of the base. In other base geometries, the settlement is widely distributed. In addition, the numerical observations clearly show that 0.55m invert trap depth of right triangular (G3) trap geometry is the optimum invert trap depth for all flow depth and slot openings, under the given sediment parameter.

Contents

Acknowledgements.....iv

Abstract.....vi

Contents.....viii

List of Figures.....xiii

List of Tables.....xvi

CHAPTER 1.....1

INTRODUCTION.....1

1.1 General.....1

1.2 Sediment.....5

1.3 Sedimentation.....6

1.4 Settling Velocity.....6

1.5 Sediment Transportation.....7

1.6 Invert Trap.....8

1.7 Particle Trap Efficiency.....8

1.8 Computational Fluid Dynamic (CFD) Modeling.....9

1.9 Critical Review.....9

1.10 Research Gaps.....10

1.11 Research Objectives.....10

1.12 Research Program.....11

1.13 Need for the Study.....12

1.14 Organization of the Thesis.....12

CHAPTER 2.....14

LITERATURE REVIEW.....14

2.1 Literature Review on Invert Traps.....15

2.2 Literature Review on Settling Velocity Expressions.....22

2.3.1 Origin of Sediments.....25

2.3.2 Properties of Sediments 26
2.3.3 Incipient Motion of Sediment Particles 28
2.3.4 Bed Forms 29
2.3 Bed Load Transport and Saltation 33
2.4 Estimation of Bed Load 34
2.5 Suspended Load Transport 35
2.6 Mechanism of Suspension 35
2.7 Estimation of Suspended Load 36
2.8 Sediment Management 37
2.9 Grit Chambers 38
2.10 Invert Traps (Silt Traps) 39
CHAPTER 3 41
EVALUATION OF SEDIMENT'S SETTLING VELOCITY 41
3.1 General 41
3.2 Analysis of Existing Settling Velocity Equations 42
3.2.1 Overview 42
3.2.2 Data Description 42
3.2.3 Existing Equations for Settling Velocity of Sediments 43
3.2.4 Statistical Performance Analysis of Equations 48
3.2.5 Results and Discussions 49
3.2.6 Conclusions 54
3.3 Estimation of Settling Velocity Using Machine Learning Algorithms 56
3.3.1 Overview 56
3.3.2 Methodology 56
3.3.3 Results and Discussion 58
3.3.4 Conclusions 64
CHAPTER 4 66

COMPUTATIONAL FLUID DYNAMICS MODEL THEORY 66
4.1 General 66
4.2 Assumptions of the Model 66
4.3 CFD Model for Multiphase (Two-Phase) Flow 67
4.4 Euler–Euler Approach 67
4.4.1 Volume of Fluid (VOF) Model 68
4.4.2 Volume Fraction Equation 70
4.4.3 Momentum Equation 71
4.4.4 Open Channel Flow 72
4.5 Discrete Phase Model (DPM) 73
4.5.1 Particle Tracking 73
4.5.2 Drag Coefficient of Sphere (C_D) 73
4.5.3 Particle Trajectories 74
4.6 CFD Model Setup 75
4.6.1 Two-way Coupling 76
4.6.2 Turbulence Models 76
4.6.3 Near Wall Treatment 77
4.6.4 Surface Tension and Wall Adhesion 80
4.6.5 Grid Generation 80
4.6.6 Grid Quality 80
CHAPTER 5 82
TWO DIMENSIONAL CFD MODELING AND SIMULATIONS 82
5.1 General 82
5.2 Source of Data 83
5.2.1 Experimental Setup 83
5.2.2 Dimensions of Laboratory Channel 84
5.2.3 Particle Trap Efficiency 84

5.2.4 Sedimentation Parameter 84
5.2.5 Materials and Properties 85
5.3 Methodology 86
5.3.1 CFD Model Geometry 87
5.3.2 Invert Traps 88
5.4 CFD Model Setup 91
5.4.1 Boundary Conditions 92
5.4.2 Convergence Criterion 93
5.5 Results and Discussion 93
5.5.1 Validation of 2D CFD Model 94
5.5.2 Analysis of the Effect of Invert Trap Geometry on Sediment Retention Efficiency 96
5.5.3 Analysis of the Effect of Invert Trap Depth on Sediment Retention Efficiency 101
5.6 Conclusions 105
CHAPTER 6 107
FINANCIAL VIABILITY OF INVERT TRAP 107
6.1 General 107
6.2 Methodology 108
6.3 Location and Dimensions of Drainage Channel 109
6.4 Standard Rates 112
6.5 Estimation and Costing 112
6.5.1 Cost Estimation for Conventional Drainage Channel 112
6.5.2 Cost Estimation for Hypothetical Drainage Channel 113
6.6 Cost Comparison 115
6.7 Conclusions 115
CHAPTER 7 116

CONCLUSIONS AND SCOPE FOR FUTURE WORK 116
7.1 Conclusions 116
7.2 Scope for Future Work 118
Appendix-I 119
Publications from Present Research Work 119
Appendix-II 120
List of symbols 120
References 123

List of Figures

Figure 1. 1 Schematic view of Drainage and Sewer water system.....1
Figure 1. 2 Photo view of blocked drainage channel at Vijayawada.....2
Figure 1. 3 Photo view of desilting of drainage channel at Thiruvananthapuram (India).....3
Figure 1. 4 Photo view of drainage flow in blocked channel and cleaned channel at Bengaluru (India) 3
Figure 1. 5 Sedimentation in storm drains during dry weather conditions.....4
Figure 1. 6 Schematic view of invert trap in an open rectangular channel 5
Figure 1. 7 Frame work of the proposed research program.....11
Figure 2. 1 Different shapes of sediment particles……26
Figure 2. 2 Bed forms in alluvial channels (K Subramanya, 2009) 32
Figure 2. 3 Processes of erosion, transport, and sedimentation (Julien, 2010) 33
Figure 2. 4 Sketch of the bed and suspended load layer (Julien, 2010) 34
Figure 2. 5 Suspended load concentration and velocity profile in a channel 36
Figure 2. 6 Conventional French grit chamber (Ashley et al., 2004) 38
Figure 2. 7 Schematic diagram of invert trap and cleaning process (Ashley, 2004) 39
Figure 3. 1 (a-k): Observed versus predicted settling velocity without shape factor using; (a) Rubey (1933), (b) Zanke (1977), (c) Rijn (1989), (d) Zhang (1993), (e) Zhu and Cheng (1993), (f) Julien (1995), (g) Cheng (1997), (h) Soulsby (1997), (i) Jimenez and Madsen (2003), (j) Wu and Wang (2006) and (k) Camenen (2007)……52
Figure 3. 2 (a-c): Observed versus predicted settling velocity with shape factor using; (a) Jimenez and Madsen (2003), (b) Wu and Wang (2006), and (c) Camenen (2007). 53
Figure 3. 3 Flow chart of methodology. 58
Figure 3. 4 Observed and calculated settling velocity using training datasets as per; (a) Jiménez and Madsen (2003), (b) Wu and Wang (2006), (c) Camenen (2007), (d) GRG approach, and (e) Hybrid GRG-GA approach.....61
Figure 3. 5 Observed and calculated settling velocity using validation datasets as per; (a) Jiménez and Madsen (2003), (b) Wu and Wang (2006), (c) Camenen (2007), (d) GRG approach, and(e) Hybrid GRG-GA approach.....62
Figure 3. 6 Percentage error vs percentage datasets using Jiménez and Madsen (2003); Wu and Wang (2006); Camenen (2007); GRG approach, and Hybrid GRG-GA approach. 63
Figure 4. 1 Schematic diagram of the present CFD model approach……69
Figure 4. 2 Schematic diagram of Wall function and Near wall modeling approaches. 78

Figure 5. 1 Schematic diagram of plan and elevation of experimental setup …….83
Figure 5. 2 Flow chart for CFD model validation and evaluation of Invert trap geometry.....87
Figure 5. 3 Two-Dimensional geometry of an open channel and an invert trap for CFD study. 88
Figure 5. 4 (a-d) Line diagram of proposed Invert trap geometries: (a) Invert trap of rectangular chamber with a base geometry (BG) of trapezoidal bottom; (b) Invert trap of rectangular chamber with a base of arc shape passing through three points (G1); and (c) Invert trap of rectangular chamber with an isosceles triangular base (G2); (d) Invert trap of rectangular chamber with a right triangle base (G3). 89
Figure 5. 5 Generation of Mesh of Invert Trap and Channel. 90
Figure 5. 6 Volume fraction of water in the channel after convergence. 93
Figure 5. 7 2D predicted velocity contours and velocity vector of base geometry (BG) coloured by velocity magnitude for a flow depth of 5 cm: (a) 2D velocity contours of base geometry (BG) with slot opening, Δx = 9 cm; (b) 2D velocity contours of base geometry (BG) with slot opening, Δx = 15 cm; and (c) 2D velocity vector of base geometry (BG) with slot opening, Δx =15 cm. 95
Figure 5. 8 Validation of 2D CFD model using Mohsin and Kaushal (2017b) experimental data. 95
Figure 5. 9 2D predicted velocity contours and velocity vector of Geometry 1 (G1) coloured by velocity magnitude for a flow depth of 5 cm: (a) 2D velocity contours of G1 with slot opening, Δx = 9 cm; (b) 2D velocity contours of G1 with slot opening, Δx =15 cm; and (c) 2D velocity vector of G1 with slot opening, Δx =15 cm. 97
Figure 5. 10 2D predicted velocity contours and velocity vector of Geometry 2 (G2) coloured by velocity magnitude for a flow depth of 5 cm: (a) 2D velocity contours of G2 with slot opening, Δx = 9 cm; (b) 2D velocity contours of G2 with slot opening, Δx =15 cm; and (c) 2D velocity vector of G2 with slot opening, Δx = 9 cm. 97
Figure 5. 11 2D predicted velocity contours and velocity vector of Geometry 3 (G3) colored by velocity magnitude for a flow depth of 4 cm: (a) 2D velocity contours of G3 with slot opening, Δx = 9 cm; (b) 2D velocity contours of G3 with slot opening, Δx =15 cm; and (c) 2D velocity vector of G3 with slot opening, Δx = 9 cm. 98
Figure 5. 12 2D predicted velocity contours and velocity vector of Geometry 3 (G3) colored by velocity magnitude for a flow depth of 5 cm: (a) 2D velocity contours of G3 with slot opening,

Δx = 9 cm; (b) 2D velocity contours of G3 with slot opening, *Δx* =15 cm; and (c) 2D velocity vector of G3 with slot opening, *Δx* = 9 cm. 99
Figure 5. 13 Particle trajectories inside the G1 and G3 invert trap for slot size of Δx = 9 cm: (a) particle trajectories inside the G1 for a flow depth of 5 cm; and (b) particle trajectories inside the G3 for a flow depth of 4 cm..... 99
Figure 5. 14 Predicted trap efficiency with the different flow depths for two slot size; (a) *Δx* = 9 cm, and (b) *Δx* =15 cm..... 101
Figure 5. 15 (a-d) Numerically simulated velocity distribution inside right angular (G3) invert trap at depth of flow (*Y*) = 0.05 m and average velocity (*U*) = 1.1 m/s with slot opening size (*Δx*) = 0.15 m. 103
Figure 5. 16 Predicted trap efficiency with the different flow depths for two slot size; (a) *Δx* =15 cm, and (b) *Δx* = 9cm..... 104
Figure 6. 1 Flow chart of Methodology..... 108
Figure 6. 2 Preparation of formwork to construction open drainage channel by TS Panchayat Raj Dept. at Bollaram village. 110
Figure 6. 3 Conventional drainage channel construction by TS Panchayat Raj Dept. at Bollaram village. 110
Figure 6. 4 Placing of concrete while construction of open drainage channel at Bollaram village. 111
Figure 6. 5 Photo view of under construction open drainage channel. 111

List of Tables

Table 3. 1 Data description and properties 43
Table 3. 2 Statistical values 54
Table 3. 3 Values of performance evaluation criteria for different methods 64
Table 5. 1 Sedimentation parameter (SP)-based classification of sediment transport modes…85
Table 5. 2 Inlet flow properties for CFD model (b = 1m and So= 0.006) (from Mohsin and Kaushal, 2017b).....86
Table 5. 3 Physical properties of the sediment particles.....86
Table 5. 4 Physical parameters of open channel and invert trap geometry. 88
Table 5. 5 Two-dimensional mesh quality details 91
Table 5. 6 Mass Balance of water at Convergence (for y = 5cm and Δx = 9cm).....93
Table 5. 7 Validation of 2D CFD model with experimental (Mohsin and Kaushal 2017b) results for NSS1 particles.....94
Table 5. 8 Predicted trap efficiency for different geometries using NSS1. 100
Table 5. 9 Predicted trap efficiency for different invert trap depth using NSS1 102
Table 6. 1 Parameters of open drainage channel and invert trap geometry……109
Table 6. 2 Standard rates for earth and PCC work from P.R department 112
Table 6. 3 Estimation and costing for conventional drainage channel for stretch of 1 km 113
Table 6. 4 Estimation and costing of hypothetical drainage channel for stretch of 1 km.....114

CHAPTER 1

INTRODUCTION

1.1 General

Solid-liquid flow interaction in open channels occurs in many natural systems, e.g., sediment transport in rivers, streams, coastal areas, lined and unlined irrigation canals, drainage and sewer channels, surface runoff etc. In recent years, the world is in its rapid pace of urbanization and concretization of rural areas, that makes the amount of waste water and storm water going into the combined sewer systems has been increased significantly. The combined storm and sewer system includes different components such as sources, drains and sewers, treatment plant and receiving water bodies, which can be seen in Fig. 1.1. These storm water contains industrial and domestic waste, natural solids, construction waste etc.

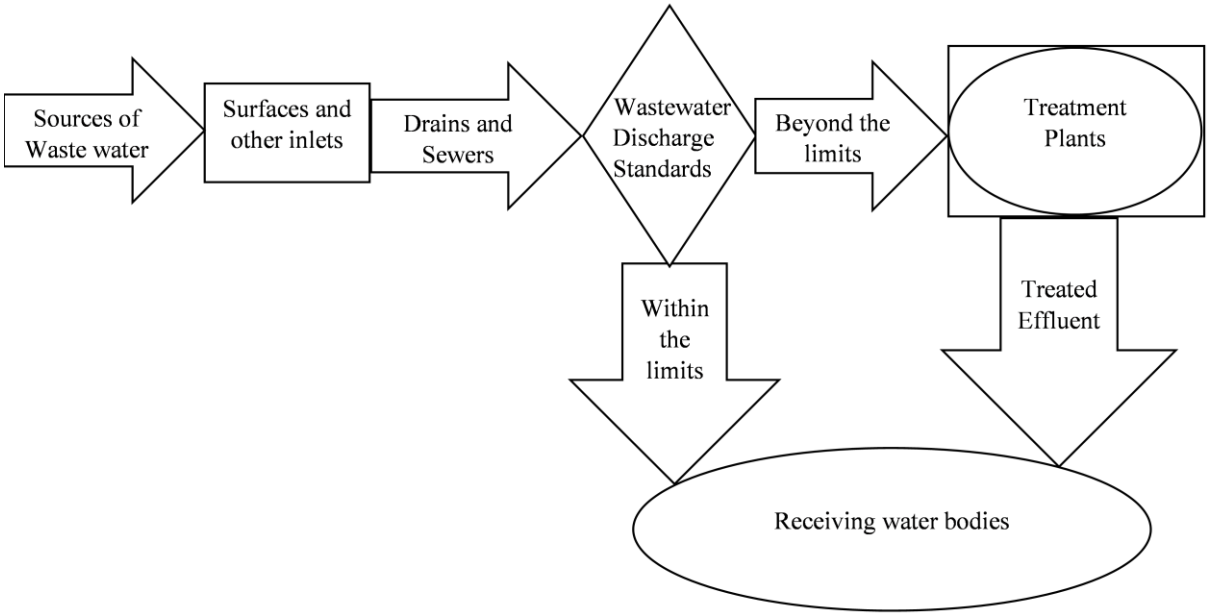

Figure 1. 1 Schematic view of Drainage and Sewer water system

A combined open drainage and sewer is a channel that is used to discharge sewerage and rainwater into treatment plants or into other bodies of water. Sediment transport, erosion and deposition in sewers and drainage channels is a significant issue that is faced by the whole world. Sediments such as natural sediment particles, construction debris and particles that come from industrial and domestic waste enter into drainages and sewer channels from the surrounding areas and get accumulated, it can cause blockage of drainage channels. As a result,

the surrounding area becomes hazardous for the nearby residents. Some news articles were also published, which describes the drainage system of various cities in country like India. Due to the traditional drainage systems, various problems were emerged, such as, sediments enter the sewer channel and get deposited along the drainage channels, it causes stagnation of storm and sewer water in the channel which leads to mosquitoes growth. The carrying capacity of channel has been decreasing. It is very difficult to clean the channel to its total length. The suspended sediments in flowing water might be settleable by providing suitable trap and drainage structures.

Figure 1. 2 Photo view of blocked drainage channel at Vijayawada

(Source: The Hans India/ 22-12-2021)

Sediments such as natural sediment particles, construction debris and particles that come from industrial and domestic waste enter into drainages and sewers from the surrounding areas and create several problems like reduced hydraulic efficiency, which leads to overflow, clogging problems, and hinders the pumping of sewer treatment plants as shown in Fig. 1.2 - 1.5, and to overcome this, many excluding or sediment trapping devices have been proposed and are being used practically at appropriate locations along the length of the channel to reduce the sediment concentration and to make sure the smooth and best possible functioning of the drainage system. Researchers are still working on a better design of sediment trap devices.

Figure 1. 3 Photo view of desilting of drainage channel at Thiruvananthapuram (India)

(Source: Deccan Chronicle/ 08-07-2017)

Figure 1. 4 Photo view of drainage flow in blocked channel and cleaned channel at Bengaluru (India)

(Source: Times of India/ 18-05-2019)

Figure 1. 5 Sedimentation in storm drains during dry weather conditions

An invert trap is a device which is used to reduce the sediments in sewer systems and drainage channels by settling them in the chambers. Invert traps are generally installed at a suitable location on the bottom of a channel and sediments are supposed to fall and collect in an invert trap along the length of the channel. The settled sediment particles are then taken out from the chamber periodically, by breaking the flow into the invert trap using retaining gates. Among all sediment excluding and trapping devices, invert traps are very effective method of reducing the amount of sediment flowing in a drainage system and irrigation channels (Gupta et al., 2005).

Originally, the ideology of invert traps has come from the sediment sampling devices. In the olden days, sediment sampling was done using a device called a sampler which can disturb the flow field. Hubbell (1964) introduced a sampler called pit trap which can reduce the interference problem with the existing sediment sampling devices. First, experimentally in a rectangular open channel, an invert trap was explored by Poreh et al. (1970). They have conducted laboratory tests on slotted traps and illustrated a range of curves of sediment trapping efficiency versus dimensionless slot size.

An experimental investigation is required to know the insight knowledge and performance of the invert trap devices. However, experimentation is very difficult to conduct all the time, or else it involves huge setup costs. In the recent years, Computational Fluid Dynamics (CFD) models have been used effectively to improve the design of invert trap devices and optimize their structures. Figure 1.6 represents the creation of invert trap geometry in an open rectangular channel by CFD Tool.

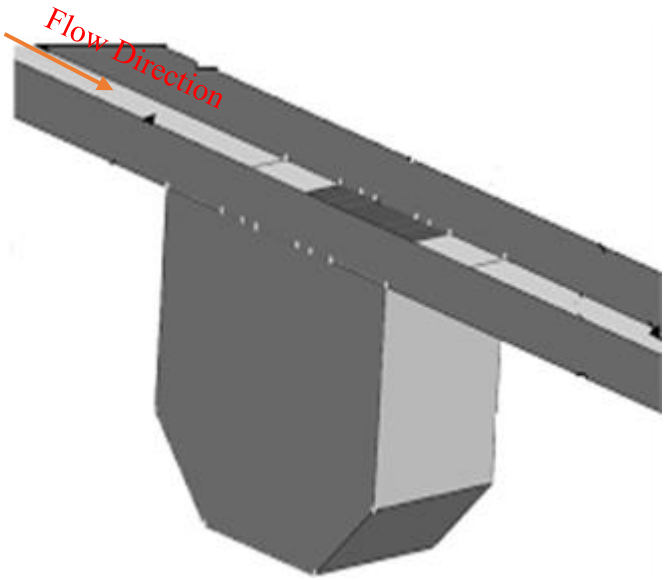

Figure 1. 6 Schematic view of invert trap in an open channel

(Source: Thinglas and Kaushal, 2008)

Therefore, in the current study, a thorough literature review and two-dimensional CFD analysis has been conducted using ANSYS Fluent software for varied parameters of flow (U, y), particle (d_p, ρ_p), and invert trap geometry (base shape, trap depth and slot opening size i.e., $\boldsymbol{\Delta}x$). The study utilized a Volume of Fluid (VOF) model coupled with a realizable k-ε turbulence model to determine flow velocity and free surface, while a stochastic Discrete Phase Model (DPM) was employed to assess sediment trap efficiency. The impact of the size and shape of the invert trap on efficiency was assessed using various flow parameters. To enable the proposed CFD model to be used in place of experiments for future design and performance analysis of invert traps, the CFD predictions were compared with experimental data.

1.2 Sediment

According to the American Geophysical Union's 1947 report from the subcommittee on sediment term, which was headed by E. W. Lane, the sediment is stated as:

"Fragmental material transported by, suspended in, or deposited by water or air, or accumulated in the beds by other natural agents; any detrital accumulation, such as loess".

1.3 Sedimentation

Generally, Sedimentation is the process of erosion of sediment particles from the surrounding catchment, transportation of particles in suspension, deposition of particles in the fluid against an obstruction or barrier. The sedimentation process is affected by particle settling velocity which makes the particle to settle down. Basically, the settling velocity of particle depends on particle properties like shape, size and density, and the fluid properties like density and viscosity of fluid (Graf, 1984; Pu et al., 2021).

1.4 Settling Velocity

The settling velocity of a particle is the speed at which it falls through a low-density fluid without any external forces acting upon it, also referred to as the terminal fall velocity. At this velocity, the drag force (F_D) acting on the sediment particle is equal to the buoyancy force, counterbalancing the force of gravity (F_G) acting downwards. Consequently, the particle ceases to accelerate and continues to fall at a constant speed, known as the terminal velocity. The particle's acceleration is arrested by the combination of fluid drag and the particle's submerged weight. Essentially, particle fall velocity is determined by equating the gravity and drag forces. Precise knowledge of settling velocity is crucial in accurately predicting sediment transport processes in rivers and combined sewers.

When suspension is the dominant process, the settling velocity of sediment is a crucial parameter for studying the transportation of sediment in flowing water and freshwater reservoirs. Settling velocity is a complex due to the sediment and water interactions (Rushd et al., 2021). Possibly, the most significant instances are the wastewater treatment, hydraulic fracturing, dredging and sediment transport with flowing water.

Many empirical and semi-empirical equations have been developed by researchers to address issues related to particle fall velocity and sediment transport processes. The origins of these equations can be traced back to Stokes in 1851. The initial settling velocity equations for sediment were based on the assumption that the particles are spherical in shape (Gibbs et al., 1971). However, in reality, sediment particle shapes are often non-spherical, which can result in a reduction in settling velocity when compared to spheres (Swamee and Ojha, 1991a; Wang, 2006). To account for these practical considerations, numerous equations have been developed to calculate the settling velocity of natural sediments using a nominal diameter.

1.5 Sediment Transportation

Sediment movement in open channels can be divided into two categories: channels with loose boundaries and channels with rigid boundaries. Present channel design research has concentrated on the problem of sediment flow in a rigid boundary channel. The presence of sediment has a considerable impact on the hydraulic performance of a channel. It should be taken into account while designing irrigation, navigation, drainage, and sewer systems. The deposition of sediments in the channels changes the hydraulic resistance, the distribution of wall shear stress, and the flow velocity. On the other hand, the channel's cross-sectional area has decreased, resulting in a reduction in the channel's hydraulic capacity. Sedimentation has adverse effects on the environment because it spreads contaminants throughout the urban area. Sediment transport modeling is a difficult undertaking because of the above-mentioned problem. Although, all the sewer and drainage channels are designed for a self-cleaning velocity to meet the intended design purpose i.e., no silting and no scouring condition. Because of the practical complications regarding the channel geometry, different flow conditions and different sediment particles, the no silting and no scouring criteria will not be achieved every time. Hence, the deposition of sediments in the open sewer and drainage channels can’t be controlled completely by following the design criteria.

Further, the sediment problem in sewer and drainage channels can be controlled by following ways:

(i) Preventative measures
(ii) Curative Measures

1.5.1 Preventative Measures

As part of preventive measures, the particles flowing into the systems are significantly reduced by a variety of means, including increasing public awareness of the types and quantities of solid wastes that cannot be transported through sewer or drainage systems, covering manholes with mesh covers, regularly cleaning of roads, taking adequate precautions at construction sites to prevent the construction debris from entering the drainage systems, etc.

1.5.2 Curative Measures

As part of curative measures, a suitable device is employed to remove the flowing sediments which have been entered into the sewer or drainage system from the surrounding areas. Various

sediment trapping devices, such as sediment ejectors, interceptors, excluders, vortex separators, and trapping devices, have been invented and are currently in use to minimize sediment accumulation in sewers or drainage channels.

1.6 Invert Trap

An invert trap is a device that is used to reduce the sediments in sewer and drainage systems by making them settled in the device chambers. Invert traps are generally installed at a suitable location on the bottom of a channel and sediments are supposed to fall and collect in that trap. The settled sediment particles are then taken out (manually or by using vacuum suction vehicles) from the chamber periodically, by temporary breaking or stopping the flow into the invert trap using some means. Many engineers and researchers are still working to find out better design of sediment trap devices to improve the trapping efficiency of devices through experimental studies or numerical studies.

1.7 Particle Trap Efficiency

For given characteristics of the sediment particle, the particle trap efficiency (η) is defined as

$$\eta(\%) = \frac{N_T}{N_I} \times 100 \tag{1.1}$$

Where N_T is the total number or mass of the sediments that are retained inside the invert trap chamber, and N_I is the total number or mass of the sediments that are injected into the channel (sediments are fed into the channel).

The flow field and sediment trapping tendency of several trap designs (slotted cylinders, domed bottles, funnels, etc.) were investigated by Gardner (1980). They stated that the sediment trapping ability of the trap depends on the particle resident time and flow patterns of the fluid within the trap. Bachoc (1992) carried out an experimental study on sedimentation and found that the influencing parameters for sedimentation are steady slope with channel geometry, downstream flow conditions, and rapid change in channel geometry. Chebbo et al. (1996) suggested that the invert traps are suitable devices for sediment trapping.

1.8 Computational Fluid Dynamic (CFD) Modeling

Computational Fluid Dynamics (CFD) modeling is a simulation technique that uses mathematical algorithms to solve and analyse problems related to fluid flow, heat and mass transfer, chemical reactions (Malalasekera & Versteeg, 2007). It is an interdisciplinary field that combines the principles of physics, mathematics, and computer science to create virtual models of fluid systems.

In CFD modeling, a fluid system is represented by a set of mathematical equations that describe the behaviour of the fluid under various conditions. These equations are then solved using numerical methods on a computer to create a simulation of the flow. CFD modeling has numerous applications in various fields such as aerospace, automotive, biomedical engineering, environmental engineering, hydraulic engineering and many others. It is used to optimize the design of aerodynamic structures, simulate multiphase flows, irrigation and water resource related structures i.e., dams, bridge piers etc, simulate combustion processes, model blood flow in the human body, and even predict weather patterns.

The accuracy of CFD modelling depends on the accuracy of the mathematical equations used and the quality of the numerical methods employed to solve them. Therefore, CFD modelling requires a high level of expertise in both mathematics and computer science. Overall, CFD modeling is a powerful tool that allows engineers and scientists to study fluid flow and its effects on various systems without the need for costly and time-consuming experiments.

1.9 Critical Review

1. Genetical Algorithm and machine learning approaches are effective for various hydrological and hydraulic applications.
2. Fixed lid approaches were not able to model the free water surface profile.
3. VOF model is an appropriate model for free surface flow.
4. Realizable k-ε turbulence model is effective in simulating the turbulence effects of open channel flow.
5. Trap efficiency varies with flow depth, slot opening, particle parameters, and geometry of the invert trap.

1.10 Research Gaps

1. Limited studies were reported so far comparing the accuracy of various equations to estimate the settling velocity of sediment particles.
2. No study has been reported in the literature that employs machine learning approaches to estimate settling velocity.
3. Very few researches were carried out by using Pressure based coupled solver for simulation of two-phase flows.
4. Limited work has been done on the optimization of invert trap geometry in order to improve the retention efficiencies.
5. Less work was performed on effect of invert trap depth on trap efficiency.

1.11 Research Objectives

The focus of present study is to optimize the invert trap design with respect to base geometry and depth of invert trap using Computational Fluid Dynamic (CFD) based software i.e., ANSYS Fluent. The VOF model will be used to predict the flow behaviour in the open channel with invert trap and sediment movement and deposition will be simulated using Discrete Phase Model (DPM). The cost estimation analysis is also studied for practical implication of invert traps in rural drainage and sewer channels.

This main objective is, for the sake of more clarity, subdivided into four sub objectives as given below.

1. To develop an expression for the settling velocity of sediment particles using machine learning methods. In this regard, the present study proposes the application of Generalized Reduced Gradient (GRG) and Hybrid Generalized Reduced Gradient-Genetic Algorithm (Hybrid GRG-GA) based settling velocity approaches, and to compare the proposed approaches with well-known proposed empirical equations.

2. To analyze and optimize the invert trap geometry for increased sediment retention efficiency. For this purpose, a 2D-CFD model is developed to simulate the sediment retention efficiency of invert trap fitted in open channel using coupled VOF and DPM present in ANSYS Fluent software for a range of flow depths, slot openings and a given sediment type. The proposed model is validated with the literature data.

3. To assess the impact of the depth of invert trap on sediment retention efficiency for the optimal invert trap geometry obtained from the previous study. By employing a validated 2D CFD model, the study aims to analyse how varying trap depths affect the sediment retention efficiency of Invert Trap.

4. To estimate the financial viability of optimized sediment invert trap design for rural applications. To get this, the cost estimation analysis is done for conventional drainage channel to a stretch of 1km with and without invert trap.

1.12 Research Program

The framework of the proposed methodology for the present research program has been shown in Fig 1.7.

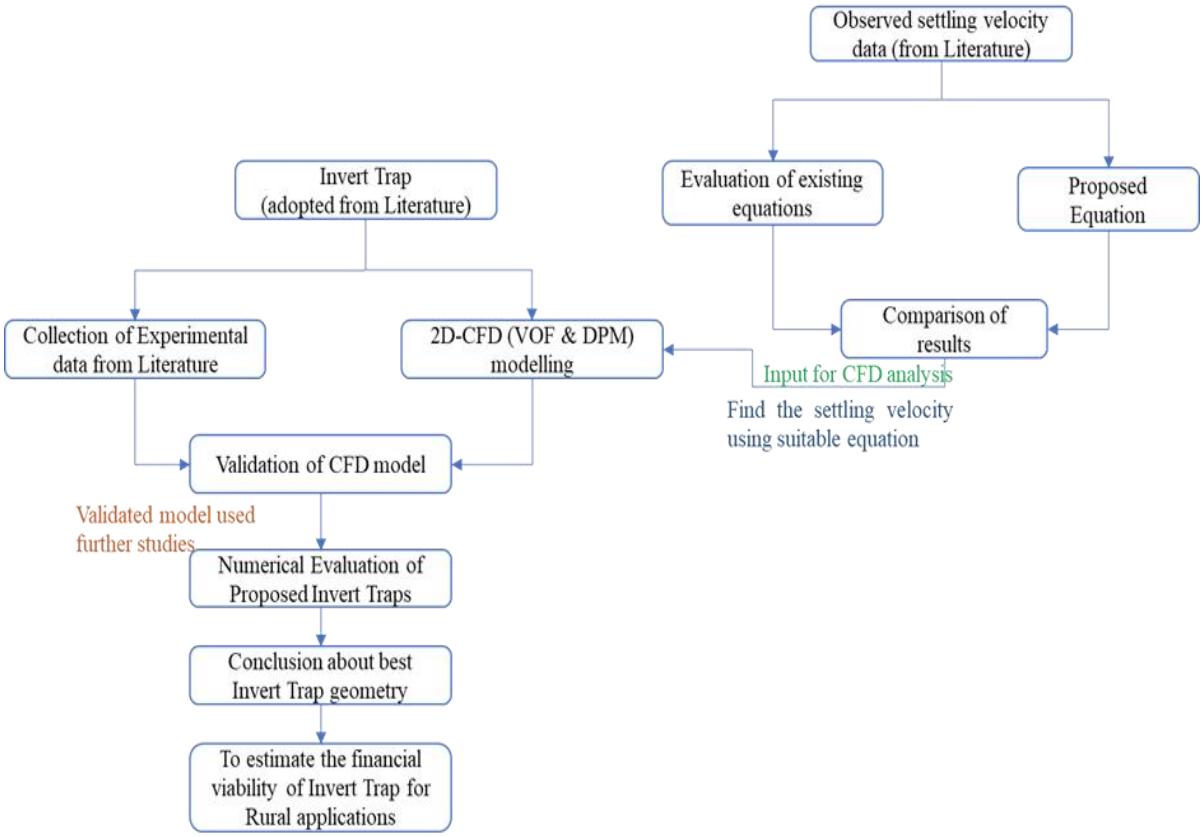

Figure 1. 7 Frame work of the proposed research program

1.13 Need for the Study

The need of the present research activity can be summarised according to the comprehensive literature review as follows:

1. The investigations that have been carried out so far have used a limited set of sediment measurements, flow characteristics, and trap design (base geometry). As a result, it is proposed in this research to numerically evaluate the sediment trap efficiency for a wide range of trap configurations (i.e., base geometries), sediment parameters, and flow characteristics, as well as to perform CFD (VOF model) simulations using ANSYS Fluent 2021 software and compare the CFD predicted results with the experimental results of Literature.
2. Although previous researchers claimed that the invert trap was useful for sewer solid management, none of them evaluated the influence of invert trap depth of best suited geometry on trap performance. As a result, it is proposed in this study to use different trap depths to explore the influence of invert trap depth on trap efficiency.
3. The previous researchers did not compare the sediment particle settling velocity equations, which will be supplied into a CFD model to evaluate the sediment trap efficiency of an invert trap. In the present study, therefore, it is proposed to compare existing equations and develop a new equation to increase the accuracy of sediment settling velocity prediction.
4. Limited study has been addressed for the economical sustainability of optimised sediment invert trap design for rural applications. To obtain this, a cost estimation analysis is performed for a conventional drainage channel along a 1 km segment with and without an invert trap.

1.14 Organization of the Thesis

The thesis has been composed of 7 chapters, as mentioned:

Chapter 1: The "Introduction" chapter outlines the research background such as purpose of drainage channel, sediments and sediment transport and deposition, sediment related problems and available solutions, research gaps, research objectives, research program, need for the study, and scope of the research.

Chapter 2: The "Literature Review" chapter analyses the studies available in the literature that are relevant to the present investigation. It has two sub-sections which can elaborate

the research gaps. It also provides the research approach that will be used in the present study.

Chapter 3: The " Evaluation of Sediment's Settling Velocity " chapter outlines the analysis of existing equations for calculating the settling velocity, estimation of settling velocity using Generalized Reduced Gradient (GRG) and Hybrid Generalized Reduced Gradient-Genetic Algorithm (Hybrid GRG-GA). It assists in the development of an equation for settling velocity that appropriately predicts sediment mode of transport.

Chapter 4: The title of this chapter is "CFD (VOF and DPM) Model Theory." This contains the detailed theoretical approach to Computational Fluid Dynamics (CFD) that was applied in the present research work. The theory relies on the documentation of ANSYS Fluent 2021.

Chapter 5: The "2D CFD (Coupled VOF and DPM) Modelling " chapter describes validation of proposed 2D CFD model, analysis of different Invert Trap geometries by considering various parameters, and comparison of simulated results.

Chapter 6: The " Financial Viability of Invert Trap" chapter provides a cost comparison study of two types of drainage channels: conventional drainage channels and hypothetical drainage channels with invert traps, as well as the financial viability of Invert Traps for rural applications.

Chapter 7: The "Conclusions and Scope for Future Work" chapter addresses the main conclusions of the present research as well as the scope for future research, along with a few recommendations for practical applications.

CHAPTER 2

LITERATURE REVIEW

A thorough literature review reveals that considerable work has been done in the optimization of invert trap design in terms of slot opening, flow parameters, and sediment properties (Buxton et al., 2002; Kaushal et al., 2012; Thinglas and Kaushal, 2008b, 2008b), but very little work has been done in terms of base geometry and depth of invert trap. The invert trap chamber design was numerically analysed using a Volume of Fluid (VOF) model for a multi-phase open channel flow (Beg and Kaushal, 2022; Mohsin and Kaushal, 2017b, 2017a). However, in order to predict the flow and sediment interactions in the open channel and invert trap chamber, the sediment settling velocity must be estimated with greater precision.

Since the early twentieth century, sediment transport in rivers has been intensively investigated (Wang, 2006). The sediment motion in a fluid medium is characterized by relevant variables and can be determined based on the fluid and sediment-related parameters. Many critical problems have been addressed through the development of theories and procedures that provide answers or solutions, such as sediment property quantification, sediment transport rate estimation under various flow circumstances, river morphological change prediction and so on (Pu et al., 2021; Singh et al., 2019). Settling velocity (w_s) is one of the most significant terms in the sediment transport phenomenon. The settling velocity of a solid particle in a flowing fluid is the continuous free-falling velocity of the particle when the opposing gravity and drag forces acting on it are approximately equal.

According to the literature, two major components dominate the prediction of sediment trapping inside the invert trap: proper model setup to improve the shape of the invert trap geometry and proper estimation of the settling velocity of sediment particles. As a result, the section on literature review has been divided into two subsections.

1. Review of the literature on the sediment retention efficiency of invert traps and the associated numerical models.
2. A review of the literature on the settling velocity expression of sediment particles.

2.1 Literature Review on Invert Traps

Hubbell (1964) developed the pit trap sampler to address the issue of sediment sampling devices interfering with flow, which was common with other bed load sampling devices. In the olden days, sediment sampling was done using a device called a sampler which can disturb the flow field. However, pit samplers have higher and more consistent efficiencies than other types of samplers. Because pit traps must be placed in the streambed, their application is limited.

Hunt (1969) illustrated using a diffusion equation that, for a mixture with various grain sizes of sediment particles in suspension, the concentration of the smaller size particle increased upwards while the heavier particles were necessarily transported primarily near the bed, which was consistent with the observations.

Poreh et al. (1970) first investigated an invert trap experimentally in a rectangular open channel. In the laboratory, they tested slotted traps using eight different sand and gravel samples that varied in size from 0.2 mm to 4.5 mm. They generated a range of curves that illustrated the efficiency of sediment trapping versus dimensionless slot size. For the bed load transport range, they discovered a universal relationship between efficiency, Froude number, and particle size. Although the sampling efficiency decreased slightly with particle size in this range, it approached unity for larger slot openings. On the other hand, the sampling efficiency of smaller particles, which do not move as much as the bed load, increased with particle size. However, it remained less than unity even at extremely large slot size to particle size ratios.

Reynolds (1976) examined the large-eddy turbulence model and discovered that a very coarse grid produces remarkably good results, leading him to believe that large-eddy simulations could eventually be suitable for real-world engineering applications after considerable development.

Gardner (1980) conducted a study on flow dynamics and sediment particle trapping behavior, using various trap designs such as slotted cylinders, domed bottles, funnels, and more. The experiment involved the use of dye, marine water, and deep-sea lutite in a re-circulating open channel and fish tank. Gardner's findings revealed that sediment trapping efficiency depends on both the residence time and fluid flow circulation pattern within the trap.

Hirt and Nichols (1981) presented a simple but powerful method for tracking free surface of fluid flow (incompressible) based on the concept of a fractional volume of fluid

(VOF). This method is demonstrated to be more adaptable as well as productive than other methods for addressing complicated transient flow configurations.

Atkinson (1992) given two numerical models for the simulation of sluiced settling basin design. The first model was developed to predict the particle deposition pattern as well as the amount of sediment that would pass through the basin. The second model anticipated the sluicing process as well as the time required to empty a basin. Using field data, the models were precisely validated.

By physically analysing existing field sewers, **Bachoc (1992**) explored the most significant parameters responsible for sewer sedimentation and clogging. He came to conclude that a low slope is insufficient, and that channel geometry, sudden changes, and downstream flow characteristics are all important elements in sedimentation.

Chebbo et al. (1996) investigated sewer manhole clogging and contamination in urban sewers wet-weather discharges actually contains suspended sediment particles. They emphasised for selective trapping of bed load solids in man-entry sewers as well as dewatering to reduce contamination in urban wet-weather flows.

Stovin and Saul (1996) developed two approaches for estimating the sedimentation process in storage chambers using FLUENT's CFD tools. The initial method predicted the distribution of bed shear stress and sediment deposition. However, sediment deposition assumed in places where bed shear stress fell below a critical threshold (τ_{oc}). The second method used FLUENT's particle tracking facility to estimate efficiency based on the percentage of sediment particles that resided inside the chamber.

Stovin and Saul (1998) used the particle tracking technique in FLUENT to predict sediment particle deposition in storage components. They also highlighted how this technique could be used to predict the probable spots of sediment deposits.

Schmitt et al. (1999) conducted simulations of inverted traps with different slot opening sizes and upstream and downstream lid heights. The simulations included a centrally located slot with identically sized lids, a slot with an elevated downstream lid, a slot at the trap's downstream edge, and an opening at the trap's upstream edge. The results showed that the most effective design for an invert trap was one with a slot opening located at the center, with a width equal to the channel, and with upstream and downstream lids at the same level, leading to the highest trap efficiency.

Mohapatra et al. (1999) performed numerical computations for Dam-Break Flow study in a vertical plane utilising two-dimensional flow model. For surface tracking, the mathematical model employs the established marker and cell method mixed with the volume of fluid technique. For both wet and dry bed instances, the time development of flow depth at the dam's location and the development of the pressure distribution are explored. The long-term variations of free surface and wave propogation are investigated as a result of the initially nonhydrostatic state. These long-term effects are discovered to be insignificant in wet-bed circumstances but significant in dry-bed instances.

Ashley et al. (2000a) gave an extensive overview of sediment management in combined sewers and concluded that a methodology is still needed to properly evaluate sediment accumulation within sewer systems under varying operations and maintenance regimes and choose the most adequate control strategy.

Faram and Harwood (2000) stated that Computational Fluid Dynamics (CFD) can be a cost-effective and dependable method for enhancing the design of an already established system or identifying superior alternatives. By utilizing a particle tracking model in CFD, they successfully conducted a performance and sediment retention efficiency analysis for sediment separator devices, yielding favorable and practical outcomes. CFD predictions have the potential to offer either a relative trend or an absolute forecast.

Wu et al. (2000) created a numerical model with three-dimensional capabilities to compute the flow and sediment transport within an open channel. The model used the k-ε turbulence model to solve the complete Reynolds-averaged Navier-Stokes (RANS) equations to simulate the flow. Special treatments for free-surface and roughness were implemented to account for open-channel flow, specifically through the use of a 2D Poisson equation derived from 2D depth-averaged momentum laws to govern the water level. The accuracy of the 3D computational fluid dynamics (CFD) model was validated by estimating the flow and sediment transport in a movable bed 180^0 channel bend.

Harwood and Saul (2001) examined some of the experimental studies conducted in the United Kingdom to assess the efficiency of combined sewer overflow (CSO) systems. Computational fluid dynamics (CFD) was acknowledged as a viable substitute for experimental studies. The revolution of chamber modelling will be an integration of CFD and physical techniques, it was concluded.

Stovin et al. (2002) reported that the choice of modelling parameters affects the results of CFD models. Several modelling refinements were implemented within one turbulence model, the RSM (Reynold's Stress Model), that dramatically affected the simulated velocity and bed shear stress developed within a trapezoidal open channel.

Buxton et al. (2002) predicted the sediment trapping ratios of rectangular invert traps with different slot sizes viz. 2.25 cm, 4.5 cm, and 9.0 cm using a 2D-CFD model and compared the results obtained from laboratory investigations. A renormalization group (RNG) k-ε model and fixed lid model were used to simulate turbulence and free surface tracking, respectively. They concluded that the sediment tracking with the 2D-CFD model is slightly over-predicts compared to experimental analysis.

Faram and Harwood (2002) investigated the performance of various stormwater treatment components such as advanced vortex separator (AVS), simple vortex separator (SVS), simple catch basin (SCB), and gravity sedimentation device (GSD) using CFD modelling with Lagrangian particle tracking model. They noted that vortex chambers' performance is prominent compared to linear-shaped chambers.

Ashley et al. (2003) presented experimental and 3D-CFD simulated sediment retention ratios of rectangular shaped invert traps from a joint study in the United Kingdom aimed at refining and utilising new knowledge acquired from field data, laboratory test results, and CFD simulations to implement economical design tools for the application of small invert traps to localise sediment deposition in sewers for collection.

Gupta et al. (2005) solved the continuous flow phase and estimated the velocity distribution using a 2D CFD model in FLUENT. They experimented with three distinct trap configurations with various particle types at six different discharges (low, medium, and high). Early results showed that trap performance is affected by the discharge and trap configuration. They stated that additional research is being conducted to discover the optimum shape for solid trapping efficiency under Indian conditions.

Naser et al. (2006) developed a steady, two-dimensional numerical model to examine the hydraulic behavior of a rectangular sedimentation tank under turbulent conditions. The strip integral method was used to write the flow equations, and a forward discretization scheme was employed to solve the governing partial differential equations of continuity (mass conservation), momentum (momentum conservation), advection-diffusion, turbulent kinetic

energy (k), and its dissipation (ε). A two-equation k-ε turbulence model was used to compute the turbulent shear stresses. The simulation results were compared to experimental data, and there was generally a high degree of agreement (within 5-10%).

Thinglas and Kaushal (2008a) developed and compared the 2D and 3D CFD (fixed lid approach) model with the Discrete Phase Model (DPM) of invert trap used in sewer solids management. They stated that the 2D CFD model estimates higher sediment trapping efficiency than the 3D CFD model.

Thinglas and Kaushal (2008b) investigated the flow field and sediment retention efficiency of invert traps through experimental and computational methods. They considered five different geometries of invert traps (trapezoidal chamber, rectangular chamber with and without side lids, trapezoidal chamber with rectangular base, and rectangular chamber with trapezoidal base) and simulated with different flow and sediment parameters. The most productive trap geometry is the rectangular chamber with a trapezoidal base and lids on both sides at the same level based on experimentation and 3D CFD simulations.

Gandhi et al. (2010) used the Volume of Fluid (VOF) model to simulate a free surface flow and investigate the effects of upstream bend, channel width, and channel bed slope on the velocity profile. Due to the lack of ideal flow conditions, they discovered that the real velocity profile was incompatible with the theoretical velocity profile.

Zhou and Tian (2010) devised a novel approach, along with refined operation strategies, for effectively handling the sediment deposition in sewer systems and its associated complications. Their study demonstrated that the implementation of optimized operations is a ground-breaking concept that can enhance overall performance and mitigate the problem of sediment accumulation in Shanghai's sewage network.

Kouyi et al. (2011) utilized CFD modeling to enhance the downstream-controlled dual-overflow structure's components. The said structure includes two combined sewer overflows (CSOs) linked by a rectangular drainage channel and controlled by a downstream gate at the Meyzieu waste water treatment plant entrance. The CFD simulations improved the understanding of the CSOs' interaction and enabled the optimization of the water depth sensor's placement. A numerical correlation was also established to compute the overflow rate based on the measured water depth.

According to **Khazaee and Mohammadiun (2012)**, numerical examinations of open channels are minimal when it comes to empirical analysis. Because the free surface fluctuates with time and space, they concluded that estimating flows in an open channel is more difficult than in a closed conduit.

Kaushal et al. (2012) conducted experiments and 3D CFD investigations to increase the efficiency of sediment trapping for sewer systems. To predict the free surface and sediment trapping efficiency of an invert trap with a rectangular chamber and a trapezoidal base, they used a fixed lid model and the DPM model. They discovered that the proposed model agreed fairly well with the experimental results.

Ghani et al. (2013) discussed the significance of sediment flushing in an open storm drain by using tipping flush gate. The study was conducted in an open concrete storm drain in Taman Pekaka, Nibong Tebal, Penang, Malaysia, to investigate the scouring effect of flushing arrangements on sediment in the drain channel and the practicality of employing a tipping flush gate in an open drainage system. The study's findings demonstrate that in a closed drainage system, the flush gate is more successful at sediment removal and has a longer flushing duration than the Hydrass gate.

Aslam (2013) conducted comprehensive research on the settling of sediment particles and inert materials in raw urban wastewater conveyance lines and various components of sewage water treatment plants such as primary settling tanks. He additionally developed a new component for assessing the solids settling in wastewater.

Yan (2013) introduced a new approach for predicting sediment transport, settling, and erosion as part of transient conditions in field detention basins using CFD to enhance predictions for deposition zones and settling efficiency. Using the suggested method for simulating particle transport, settling, and erosion processes under unstable conditions, multiple simulations with variable bed boundary conditions were performed in a rectangular basin. They came to the conclusion that the sediment removal efficiencies and sediment deposition zone predictions were accurate.

Aryanfar et al. (2014) conducted many laboratory experiments and examined the impact of lid's inlet and outlet angles on sediment trapping efficiency. They discovered that sediment trapping efficiency is highest with a 90^{o} inlet angle and a 34^{o} outlet angle.

Yan et al. (2014) predicted basin sediment trapping efficiency in a massive storm water detention and settling basin using 3D CFD (Eulerian based VOF Model) and a Lagrangian particle tracking model (Discrete Phase Model) with a novel boundary condition based on the interaction of particle energy and turbulent kinetic energy. They also claim that simulation models are inexpensive, more efficient, and more flexible than field measurements and laboratory studies.

The VOF model was used by **Mohsin and Kaushal (2017a and 2017b)** to estimate the free surface flow of sewer systems fitted with invert traps. They observed that the performance of the VOF model is superior to the fixed lid model in the comparison of simulated results with the experimental studies. Numerical studies of invert traps in open rectangular drains have been done using 2D and 3D CFD (VOF model along with stochastic DPM) models and stated that the sediment trapping efficiency is low for 2D CFD as compared to 3D CFD model.

In their study, **Beg et al. (2019)** utilized 2D Particle Image Velocimetry and experimental methods to examine the velocity distributions within invert traps of varying shapes and depths. The experiments were conducted in a glass-sided rectangular recirculating tilting flume, with the trap affixed to the flume's base. The researchers observed low-velocity areas near the trap's boundary surfaces, corners, and central region. Furthermore, they noted that the water velocity inside each invert trap was lower than the average velocity of the flume at each flow depth.

Beg and Kaushal (2022) investigated the performance of rectangular sediment invert trap (SIT) by both experimentally and computationally. Variation of Sediment trap efficiency of rectangular SIT was studied with the influence of trap depth, particle parameters, flow depth and slot opening size. They concluded that the 2D CFD based VOF and DPM model has capability to simulate the flow phenomenon and sediment retention efficiency of invert trap installed at the bottom of open rectangular flume.

Buxton et al. (2002); Thinglas and Kaushal (2008a and 2008b); Kaushal et al. (2012); and Mohsin and Kaushal (2017a and 2017b); as previously stated, conducted experimental and numerical studies (CFD) to improve the design of invert traps in order to achieve maximum sediment trap efficiency. Buxton et al. (2002) found that the 2D Computational fluid dynamics (CFD) model simulated significantly higher retention ratios than the experimental results, and they expected that 3D modelling, rather than 2D modelling, would predict lower retention efficiencies. Thinglas and Kaushal (2008a)observed the same thing with their CFD (fixed lid

model) results. Mohsin and Kaushal (2017a and 2017b) used the VOF model to estimate the free surface flow of invert trap-equipped sewer systems. In their comparison of simulated and experimental results, they discovered that the VOF model is superior the fixed lid model.

The above said researchers investigated trap efficiency with various invert trap geometries using both experimental and numerical (i.e., fixed lid model, VOF, and DPM) analysis. In this study, we looked at three different invert trap shapes to improve trap efficiency and looked at the effect of trap depth on trap efficiency with different flow parameters.

Initially, the settling velocity of sediment equations were derived on the assumption that the particles are in spherical shape (Gibbs et al., 1971). When the shape of sediment particles differs from that of a spherical, the settling velocity decreases (Swamee and Ojha, 1991) and (Wu and Wang, 2006). As a result of these practical implications, many equations have been developed to compute the settling velocity of natural sediments with an assumption of sphere with the nominal diameter (diameter of the sphere that has the same volume related to sediment particle) (Rubey, 1933; Zanke, 1977; Hallermeier, 1981; Van Rijn, 1984; Zhu and Cheng, 1993; Cheng, 1997; and Jiménez and Madsen, 2003). Investigators have also attempted soft computing and machine learning based approaches to calculate the settling velocity. In fact, past studies have shown that soft computing technique has a wide range of applications in the subject of fluvial hydraulics and its sub-disciplines (Azamathulla et al., 2009; Azamathulla et al., 2012) and (Pandey et al., 2020a, b). Machine learning is a collection of optimization techniques that has been widely used to the study of sediment transport and fluid flow (Bhattacharya et al., 2007; Bowden et al., 2012; Oehler et al., 2012; Yoon et al., 2013). Goldstein and Coco (2014) effectively applied genetic programming for calculating the settling velocity in flowing fluid, while Rushd et al. (2021) used artificial intelligence for calculating the settling velocity of particle in Newtonian and non-Newtonian fluid. When observational datapoints are big and correlations between variables are unclear and nonlinear, machine learning is a promising technique for developing prediction systems (Goldstein and Coco, 2014). Mahtabi et al. (2020) were used the machine learning techniques (decision tree classifier (J48), a multi-layer neural network) and compared them with the performance analysis on hydraulic jump over rough beds.

2.2 Literature Review on Settling Velocity Expressions

Researchers are still working on improving sediment trap device design. To optimize the design of the invert trap, it is important to know the sediment transport mode in the drainage and sewer

channels. One of the most important terms in the sediment transport phenomenon is settling velocity (w_s). A solid particle's settling velocity in a flowing fluid is its continuous free-falling velocity when the opposing gravity and drag forces acting on it are approximately equal. The settling velocity of a particle is affected by particle properties such as shape, size, and density, as well as fluid properties such as density and viscosity (Graf, 1984 and Pu, 2019). The settling velocity (w_s) of a particle in a quiescent fluid can be calculated by matching the effective weight force to the drag force (Stokes, 2010). Since 1851, researchers have developed a number of empirical and semi-empirical equations for calculating particle settling velocity in flowing fluid.

Stokes (1851) derived an equation for settling velocity (w_s) by equating particle drag and submerged weight with a nominal diameter assumption. Stokes' (1851) developed an equation that is discussed in Chapter 3. To predict the settling velocity of particles, the equation relies heavily on particle size, flow, and fluid parameters.

Cheng (1997) proposed a simple equation to predict the settling velocity of natural sediment particles. The shape factor and roundness value were not directly considered in his study; perhaps he assumed the standard shape factor for natural sediments to be 0.7. The equation suggests an explicit connection between the particle's Reynolds number and a non-dimensional particle parameter, and it works for a wide range of Reynolds numbers, from Stokes flow to turbulent flow.

Ahrens (2000) developed an equation to compute sediment fall velocity, which was demonstrated to fit a large data set covering a wide range of situations. The formula was rigorously calibrated to the sand portion of the data and was found to match that subset extremely well; the RMS error was roughly 8%; and the equation approaches acceptable limiting values in both laminar and turbulent flow systems.

Jimenez and Madsen (2003) developed a straightforward formula for calculating the settling velocity of natural sediments with grain sizes varying from 0.063 to 1 mm. The prior work of Dietrich (1982) was used to create the formula, which forecasts the non-dimensional settling velocity as an expression of a fluid-sediment parameter. In the lack of details on shape and roundness factors, they found that for natural sediment particles, the formula with a shape factor of 0.7 and a roundness factor of 3.5 should be used.

Wu et al. (2006) used comprehensive data collected from many countries and regions to explore and modify numerous established equations for both the initial porosity and settling velocity of sediment. They concluded that the new formula had roughly the same accuracy as the original Interagency Committee curves for sediment particles larger than 0.2 mm. Because it was calibrated using measured data rather than the assumption that it approaches the Stokes' law of spheres, the new formula should be more accurate than the original curves for sediment smaller than 0.2 mm.

Bhattacharya and Solomatine (2007) used measured data to model bedload and total load sediment transport using two Machine Learning methods: artificial neural networks and model trees. Bed-load transport models were compared to Bagnold, Einstein, Parker and van Rijn models. The models for total load transport were compared to those of Ackers and White, Bagnold, Engelund and Hansen, and van Rijn. They concluded that Machine learning (ML) is an another way to reducing the inaccuracies of sedimentation models using the selected data sets on sediment transport.

Camenen (2007) developed a simple, robust, and general equation for a particle's settling velocity that accounts for particle shape and roundness. It is based on the drag coefficient's asymptotic behaviour for low and high Reynolds numbers, respectively. They concluded that the given relationship produced the best results for a wide range of particle sizes, shapes, roundnesses, and densities among the tested formulas.

Based on Cheng's general correlation among the drag coefficient and the Reynolds number of a particle, **Zhiyao et al. (2008)** proposed a new relationship between the Reynolds number and a dimensionless particle property. They employed a trial-and-error process to minimise errors, established the coefficients, and developed a formula for predicting the settling velocity of natural sediments.

Goldstein and Coco (2014) developed a machine learning model that utilized genetic algorithms for simulating the fall velocity of noncohesive sediments. Their algorithm included a unique selection process that extracted training data from a database of 985 previously published studies. Their findings indicated that the machine learning model for settling velocity outperformed two commonly used predictors from existing literature. They further concluded that particle settling velocity is an exponential function of three independent variables: particle nominal diameter, fluid kinematic viscosity, and particle submerged weight.

Pandey et al. (2020b) utilized a genetic algorithm (GA) and multiple linear regression (MLR) to determine the maximum scour depth under equilibrium scour conditions. Through their analysis of 300 sets of experimental data from various studies and other researchers, they established a clear water scour interaction model for circular bridge piers. Their findings revealed that the GA-based approach provided more accurate results in predicting the maximum scour depth compared to MLR. Therefore, their study suggests that the GA method is a promising technique for estimating the maximum scour depth around bridge piers.

Bizimana et al. (2021) employed machine learning techniques to examine how sediment entrainment begins in rectangular and circular channel cross sections. They found that circular channels possess a self-cleansing open channel design advantage. Additionally, they devised an innovative hybrid geno-fuzzy inference system (GENOFIS) and adaptive neural fuzzy inference system (ANFIS) methodology to predict the incipient motion of sediment entrainment by utilizing experimentally derived data.

2.3 Sediment Transportation

2.3.1 Origin of Sediments

Sediments are a natural accumulation of solid materials that have been transported and deposited by wind, water, or ice. The origin of sediments can be traced back to the processes of weathering, erosion, and transportation of rocks and minerals on the Earth's surface. Weathering is the breakdown of rocks and minerals into smaller particles due to exposure to natural forces such as wind, water, and temperature changes. This process can be physical or chemical, and it can happen in situ or during transportation. Erosion occurs when weathered materials are detached and removed from their original location by agents such as water, wind, or ice. The eroded materials can be transported over long distances before being deposited. Transportation involves the movement of the eroded materials by the agents of erosion. Water is the most common agent of transportation, but wind and ice can also transport sediments over long distances. Deposition occurs when transported materials settle and accumulate in a new location. Deposition can occur in various environments such as rivers, oceans, lakes, deserts, sewer and drainage systems.

2.3.2 Properties of Sediments

Sediments are the collection of small particles of minerals, rocks, organic matter, and other materials that have been transported by water, wind, or ice, and deposited in layers on the earth's surface. The properties of sediments depend on several factors, including the composition of the sediments, the source of the sediments, and the environment in which the sediments were deposited. Some common properties of sediments include:

(i) *Grain size*: The size of the particles in sediments can range from coarse gravel to fine clay. The size of the particles can be used to infer the energy of the environment in which the sediments were deposited. Larger particles usually indicate high energy environments, such as fast-flowing rivers or waves, while smaller particles are more commonly found in low energy environments, such as lakes or sewer systems.

(ii) *Shape*: The particle shape is an important property because it influences the mean velocity of the flow as the particle moves on the bed, the settling velocity, the stability of beaches, and the bed load transport. The shape of coarse particles also indicates the mode of transport and deposit to which they belong. It also aids in determining the porosity, permeability, and cohesiveness of soils.

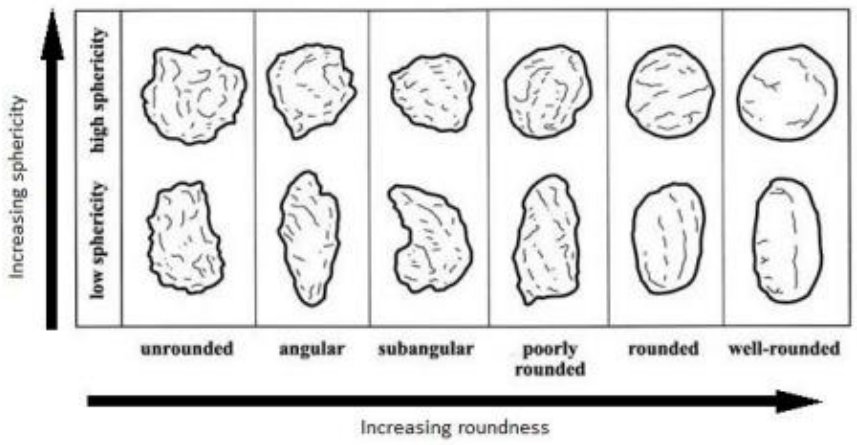

Figure 2. 1 Different shapes of sediment particles

(iii) *Settling velocity*: The settling velocity is an important parameter in analysing freshwater reservoirs and transporting sediment in water that flows, particularly when dispersion is the dominant process. First, Stokes (1851) derived an expression for terminal fall velocity (w_s) by equating the drag and submerged weight of the particle as

$$w_s^2 = \frac{4}{3C_d}\frac{(\rho_s - \rho)}{\rho} gd \quad (2.1)$$

where ρ_s= sediment density, ρ = water density, g = gravitational acceleration, C_d= drag coefficient and d = nominal diameter. The above equation is valid for particle's Reynold number, $Re_p < 1$

In the present study, the fall velocities of natural sediments (NSS1) have been estimated using newly developed GRG and Hybrid Hybrid GRG-GA described in Chapter 3 (Eq. 3.17 and 3.18).

(iv) *Composition*: Sediments can be composed of a variety of materials, including minerals, rocks, organic matter, and even anthropogenic waste. The composition of the sediments can be used to infer the source of the sediments and the geological history of the area.

(v) *Sorting*: The degree of sorting refers to how uniformly sized the particles in the sediment are. Well-sorted sediments have particles that are similar in size, while poorly sorted sediments have a wide range of particle sizes. The degree of sorting can be used to infer the energy of the environment in which the sediments were deposited.

(vi) *Porosity (P)*: It is expressed as a percentage of volume of voids to the total bulk volume of the soil. Fine-grained material has greater porosity than coarse-grained material.

(vii) *Specific Gravity*: The specific gravity of a sediment particle is the ratio of the weight of a sediment particle to the weight of an equal volume of water at a specific temperature. It is a measure of the density of the sediment particle relative to water. The specific gravity of sediment particles can vary depending on the type of sediment, as well as the composition and density of the minerals that make up the sediment. For example, quartz has a specific gravity of about 2.65, while feldspar has a specific gravity of about 2.56. The specific gravity of sediment particles is an important factor in many geologic processes, including sediment transport and deposition.

(viii) *Angle of Repose*: The angle of repose of sediment particles is the steepest angle at which a pile of sediment can maintain its stability without sliding or slumping. It is a characteristic property of the sediment particles and is influenced by various factors such as the shape, size, and packing arrangement of the particles, the amount of moisture in the sediment, and the external forces acting on the pile. Gibson proposed the Eq. 2.2 for calculating the angle of repose (Garde and Raju, 2000).

$$\tan(\emptyset) = kd^{0.125}S^{0.19}r^{0.25} \quad (2.2)$$

Where, $\emptyset$ = Angle of repose under water,

d = mean diameter of sediment (mm),

S = Relative density of sediment in water,

r = Mean ratio of longest and shortest diameters,

k = a constant (=0.6).

2.3.3 Incipient Motion of Sediment Particles

The incipient motion of sediment particles refers to the point at which the forces acting on a particle are sufficient to overcome the particle's weight and cohesive forces, causing it to start moving. This can occur in various environments, such as rivers, oceans, drainage and sewer systems, or wind, and is an important concept in understanding sediment transport.

The critical condition at which incipient motion occurs depends on various factors such as the size, shape, and density of the particle, the viscosity of the fluid, and the fluid velocity. Understanding the incipient motion of sediment particles is important for predicting sediment transport rates and designing erosion control measures in river, coastal, canal, and drainage environments.

Three different techniques have been utilized to determine the condition for the bed's incipient motion of sediment particles. (Garde and Raju, 2000)

(i) *Competency*: In this case, the bed material size, p_d, is proportional to either bed velocity or average velocity of flow, which simply makes the particle to move.

(ii) *Lift Concept*: It is considered that when the force acting on the particle in upward direction, is just larger than the particle's submerged weight, the condition of incipient motion is established. The lift force results from the pressure difference between the top and bottom of a sediment particle, which occurs when water flows over the particle. The pressure difference creates a lift force perpendicular to the flow direction. As the flow velocity increases, the lift force becomes greater, eventually exceeding the weight of the particle and causing it to lift off the bed.

(iii) *Critical Tractive Force Approach*: The critical tractive force approach is a method used to determine the threshold for sediment transport in a fluid flow, such as a river or a coastal environment. In this approach, the critical tractive force (or critical shear stress) required to initiate sediment movement is compared to the shear stress exerted by the fluid on the sediment bed. If the shear stress exceeds the critical tractive force, sediment transport will occur. This approach can be useful for predicting sediment transport rates in natural and engineered environments, such as urban, rivers, estuaries, and coastal zones. However, it is important to note that sediment transport is a complex process that can be affected by many other factors, such as turbulence, sediment cohesion, and bed roughness. Therefore, this approach should be used in conjunction with other sediment transport models and empirical data to accurately predict sediment transport rates.

2.3.4 Bed Forms

The nature of both the bed surface and the water surface changes when the sediment features, flow properties, and/or fluid properties vary in alluvial channels. Flow regimes are used to classify these types of bed and water surfaces depending on their attributes.

These regimes of flow can be divided into different categories, schematically, these bed forms are shown in Fig. 2.2. (Simons and Richardson, 1966; Garde and Raju, 2000; K Subramanya, 2009; Dey et al., 2019).

(i) A Plane bed with no sediment movement
(ii) Ripples and sand dunes
(iii) Transition
(iv) Antidunes

2.3.4.1 A Plane Bed with no Sediment Movement

This scenario occurs when the actual shear stress τ_0 is smaller than the critical shear stress τ_c. The sediment will not move, and the bed will remain flat. The resistance of the particles is the only source of flow friction.

2.3.4.2 Ripples and San Dunes

(a) *Ripples*: Individual particles on the bed begin to move when the average shear stress on the bed equals the critical shear stress for the given size of the bed material. After the motion begins, there is a range of shear stress at which the particles move in a general motion, but the bed is geometrically plane. In the case of an alluvial stream, when the

slope remains constant at various stages, an increase in discharge will disturb the bed sufficiently to cause ripples to form. If they are generated by unidirectional water current, they are termed current ripples; if they are formed by wind, they are called ballistic ripples. The downstream face of the ripples is significantly steeper than the upstream face, and the ripples move very slowly in the downstream direction. The flow, sediment, and fluid parameters influence the height, length, and speed of the ripples.

(b) *Dunes*: Dunes are another type of bed form that appears when the shear stress on the bed increases and the ripples grow larger. Dunes are characterized by a wave pattern on the bed, with ripples riding over it. As the shear stress continues to increase, the ripples disappear, leaving only the dunes pattern. Unlike ripples, dunes have a low height-to-length ratio and are larger. The surface of the water above the dunes will be wavy and out of phase. Sediment movement is more significant in dunes than in ripples, but the dunes move downstream at a slower rate than the water flow. The flow rate in channels with dune beds is subcritical, and flow separation occurs on the lee side of the bed form, leading to significant energy losses, especially in dune beds. The separation region on the dunes' lee side sheds vortices, causing the free water surface to ripple. The bed form erodes on the upstream side of both ripples and dunes, and the material is continuously deposited on the lee side of the bed form, resulting in the downstream movement of the bed wave pattern's crest.

2.3.4.3 Transition

(d) *Plane bed with sediment motion*: Increased shear stress following the dune bed pattern phase will result in a transition phase in which the bed undulations are gradually wiped away, eventually resulting in an essentially plane bed surface. The sediment movement rate would be much higher than in the dune phase. The flow, on the other hand, will be in the subcritical area, with a Froude number closer to unity.

(e) Standing wave: Continued augmentation of shear stress after the plane bed phase would generate symmetrical sand waves, accompanied by standing waves on the water surface. This would cause the Froude number to approach and surpass unity. The ripples on the water surface would synchronize with the sand waves. Both the plane bed with sediment motion and the standing wave stage are considered as transitional bed features. The bed shape during the transitional phase is quite unsteady.

2.3.4.4 Antidunes

If the shear stress within a channel surpasses the transitional stage, the symmetrical sediment wave and associated standing wave will gradually move upstream, growing steeper until they eventually break. This is known as the antidune stage, which is characterized by the absence of flow separation at the standing wave and antidune bed forms, resulting in energy loss primarily due to grain boundary roughness. It is important to note that the sand waves are considered to flow upstream only in a relative sense, due to the rapid exchange of sediment within the bed profile. The lee side of the wave will experience erosion, with some sediment deposited on the upstream side, causing the wave crest to move upstream. Overall, water flow and sediment transfer will be downstream. Antidunes have been observed solely at the water-sediment interface in alluvial channels and not at the air-sediment interface in desert environments. The flow will be supercritical during the antidune bed form stage, and the sediment transport rate will be exceptionally high.

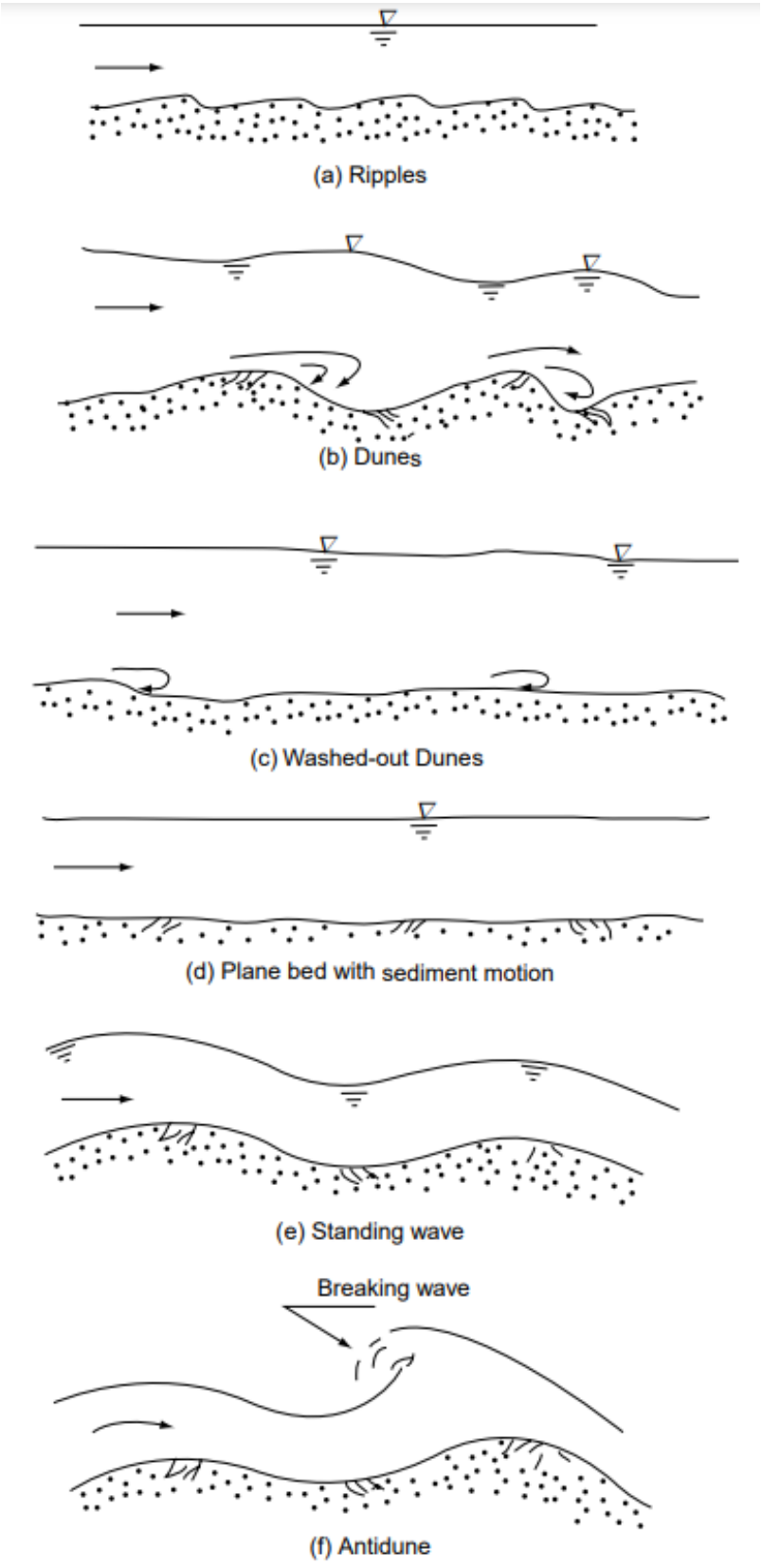

Figure 2. 2 Bed forms in alluvial channels (K Subramanya, 2009)

2.4 Bed Load Transport and Saltation

Water transports sediment as it flows through rivers and channels. Depending on the flow conditions, the density ratio of the fluid and the sediment, and the size of the sediment, the particles move in different modes. A portion of the sediment is dragged or rolled along the bed, or is in touch with the bed for the majority of the time. Contact load implies to the sediment delivered in this manner. A second method of transportation is hopping or bouncing along the bed, which causes the particle to lose touch with the bed for a short period of time. This type of material is referred to as a saltation load. The modes of sediment transport generally depend on the average shear stress on the bed for a particular ratio of sediment and fluid mass densities. For low shear stresses, the material is totally carried as contact load. At slightly greater stresses, some material is carried as saltation load. A portion of the material is conveyed in suspension as shear stress increases.

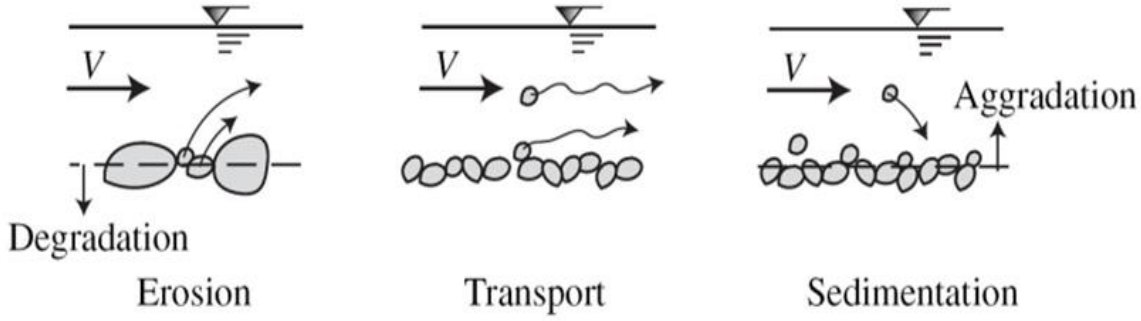

Figure 2. 3 Processes of erosion, transport, and sedimentation (Julien, 2010)

Saltation load is usually difficult to determine, because saltation load is quite low when flowing over sandy surfaces. As a result, contact load and saltation load are combined and referred to as bed load. Figures 2.3 illustrate the processes of erosion, transport, and sedimentation, as well as a Fig. 2.4 illustrate the representation of the bed and suspended load layer.

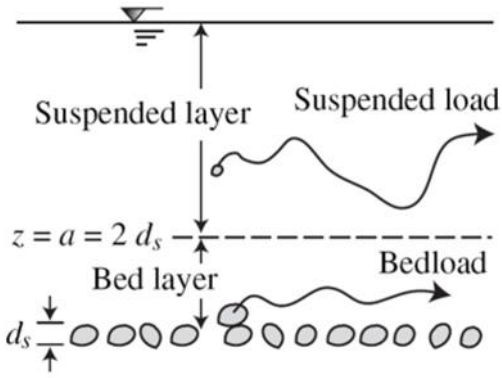

Figure 2. 4 Sketch of the bed and suspended load layer (Julien, 2010)

2.5 Estimation of Bed Load

A widely used way to measure the rate of sediment transport in the bed load (q_B) is by expressing it as the weight of sediment per second per unit width (N/s/m). There are many empirical and semi-analytical formulas that can be utilized to calculate the bed load, taking into account various factors such as the type of sediment, characteristics of the fluid, and flow parameters. Duboys (1879) proposed the first expression for q_B as a function of shear stress τ_0 excess over critical shear stress τ_c, viz.

$$q_B = \alpha(\tau_0 - \tau_c) \tag{2.3}$$

Since then, other empirical equations incorporating the parameter $(\tau_0 - \tau_c)$ have been proposed by various researchers. Meyer-Peter and Muller developed the most generally used empirical equation for q_B, which relates q_B in a dimensionless manner as,

$$\emptyset_B = 8(\tau'_* - 0.047)^{3/2} \tag{2.4}$$

Where $\emptyset_B$ = Bed load function

$$\emptyset_B = \frac{q_B}{\gamma_s (g d^3)^{1/2}} \frac{1}{\left[\frac{\gamma_s}{\gamma} - 1\right]^{1/2}} \tag{2.5}$$

And τ'_* = dimensionless grain shear stress

$$\tau'_* = \left[\frac{n_s}{n}\right]^{3/2} \frac{\gamma R' S_0}{(\gamma_s - \gamma)d} \quad (2.6)$$

In which q_B = Bed load (N/s/m)

d = Average size of sediment

R = Hydraulic radius of the channel

γ = Weight density of water

γ_s = Weight density of sediment particles

n = Manning's coefficient of channel roughness

n_s = Manning's coefficient of the particle roughness

R' = Hydraulic radius corresponding to grain roughness

S_0 = Bed slope of the channel

2.6 Suspended Load Transport

Suspended load transport is another level of bed load transport. At low shear stresses, one would expect just bed load transfer, whereas at high shear stresses, both bed load and suspended load movement would occur. In the case of non-uniform sediment, the finer portions of bed material may travel mostly as suspension, whereas the larger fractions of bed material may flow primarily as bed load.

2.7 Mechanism of Suspension

Sediment suspension is the process by which particles of sediment that have settled on the bottom of a body of water or fluid are stirred up and temporarily held in the water column. This can occur due to a variety of mechanisms, including:

(a) *Buoyancy*: Some sediment particles are naturally buoyant, meaning they float in the water column. These particles can be stirred up and suspended by water currents or by the movement of aquatic organisms.

(b) *Turbulence*: Some investigators claimed that turbulence variations near the boundary are responsible for the entertainment of sediments in the flow. Vertical turbulence fluctuations must be reduced to zero at the bed for a rigid plane bed. However, because the alluvial bed is porous, vertical turbulent fluctuations of significant magnitude can occur at the bed.

(c) *Shear stress*: The force of water flowing past a sediment bed can create shear stress on the particles at the bottom, causing them to lift up and become suspended in the water column.

(d) *Density currents*: Density currents occur when denser water sinks below less dense water, creating a current that can transport sediment and suspend it in the water column.

2.8 Estimation of Suspended Load

Considering a steady channel with a flow depth D that transports suspended sediment. Turbulence maintains the sediment particles risen from the bed upward, while gravity causes the particles to settle. As a result, a concentration profile $C = fn(y)$ is generated, with the sediment load C propagating vertically to achieve an equilibrium of the weights acting on the particles, as illustrated in Fig. 2.5.

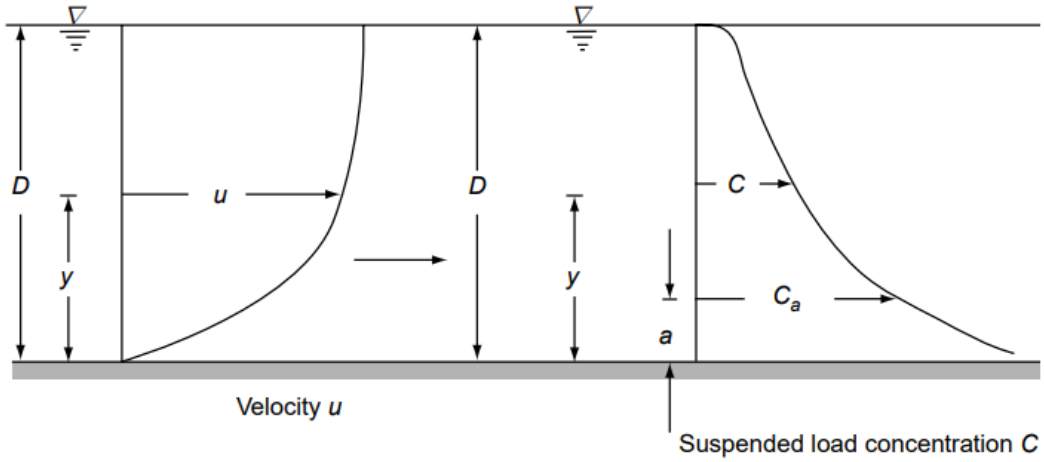

Figure 2. 5 Suspended load concentration and velocity profile in a channel

(Source: K Subramanya, 2009)

The settling of sediment particles balances the upward diffusion of sediment in a continuous flow, and the basic differential equation describing this action is given by

$$C\omega_s + \varepsilon_s \frac{dC}{dy} = 0 \tag{2.7}$$

where

C = concentration of sediment, by weight

ω_s = fall velocity of the sediment particles

ε_s = mass diffusion coefficient, generally a function of y

The Eq. 2.7 rearranged in the following form and it is known as Rouse equation.

$$\frac{C}{C_a} = \left[\left(\frac{D-y}{y}\right)\left(\frac{a}{D-a}\right)\right]^z \tag{2.8}$$

where

C_a = concentration at any height a above the bed.

The suspended sediment load q_s per unit width of channel in a vertical can be determined using Eq. 2.9 by knowing the concentration and velocity profiles in a vertical (Fig. 2.5).

$$q_s = \int_{a_1}^{D} Cudy \tag{2.9}$$

Where, a_1 = level corresponding to the edge of the bedload layer $\cong 2d$. Details of estimating q_s are available in Graf, 1971.

2.9 Sediment Management

Solids accumulation in sewers is a serious problem due to the smaller diameter of the sewer, which can cause flooding and increased pollution during overflow events to receiving waters. The solids can be gross, like garbage, with non-biodegradable high plastic components, or sediments, like sand or organic matter.

Sediment management is also critical if future systems are to be more sustainable (Ashley et al., 2000a). The primary causes of sediments in the system are hydraulic and structural discontinuities. Sewer deposits occur during dry weather and during the decelerating phases at the end of storm events. If the sediments are not removed from the system, there are two options: extract the sediments and transport them to an appropriate disposal site, or try to

move them downstream. The presence of sediment in the system can cause blockage and subsequent hydraulic problems, and anaerobic conditions, which cause hydrogen sulphide production and other problems.

The main objective of sediment management in sewers is to reduce maintenance costs, to flush sediments from Combined Sewer Overflow (CSO), and to reduce hydrogen sulphide levels in the sediment. To manage the sediments in the system, numerous devices have been developed. Erosive devices such as balling and power rodding are used to prevent or clear hydraulic restrictions, flushing systems, and silt traps. The present study concentrated on the various methods used to trap sediments that enter into the sewer and drainage systems.

2.10 Grit Chambers

Grit chambers have been utilized in France for a considerable time and can also be found in sewer inverts. They are commonly symmetrical, parallelepiped chambers as depicted in Figure 2.6. Although French grit chambers share similarities with silt traps in the UK, they are typically larger in size. Grit chambers are usually rectangular and are constructed to capture heavy inorganic sediments regardless of the flow conditions. However, Chebbo et al. (1996) noted that during dry weather, grit chambers tend to trap sediment types such as bed-load, near-bed solids, and suspended load transported within the flow. As the flow increases, the efficiency of grit chambers in trapping sediment reduces, particularly with fine-grained material.

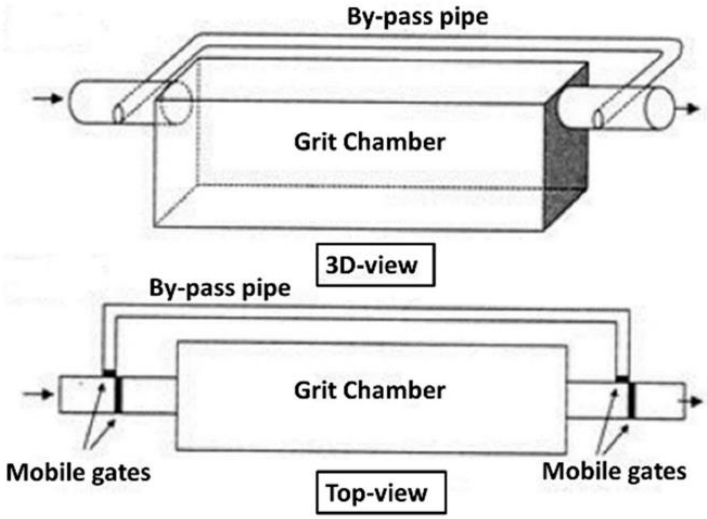

Figure 2. 6 Conventional French grit chamber (Ashley et al., 2004)

Grit chambers, which have a high trap width to sewer width ratio, are more comparable to conventional fluvial settling tanks (Ashley et al., 2004). However, studies and design guidelines for fluvial settling tanks in the United States, as well as re-evaluation of the methods, might not be applicable to combined sewers, where particle nature is highly variable and temporal variability in flow conditions is much greater across the basin.

2.11 Invert Traps (Silt Traps)

Invert traps are chambers in the sewer bottom that are used to collect sediments. In the United Kingdom and France, invert traps are commonly used. This device consists of a break in the sewer's invert (Fig. 2.7) through which the sediments fall.

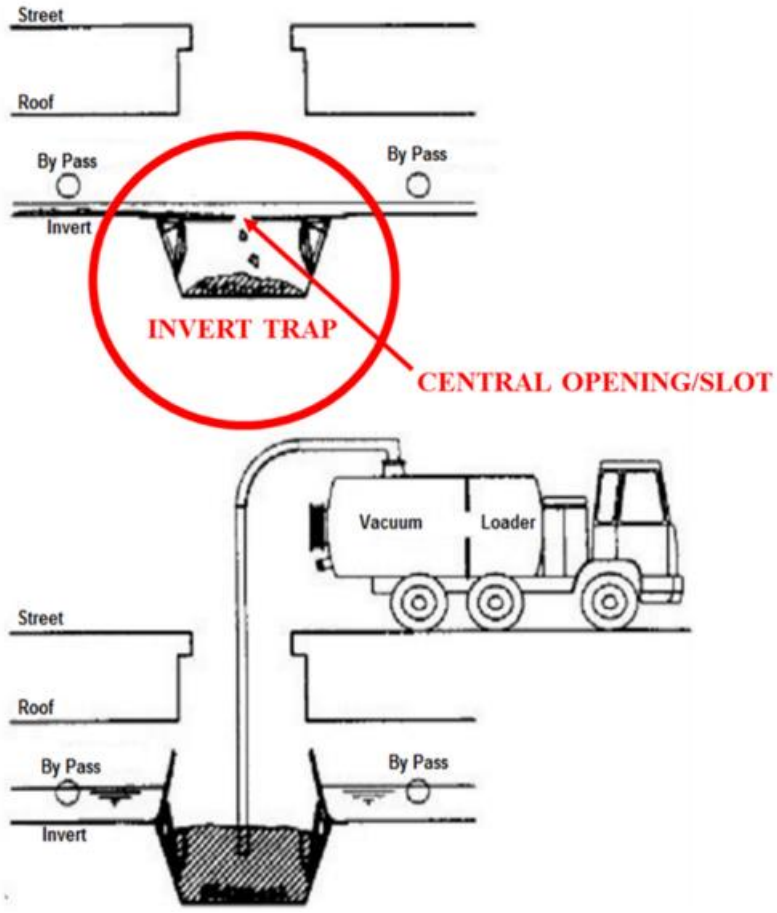

Figure 2. 7 Schematic diagram of invert trap and cleaning process (Ashley, 2004)

Regular maintenance is necessary for these traps as they must be emptied periodically. To facilitate cleaning procedures, the trap can be isolated, and the flow diverted. In combined sewers, the traps are designed to capture as much sediment bed-load as possible while

minimizing the deposition of near-bed solids, mostly inorganic in nature, that cannot be transported downstream with the flow. In dry weather, the majority of the trapped material is organic, whereas during storms, it is mostly granular in nature.

A diverse range of devices exist that aim to capture sediment across different environments and operate using different techniques. Pit-traps, invented by Hubbell (1964), were created to overcome the issue of sampling devices interfering with flow, which was commonly encountered with other bed-load sampling devices. Research has demonstrated that samplers with slot widths ranging between 100 to 200 particle diameters can capture nearly 100% of the bedload (Einstein, 1944). However, slot or pit samplers have a drawback as they must be installed in the stream bed and can only be emptied by either pumping or digging.

CHAPTER 3

EVALUATION OF SEDIMENT'S SETTLING VELOCITY

3.1 General

Before proceeding with the sediment trap efficiency of Invert trap and its CFD (VOF model) analysis, two case studies were performed to find the settling velocity equation of sediment particles using the experimental data of previous investigators and the proposed soft computing approaches, i.e., Generalized Reduced Gradient (GRG) Algorithm and Hybrid GRG-GA (to be used in the current study), to ensure that the proposed CFD model is predicting satisfactory results. These studies were published in prestigious international journals.

Since the early twentieth century, sediment transport in rivers has been intensively investigated (Wu and Wang, 2006). The Sediment motion in a fluid medium is characterised by relevant variables, can be determined based on the fluid and sediment related parameters. Many critical problems have been addressed through the development of theories and procedures that provide answers or solutions, such as sediment property quantification, sediment transport rate estimation under various flow circumstances, river morphological change prediction, and so on (Singh et al., 2019; Pu et al., 2021). Field engineers and researchers, on the other hand, find it difficult to make a judgement when many empirical methodologies yield diverse results for the same problem. As a result, a reassessment of existing procedures is required. Several empirical formulas, for example, were developed decades ago based on a small quantity of experimental and field data. To improve the reliability and accuracy of these established formulas and procedures, many new or rediscovered old datapoints from various countries and areas can be utilised. Settling velocity (ω_s) is one of the most significant terms in the sediment transport phenomenon. The settling velocity of a solid particle in a flowing fluid is the continuous free-falling velocity of the particle when the opposing gravity and drag forces acting on it are approximately equal. Settling velocity and the corresponding drag force of the sediment particle are important factors in defining the movement of sediment in suspension (Swamee and Ojha, 1991). This important term is complex due to the sediment and water interaction (Rushd et al., 2021). Possibly, the most significant instances are the wastewater treatment, hydraulic fracturing, dredging and sediment transport with flowing water. The settling velocity of particle

depends on particle properties like shape, size and density, and the fluid properties like density and viscosity of fluid (Graf, 1984; Riazi and Türker, 2019).

3.2 Analysis of Existing Settling Velocity Equations

In this section, analysis of existing equations was performed using the experimental and field data of previous investigators to predict the settling velocity of sediment particles for varying particle parameters. The predicted settling velocities were compared to observed data. This study, published in Water Journal (Switzerland), (Shankar et al., 2021), is presented here.

3.2.1 Overview

The settling velocity of sediment is one of the essential parameters in studying freshwater reservoirs and transporting sediment in flowing water, mainly when the suspension is the dominant process. Hence, their quantitative measurements are crucial. An error during the prediction of the settling velocity may be increased by a factor of three or more in the estimation of the suspended load transport in the flowing water. Despite its significance, obtaining its real value in situ is practically impossible, and it is usually derived via laboratory tests or anticipated by empirical formulas. Numerous equations are available to calculate the settling velocity of the particle. However, it is exceedingly difficult to choose the best method when giving a specific solution for the same problem. Hence, a review of the existing equations is required. In this study, extensive data on settling velocity is collected from the literature, and previously proposed equations are analysed using graphical and statistical analysis.

However, it is exceedingly difficult to choose the best method among them when numerous existing methods give a distinct solution for the same problem. Hence, a review of the existing equations is required. Predominantly, decades ago, many empirical equations were developed based on a limited number of field and experimental data. Several new or retrieved old datasets from different locations may be used to improve the consistency and accuracy of these equations. With this aim, in the present study, several existing equations for settling the velocity of particles have been tested for reliability and accuracy using the data collected from the literature.

3.2.2 Data Description

A large number of field and laboratory experimental datasets for settling the velocity of natural sediments were collected from the literature. There was 226 field, and laboratory data were taken from previous investigations. All the data sets were summarized in Table 3.1. These data

sets were categorized into two groups, viz. (i) in the first category, the shape factor has not been specified directly, and particle is represented as natural sediment grains (shape factor assumed as 0.7) and (ii) second category data set contains shape factor directly.

The first group corresponds to the fall velocity of natural sediment particles with an assumption of shape factor 0.7 were taken from Engelund and Hansen (1972); Hallermeier (1981); and Cheng (1989). Engelund and Hansen (1972) collected settling velocity data set from Hallermeier (1981). In this data, particle size was classified as sieve diameter (d_s), it has been converted into nominal diameter (d_N) by the thumb rule $\frac{d_s}{d_N}$ = 0.9. Because the kinematic viscosity ϑ and specific gravity s were not given, they were assumed to correspond to fresh water at the given temperature.

The second group data sets correspond to the fall velocity of sediment particles, including the shape factor. Briggs (1962) consists of experimental data on heavy minerals of specific gravity of about 2.65, and the shape factor ranges from 0.2 to 0.9. The data sets of settling velocities were noted by Raudkivi (1989). The data consisted of the fall velocity of sediment particles represented by their shape factor and nominal diameter. Previously, researches have showed the importance of settling velocity and suspended sediments on river health management.

Table 3. 1 Data description and properties

Parameters / Authors	No. of data	d (mm)	S (-)	CSF (-)	ϑ ($\frac{cm^2}{s}$)	w_s ($\frac{cm}{s}$)
Briggs (1962)	110	0.09-0.5	3.97-5.07	0.049-0.881	0.01	0.9-9.5
Engelund and Hansen (1972)	21	0.01-2.0	2.65	0.7	0.01-0.0131	0.5-17.0
Hallermeier (1981)	21	0.09-1.3	2.65	0.7	0.0084-0.0114	0.54-14
Raudkivi (1989)	36	0.2-2.0	2.65	0.5-0.9	0.009-0.0131	1.68-24.0
Cheng (1997)	38	0.06-4.5	2.65	0.7	0.0114-0.0141	0.235-28.1

3.2.3 Existing Equations for Settling Velocity of Sediments

Numerous field and laboratory investigations have been conducted to calculate the Settling velocity of sediment particles. To compute the variation of settling velocity for different particle

sizes and shapes, many researchers had been developed the formula for fall velocity of the natural particle. In the present study, fourteen (eleven without shape factor, S_f and three with shape factor, S_f) previously developed empirical equations are selected for checking their accuracy and these equations are listed below. A shape factor is defined as an irregularity in the shape of a particle from the sphere. Here, CSF (Corey Shape Factor) is used to measure irregularity, which is formulated as CSF = c /$(ab)^{0.5}$, where *a*, *b*, and *c* are the lengths of the longest axis, the intermediate axis, and the shortest axis, respectively.

First, **Stokes (1851)** derived an expression for terminal fall velocity (ω_s) by equating the drag and submerged weight of the particle as

$$w_s^2 = \frac{4}{3C_d}\frac{(\rho_s - \rho)}{\rho} gd \tag{3.1}$$

where ρ_s= sediment density, ρ = water density, g = gravitational acceleration, C_d= drag coefficient and *d* = nominal diameter (diameter of the sphere that has the same volume as the particle). Stokes (1851) found that, C_d for low particle Reynolds number ($R_e < 1$), is inversely proportional to R_e. $C_d = \frac{24}{R_e}$ and $R_e = \frac{\omega_s d}{\vartheta}$. He modified Eq. (4.1) as

$$w_s = \frac{1}{18}\frac{g(S-1)d^2}{\vartheta} \tag{3.2}$$

where *S* is the relative density of sediment and ϑ = kinematic viscosity of water.

On the other hand, for a higher Reynold number ($R_e > 10^5$), the C_d is found to be a constant.

Ruby (1933) was the first researcher who proposed an expression to cover all types of settling regimes and written as

$$w_s = F[dg(S-1)]^{0.5} \tag{3.3}$$

where *F* is dimensionless constant depends on particle diameter (*d*) and $F \approx 0.8$ for particles ≥ 1 mm. For particles < 1 mm, *F* is determined as

$$F = \left[\frac{2}{3} + \frac{36\vartheta^2}{gd^3(S-1)}\right]^{0.5} - \left[\frac{36\vartheta^2}{gd^3(S-1)}\right]^{0.5} \quad (3.3a)$$

Zhang (1993) proposed a simple equation with different diameter range viz. clay-sand, sand, and gravels upto 16 mm.

$$w_s = \sqrt{\left[\left(13.95\frac{\vartheta}{d}\right)^2 + 1.09(S-1)gd\right]} - 13.95\frac{\vartheta}{d} \quad (3.4)$$

Zanke (1977), Soulsby (1997), and Julien (1995) developed similar equations to compute the settling velocity and gave the relation for particle Reynolds number, which are rewritten in the following notation.

$$w_s = \frac{4A\vartheta}{d}\left[\left(1 + B\frac{(s-1)gd^3}{\vartheta^2}\right)^{0.5} - 1\right] \quad (3.5)$$

$$R_e = A\left[\left(16 + BD_{gr}^3\right)^{0.5} - 4\right] \quad (3.5a)$$

where D_{gr} is dimensionless particle size and calculated as $D_{gr} = \left[\frac{g(s-1)}{\vartheta^2}\right]^{\frac{1}{3}} d$

The only differences among these equations are given by the coefficients (*A* and *B*); the values of these coefficients are 2.5 and 0.16 for Zanke (1977), 2.59 and 0.156 for Soulsby (1997), and 2.0 and 0.222 for Julien (1995). The main reason for different coefficient values is due to the different data sets used while doing their empirical calibrations.

Rijn (1989) proposed an equation with some complexity, i.e., an equation containing trigonometric terms that depend on the non-dimensional number. He adopted the Stokes equation for $d < 0.01$ cm.

$$w_s = \frac{1}{18}\frac{g(s-1)d^2}{\vartheta} \quad \text{For } d < 0.01 \text{ cm} \quad (3.6a)$$

$$w_s = 1.1\sqrt{[(s-1)gd]} \quad \text{For } d > 0.1\text{cm} \quad (3.6b)$$

$$w_s = \frac{10\vartheta}{d}\left[\sqrt{(1 + 0.01d^3)}\right] \quad \text{For } d = 0.01-0.1\text{cm} \quad (3.6c)$$

Zhu and Cheng (1993) proposed a simple equation with the different diameter range

$$w_s = \frac{\vartheta\left[-24(cos\,\alpha)^3 + \left(576(cos\,\alpha)^6 + (18(cos\,\alpha)^3 + 3.6(sin\,\alpha)^2)D_{gr}^3\right)^{0.5}\right]}{d(9(cos\,\alpha)^3 + 1.8(sin\,\alpha)^2)} \quad (3.7)$$

Where D_{gr} is a non-dimensional particle parameter and calculated as

$$D_{gr} = \left[\frac{g(s-1)}{\vartheta^2}\right]^{\frac{1}{3}} d \quad (3.7a)$$

$$\alpha = 0 \qquad \text{For, } D_{gr} \leq 1 \quad (3.7b)$$

$$\alpha = \frac{\pi}{\left[2 + 2.5\left(log\, D_{gr}\right)^{-3}\right]} \qquad \text{For } D_{gr} \leq 1 \quad (3.7c)$$

Cheng (1997) proposed a simple equation to predict the settling velocity of natural sediment particles.

$$w_s = \frac{\vartheta}{d}\left(\sqrt{25 + 1.2D_{gr}^2} - 5\right)^{1.5} \quad (3.8)$$

Cheng (1997) directly did not consider the shape factor and roundness value in this equation and assumed the standard shape factor for natural sediments as 0.7.

Wu and Wang (2006) suggested a simple equation for calculating the settling velocity of sediment particles. In this equation, the particle shape factor considers explicitly.

$$w_s = \frac{M\vartheta}{Nd}\left[\sqrt{\left(\frac{4N}{3M^2}D_{gr}^3\right)^{\frac{1}{n}} + \frac{1}{4}} - \frac{1}{2}\right]^n \quad (3.9)$$

where *M*, *N*, and *n* are calibration coefficients and calculated as $M = 53.5e^{-0.65S_f}$,

$N = 5.65e^{-2.5S_f}$ and $n = 0.7 + 0.9S_f$. S_f is the safe factor.

Jimenez and Madsen (2003) developed an equation to predict the settling velocity. They derived this equation from the previous development of Dietrich (1982), and it calculates the fall velocity of sediment particles for a given particle shape factor, roundness parameter, and diameter.

$$w_s = \frac{\sqrt{(S-1)gd}}{A + \frac{B}{S_*}} \tag{3.10}$$

where *A*, *B* depend on the Corey shape factor (*CSF*) and particle roundness (*P*). For natural sediment particles (*CSF* = 0.7, *P*=3.5), the proposed standard values of *A*, *B* are 0.954, 5.12 respectively. S_* is dimensionless sediment parameter and calculated as

$$S_* = \frac{d}{4\vartheta}\sqrt{(s-1)gd} \tag{3.10a}$$

Camenen (2007) developed an equation to predict the settling velocity. Explicitly, the particle size, shape factor, and roundness effects have been included in this equation.

$$w_s = \frac{\vartheta}{d}\left[\sqrt{\frac{1}{4}\left(\frac{A}{B}\right)^{\frac{2}{n}} + \left(\frac{4}{3}\frac{D_{gr}^3}{B}\right)^{\frac{1}{n}}} - \frac{1}{2}\left(\frac{A}{B}\right)^{\frac{1}{n}}\right]^n \tag{3.11}$$

A, *B*, and *n* are the calibration coefficients, functions of shape factor (S_f) and roundness (*P*).

$$A = a_1 + a_2\left[1 - sin\left(\frac{\pi}{2}S_f\right)\right]^{a_3} \tag{3.11a}$$

$$B = b_1 + b_2\left[1 - sin\left(\frac{\pi}{2}S_f\right)\right]^{b_3} \tag{3.11b}$$

$$n = n_1\left(sin\frac{\pi}{2}S_f\right)^{n_2} \tag{3.11c}$$

At Particle roundness (*P* =3.5): a_1=24, a_2=100, a_3= 2.31; b_1= 0.94, b_2= 20, b_3= 2.975 and n_1= 1.62; n_2= 0.47.

3.2.4 Statistical Performance Analysis of Equations

The statistical analysis was also done to check the accuracy of these equations. Five statistical indices were taken to enhance the agreement between the predicted and observed settling velocity of sediment particles with and without shape factor. If *M* is the measured (or observed) value and *P* is the corresponding predicted (or computed) value, the various performance indices are defined as

The co-efficient of determination (R^2) explains the fraction of total variance in observed data sets, and it ranges from 0 to 1.

$$R^2 = \frac{\sum_{i=1}^{n}(M_i - \bar{M})(P_i - \bar{P})}{\sqrt{\sum_{i=1}^{n}(M_i - \bar{M})^2}\sqrt{\sum_{i=1}^{n}(P_i - \bar{P})^2}} \tag{3.12}$$

where, M_i= Observed data, P_i= Predicted data, $\bar{M}$= mean of observed data and $\bar{P}$= mean of predicted data.

Nash Sutcliffe efficiency (NSE) is the most extensively used indices, and it represents the absolute difference between measured and predicted, which is then normalized with the measured variance. The range exists between -∞ and 1, with 1 represents the perfect fit.

$$E = 1 - \frac{\sum_{i=1}^{n}(M_i - P_i)^2}{\sum_{i=1}^{n}(M_i - \bar{M})^2} \tag{3.13}$$

Kling- Gupta efficiency (KGE)

$$E = 1 - ED \tag{3.14}$$

ED is calculated as,

$$ED = \sqrt{(r-1)^2 + \left(\frac{\sigma_p}{\sigma_m} - 1\right)^2 + \left(\frac{\mu_p}{\mu_m} - 1\right)^2} \tag{3.14a}$$

where; *ED* = Euclidian distance from the ideal point, *r* = linear correlation coefficient between predicted and observed data, σ_p, σ_m= standard deviation of predicted and observed data, respectively and μ_p, μ_m = mean of predicted and observed data, respectively.

Percent Bias (PBIAS) represents the average deviation in percentage of the predicted data from the observed data.

$$PBIAS = \frac{\sum_{i=1}^{n}(M_i - P_i)}{\sum_{i=1}^{n} M_i} \times 100 \quad (3.15)$$

Mean Absolute Error (MAE)

$$MAE = \frac{1}{n}\sum_{i=1}^{n}|(M_i - P_i)| \quad (3.16)$$

3.2.5 Results and Discussions

a) Performances of Existing Equations

In this present study, total of fourteen (eleven without S_f and three with S_f) equations proposed by earlier investigators were checked with 226 field and laboratory experimental data sets. The accuracy and reliability of these equations were analysed both graphically and statistically. In Figs. 3.1(a-k) and 3.2(a-c), values on X-axis and Y-axis represent the observed and predicted data sets of settling velocity of particles, respectively. The data set has been divided into two groups; one is without shape factor (assumed as a natural particle, S_f = 0.7) another is with shape factor (shape factor considered explicitly). The first group consists of data sets of Engelund and Hansen (1972); Hallermeier (1981); and Cheng (1997). The second group consists of the data sets of Briggs (1962) and Raudkivi (1989).

Figures 3.1 (i) and 1 (k) are the graphical representation of the observed and predicted data by the equations of Jimenez and Madsen (2003) and Camenen (2007) without shape factor. Results show that the Jimenez and Madsen (2003) and Camenen (2007) equations performed well and produced nearly the same results for fine sediments (lower settling velocity); in the case of coarse sediments (higher settling velocity), these equations performed slightly under prediction and over prediction, respectively. There is a limitation for Jimenez and Madsen's (2003) equation, as it was developed for a certain diameter range (0.63 mm – 1 mm).

The equation of Cheng (2003) also shown good agreement with observed data without shape factor (natural sediment particles i.e., S_f assumed as 0.7), and slight under prediction is observed through scatter plot of Fig. 3.1(g). The Zhang's (1993) expression was over predicted for lower settling velocity between 2-9 cm/s and further observed good agreement with measured settling velocity data, shown in Fig. 3.1(d). The agreement between observed and predicted data of Zanke (1977); Soulsby (1997); and Julien (1995) expressions are shown in Figs. 3.1(b), 3.1(h),

and 3.1(f), respectively. Because of similar equations, these three expressions have shown analogous trends in their scatter plots, and Julien (1995) equation showing lower accuracy graphically and statistically. The Rijn (1989) gave over prediction with moderate performance, it has been shown in Fig. 3.1(c). Rijn (1989) divided datasets into three sediment diameter ranges (d < 0.01cm, d > 0.1cm and d = 0.01- 0.1cm) and most of the collected datasets were belonged to d > 0.01cm, that may be the reason for over prediction with moderate performance Figures 3.1(j) and 3.2(b) show the agreement between observed and predicted settling velocity by the equation of Wu and Wang (2006) with shape factor and without shape factor, respectively. Wu and Wang (2006) included the importance of the shape factor and excluded the particle roundness factor. So that, it could be used only for data that excludes the roundness factor, if not there may occur some error in particle's settling velocity calculations.

Most of the data showed incredibly good agreement graphically and statistically because of a simple equation that explicitly included the effect of the shape factor. The Camenen's (2007) expression with the inclusion of shape factor produced a low agreement with the observed data, which can be seen in Fig. 3.2(c). It would have been shown good agreement when the shape factor is considered, but the results showed low agreement because of the complex equation and insufficient data of all parameters. The expression of Jimenez and Madsen (2003) with the shape factor shown poor agreement compared to above mentioned equations for these data sets. The equations of Ruby (1933) and Zhu and Cheng (1993) shown extremely poor agreement with the observed data with under and over prediction, respectively.

The authors observed it, for computing settling velocity of sediment particles, equation proposed by Wu and Wang (2006) (with and without shape factor) illustrates better agreement with the predicted and observed data than the others. However, the reason for the poor performance of Jimenez and Madsen (2003) and Camenen (2007) with shape factors may be the complex equations and adequate data sets.

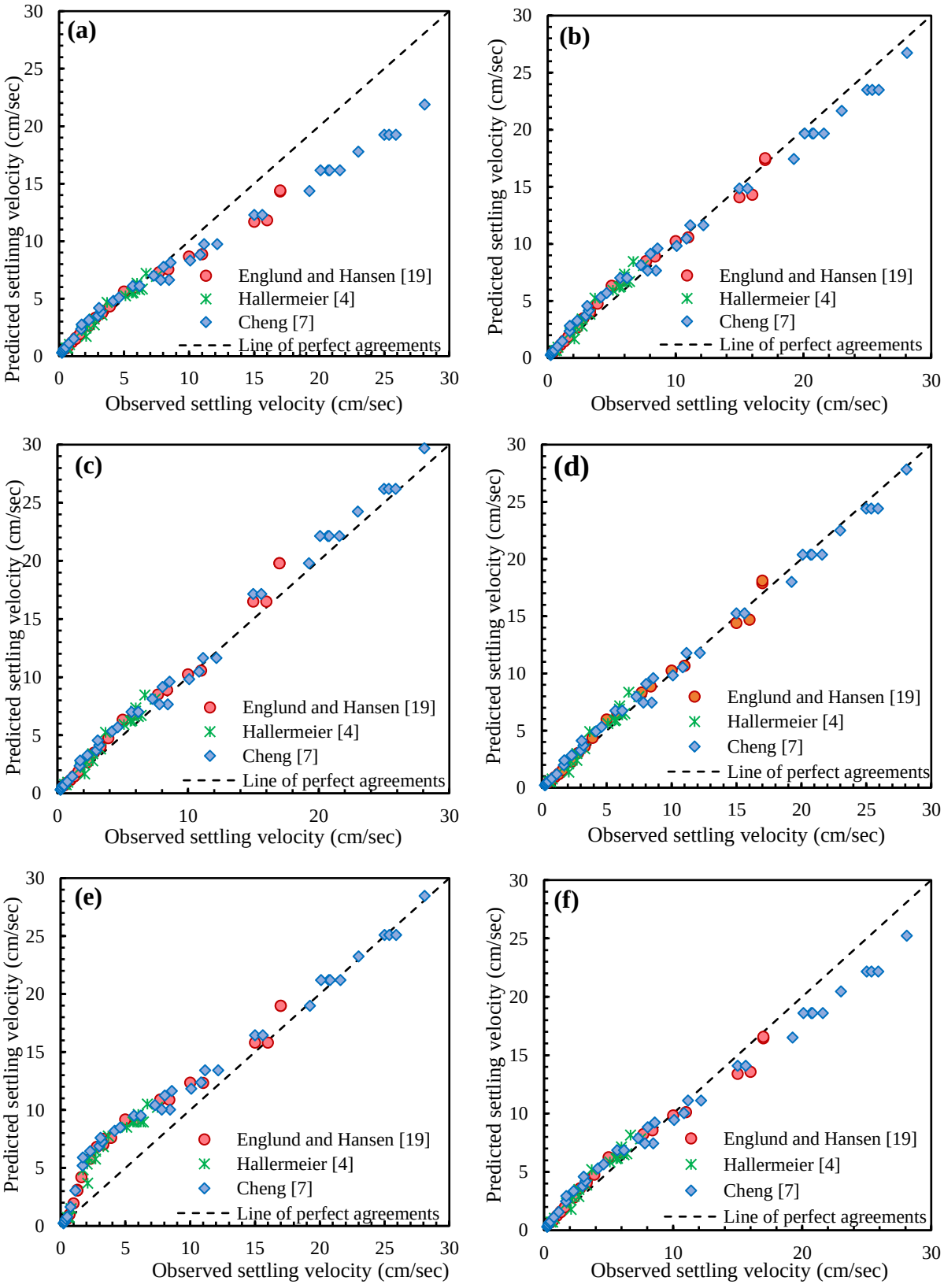
(a)
(b)
(c)
(d)
(e)
(f)
Predicted settlinng velocity (cm/sec)
Predicted settling velocity (cm/sec)
Observed settling velocity (cm/sec)
Englund and Hansen [19]
Hallermeier [4]
Cheng [7]
Line of perfect agreements
0
5
10
15
20
25
30

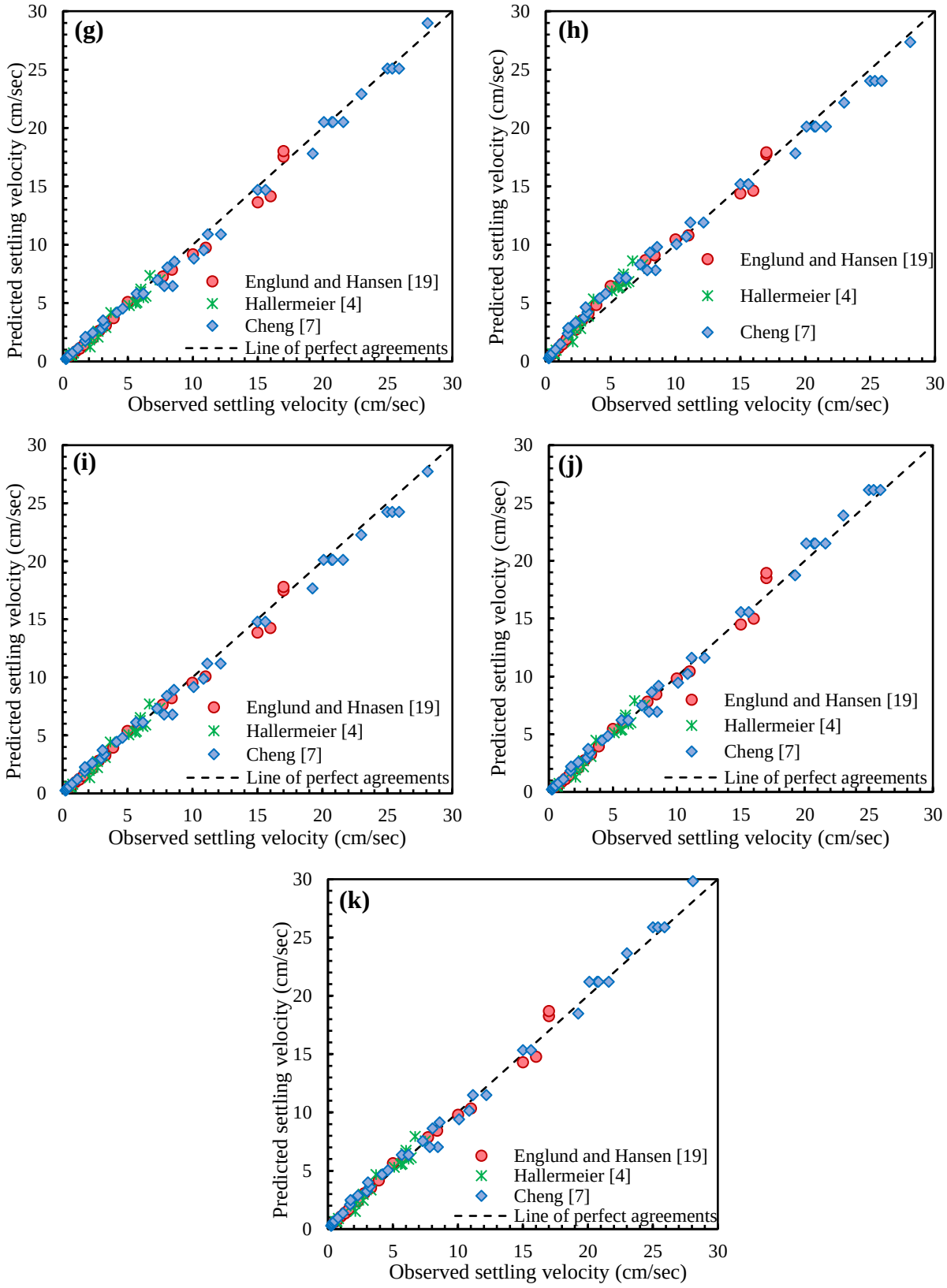

Figure 3. 1 (a-k): Observed versus predicted settling velocity without shape factor using; (a) Rubey (1933), (b) Zanke (1977), (c) Rijn (1989), (d) Zhang (1993), (e) Zhu and Cheng

(1993), (f) Julien (1995), (g) Cheng (1997), (h) Soulsby (1997), (i) Jimenez and Madsen (2003), (j) Wu and Wang (2006) and (k) Camenen (2007).

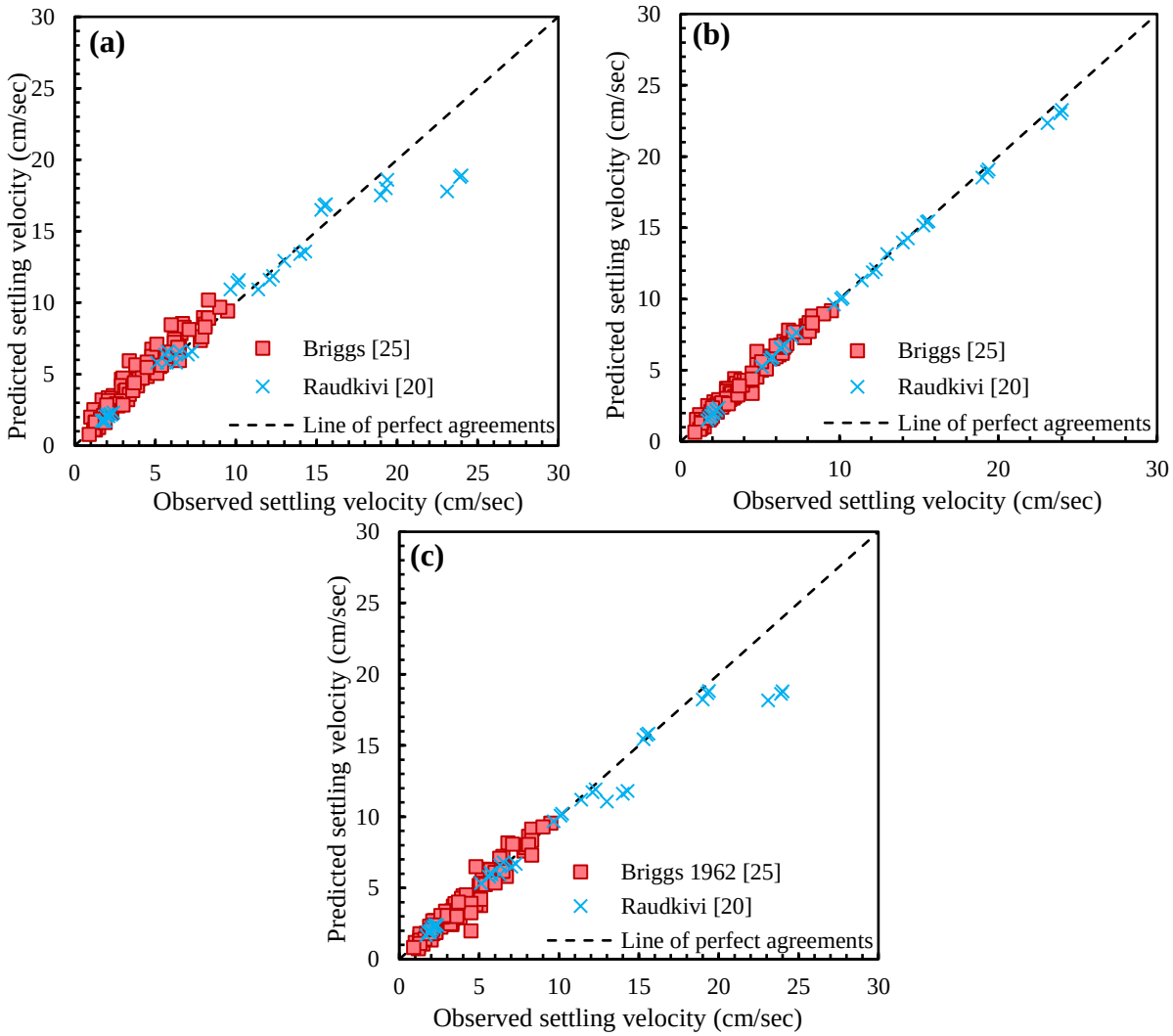

Figure 3. 2 (a-c): Observed versus predicted settling velocity with shape factor using; (a) Jimenez and Madsen (2003), (b) Wu and Wang (2006), and (c) Camenen (2007).

b) Statistical Performance Analysis of Equations

In Equations (3.12-3.16), *n* is the number of data sets, i.e., 226. Values of R^2, NSE, KGE, PBIAS, and MAE for different equations are listed in Table 3.2. The R^2, NSE, and KGE of Eq. (3.9), i.e., proposed by Wu and Wang (2006) are highest, and PBIAS and MAE are lowest than among all other equations. Statistical performances indicate that the expression of Wu and Wang (2006) predicts the better settling velocity of sediment particles than among all equations. However, it was observed graphically and statistically. The expressions proposed by Camenen (2007) and Jimenez and Madsen (2003) without shape factor give second highest agreements between observed and predicted data, as can be seen in Table 3.2 and Fig. 3.1.

Table 3. 2 Statistical values

Researchers	NSE	KGE	PBIAS	MAE	R^2
Wu and Wang (2006) with S_f	0.9937	0.976	-1.06	0.2691	0.9942
Wu and Wang (2006) without S_f	0.9931	0.9616	-1.463	0.4107	0.9948
Camenen (2007) without S_f	0.9936	0.9733	-2.3895	0.4376	0.9944
Jimenez and Madsen (2003) without S_f	0.9929	0.9512	2.6308	0.4164	0.9952
Cheng (1997) without S_f	0.9924	0.96	3.8275	0.4342	0.9941
Zhang (1993) without S_f	0.9925	0.964	-1.7206	0.4835	0.9937
Zanke (1977) without S_f	0.9847	0.9143	-2.4174	0.7276	0.9914
Soulsby (1997) without S_f	0.9861	0.9241	-4.5574	0.7057	0.9915
Rijn (1989) without S_f	0.9824	0.8998	-9.1874	0.7705	0.9933
Camenen (2007) with S_f	0.9581	0.8958	3.4168	0.5018	0.9661
Julien (1995) without S_f	0.9714	0.8582	1.0309	0.9229	0.9901
Jimenez and Madsen (2003) with S_f	0.9234	0.8648	-6.1132	0.8406	0.9354
Ruby (1933) without S_f	0.9069	0.7104	12.4768	1.3657	0.989
Zhu and Cheng (1993) without S_f	0.8707	0.7057	-28.4017	2.1954	0.9599

3.2.6 Conclusions

The present chapter describes the settling velocity phenomenon and deals with the methods of estimation of settling velocity. Total fourteen equations (eleven without S_f and three with S_f) were used for checking the accuracy and performance of particle settling velocity. The authors graphically observed it; the relationship proposed by Wu and Wang (2006) with and without shape factor gives superior agreements, as can be seen in Figs. 3.1(j) and 3.2(b). Statistically, relationships proposed Wu and Wang (2006) with and without shape factor and Camenen (2007); Jimenez and Madsen (2003); and Cheng (1997) without shape factor give approximately similar values among all, but Wu and Wang (2006) show bit higher values than other equations, as shown in Table 4.2. Graphically and statistically, it was observed that the expressions of Zanke (1977); Soulsby (1997); and Julien (1995) show the same pattern with medium performance. The low performance of Jimenez and Madsen (2003) and Camenen

(2007) equations may be strict to particular datasets. There may be the scope for checking the accuracy of the above equations with broad datasets, including particle shape factor and roundness factor. The study's main noteworthy findings are listed below.

- The settling velocity of particles must be calculated with more precision in order to define the sediment mode of transit with the flow.
- The estimates of settling velocity obtained from various methods were compared based on NSE, KGE, PBIAS, MAE, R^2 and line of perfect agreement.
- After graphical and statistical analysis, it was discovered that the Wu and Wang (2006) equation calculates the settling velocity of sediment particles with better accuracy and reliability.

Finally, it was concluded by authors after graphical and statistical investigations; the expression proposed by Wu and Wang (2006) predicts the settling velocity of sediment particles for both with and without shape factor cases, with the least errors among all equations. Hence, the present study highlights that the Wu and Wang (2006) can predict the accurate value of settling velocity of a particle.

3.3 Estimation of Settling Velocity Using Machine Learning Algorithms

Soft computing approaches, the Generalized Reduced Gradient (GRG) Algorithm, and a hybrid GRG-GA were used in this study to model particle fall velocity. Dimensional analysis was used to obtain the equation of fall velocity. According to the existing literature, the fall velocity is a function of non-dimensional particle diameter, shape factor, viscosity, and nominal diameter of the particle, so these factors were taken into account in the analysis. The predicted settling velocities were compared to observed data. This study, published in Acta Geophysica Journal, Springer, (Shivashankar et al., 2022), is presented here.

3.3.1 Overview

The modified methodology for predicting the settling velocity phenomenon is suggested in this section. The accuracy of three previously proposed settling velocity equations is also checked in this study. After graphical and statistical analysis, authors proposed GRG and Hybrid GRG-GA approaches for the estimation of settling velocity. Hybrid GRG-GA based settling velocity approach showed more precise results than GRG approach. In addition, Hybrid GRG-GA and GRG approaches were compared with previously proposed equations using 226 datapoints. Graphical and statistical analysis shows that the Hybrid GRG-GA and GRG approaches give better agreement with observed datapoints as compared to previously proposed equations. An application of Hybrid GRG-GA reduces the sum of square of error in fall velocity by over 70% and 30% on an average as compared to previous equations during training and testing respectively. This study highlights that the Hybrid GRG-GA approach could be efficiently used for calculating the settling velocity.

3.3.2 Methodology

In this study, soft computing approaches, GRG and Hybrid GRG-GA Algorithms were applied to model the fall velocity of particle. The equation of fall velocity was obtained based on the dimensional analysis. As the fall velocity is known to be a function of non-dimensional particle diameter, shape factor, viscosity, and nominal diameter of the particle from the existing literature, so, these, factors were considered in the analysis. To obtain the best fit coefficients of these independent variables, their coefficients were treated as decision variables. Thereafter, minimization of sum of square of error between observed and estimated fall velocity was set as the objective as this objective function is quite stable and has been widely used in the field of water resources (Barati, 2013; Zakwan, 2019; Nawaz et al., 2020; Niazkar and Zakwan, 2021).

Then the optimization techniques were run to obtain the optimal parameters of fall velocity expression. Outcomes of GRG and GRG-GA approaches are compared with equations proposed by Jiménez and Madsen (2003); Wu and Wang (2006) and Camenen (2007). The flow chart of the procedure is presented in Fig. 3.3. The details of GRG and GRG-GA approaches are presented in subsequent subsection.

a) Generalized Reduced Gradient (GRG) Algorithm

Generalized Reduced Gradient (GRG) is a gradient based optimization algorithm (Muzzammil et al., 2018) that utilizes steepest descent for searching the direction of optimal solution. The algorithm primarily uses Quasi- Newton method to determine the minimum gradient. GRG algorithm has been widely used for modelling in water resource engineering (Muzzammil et al., 2018; Niazkar and Zakwan, 2021; Zakwan and Niazkar, 2021; Barati, 2013; Pandey et al., 2020a and 2020b; Nawaz et al., 2020). In the present work, GRG algorithm available in MATLAB was used to develop the equation to calculate the fall velocity. For application of GRG algorithm minimization of sum of square of error was set as the objective function and initial guess values of decision variables were provided. GRG algorithm was run until the convergence was achieved. The relative change of less than 0.000000001 for five consecutive iterations marked the convergence for the present model as the default convergence rate (0.0001) was too high to meet KKT condition leading to premature stoppage of GRG algorithm.

b) Hybrid GRG-GA

Many hybrid techniques have been used for modelling in recent time. In this work hybrid GRG-GA technique has been proposed to model the fall velocity. Basically, GRG is gradient based and GA is biologically inspired non-gradient technique suitable for optimizing both continuous and discontinuous functions. “GA starts the search with random population of solutions and evolves the population based on operators derived from natural genetic variation and natural selection such as mutation, inheritance, selection, and crossover” (Pandey et al., 2020b). In the present study uniform creation function with population size 150 and rank scaling was used while the mutation function and migration were set as adaptive feasible and forward respectively in accordance with literature (Pandey et al., 2020a and 2020b).

In hybrid GRG-GA technique, the optimal values of decision variables obtained from GRG algorithm at convergence are used as an initial guess for running the GA. In this way the chances of getting trapped into local minimum of gradient based GRG technique is overcome by

applying GA. On the other hand, the number of runs required by GA are reduced by providing a suitable initial guess values of decision variable. Figure 1 represent the methodology of the present work.

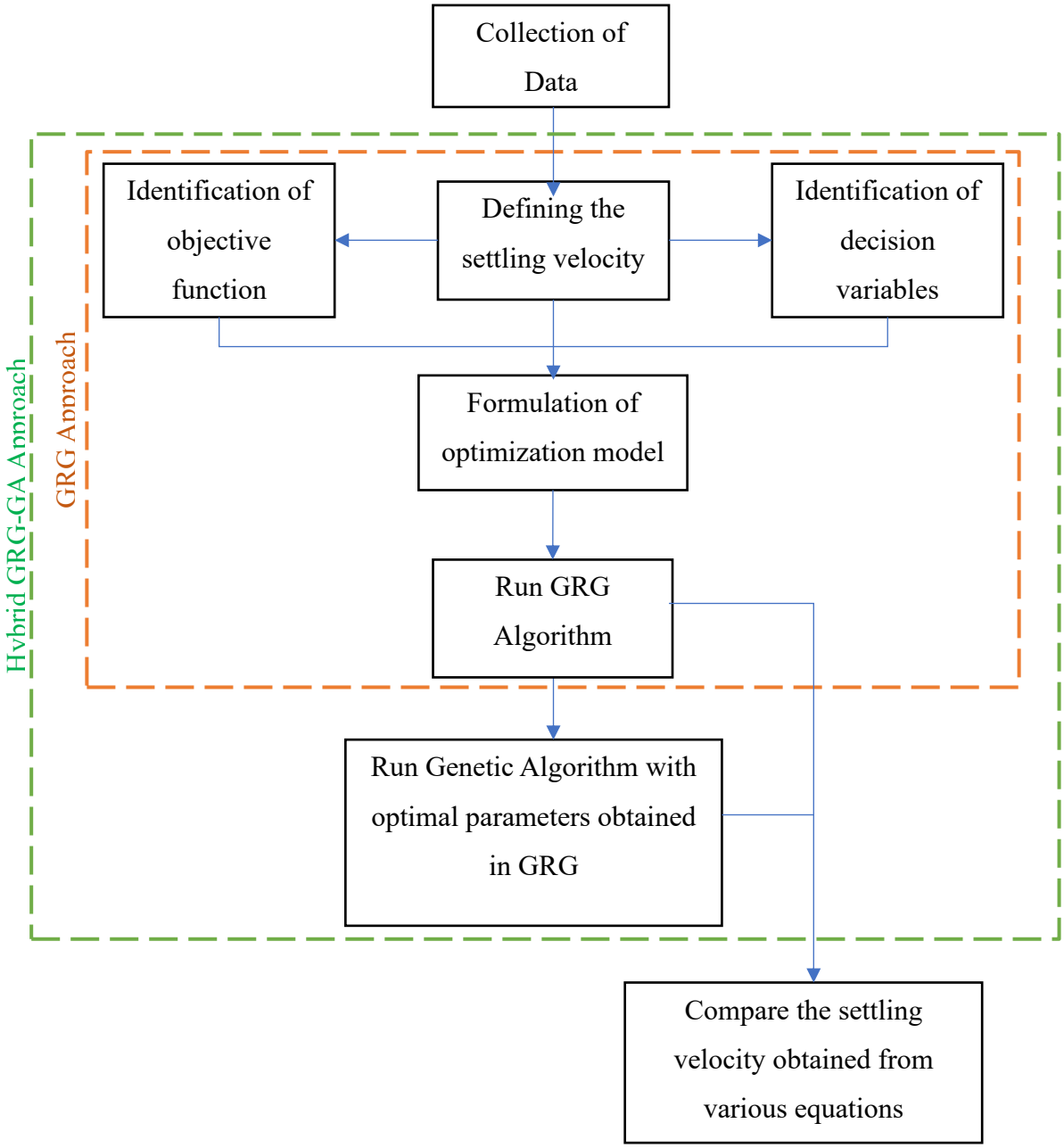

Figure 3. 3 Flow chart of methodology.

3.3.3 Results and Discussion

Different researchers have devised a variety of settling velocity formulas with and without particles shape factor. In this study we are only using three previously proposed equations (Jiménez and Madsen, 2003; Wu and Wang, 2006; and Camenen, 2007) and comparing

outcomes of these equations with GRG and hybrid GRG-GA approaches. Equations (3.17-3.18) gives the GRG and hybrid GRG-GA based relationships to calculate the settling velocity.

The parameters obtained from the two approaches were different because GRG is a gradient based technique, so it resulted in local optimal solution, which when fed as initial value of decision variables in case of hybrid GRG-GA resulted in better global optimal solution. We categorized collected data into two categories (training and validation), 75% data was used for training and 25% data was used for validation of GRG and GRG-GA approaches, as can be seen in Figs. (3.4-3.6).

$$w_s = \frac{\upsilon}{d}\left[\sqrt{\left(\frac{1990N}{M}D_*^2\right)^{\frac{1}{n}} + \left(\frac{N}{M}\right)^{53.4}} - \left(\frac{N}{M}\right)^{-1}\right]^n \qquad \text{(GRG)} \quad (3.17)$$

Where,

$$M = 0.012e^{0.054\,sin(S_f)}, N = 0.005e^{-1.37\,sin(S_f)}, \text{ and } n = 3.65 + 38.35\,sin(S_f)$$

$$w_s = \frac{\upsilon}{d}\left[\sqrt{\left(\frac{2195N}{M}D_*^2\right)^{\frac{1}{n}} + \left(\frac{N}{M}\right)^{44.5}} - \left(\frac{N}{M}\right)^{-1}\right]^n \qquad \text{(Hybrid GRG-GA)} \quad (3.18)$$

Where,

$$M = 0.012e^{0.024\,sin(S_f)}, N = 0.05e^{-1.37\,sin(S_f)}, \text{ and } n = 3.67 + 41.35\,sin(S_f)$$

These approached were analysed graphically and statistically using data collected from prior investigations, as can be seen in Table (3.2). Figures 3.4 (a-e) illustrate the ±15% error between observed and calculated settling velocity for training datapoints, while Figs. 3.5 (a-e) illustrates same for the validations datapoints. The calculated values of settling velocity using equation proposed by Jiménez and Madsen (2003) has been compared with observed settling velocity, as can be seen in Fig. 3.4 (a) and Fig. 3.5 (a). Scatter plot illustrates that the equation proposed by Jiménez and Madsen (2003) shows the slight over prediction of settling velocity for datapoints of Briggs et al. (1962) and Hallermeier (1981). The calculated values of settling velocities using the equation of Wu and Wang (2006) are illustrated in Fig. 3.4 (b) and Fig. 3.5 (b). Many datapoints of Briggs et al. (1962) and some datapoints of Hallermeier (1981) and Cheng (1997) shows equation over predicts the values of settling velocity. The equation proposed by Camenen (2007) illustrates comparatively good agreements with observed

datapoints, as can be seen in Fig. 3.4 (c) and Fig. 3.5 (c). Only few datapoints of Briggs et al. (1962), Hallermeier (1981) and Cheng (1997) are lied out of the ±15% error lines. For predicting the exact value of settling velocity, authors adopted GRG and hybrid GRG-GA approaches. Authors finalized the variables of GRG and hybrid GRG-GA approaches on the basis of previously completed sensitivity analysis on settling velocity. Figures 3.4 (d-e) and 3.5 (d-e) illustrate the comparison between observed and calculated values of settling velocity using GRG and hybrid GRG-GA approaches.

Figures (3.4-3.5) show that the computation of settling velocity using hybrid GRG-GA approach is most consistent as it also shows the least error. GRG approach also shows good agreements with observed values of settling velocity as compared to previously proposed equations. However, some datapoints lied outside the ±15% error lines. Figure 3.6 illustrates the variation of error in percentage with total datapoints (training and validation datapoints) in percentage. Figure 3.6 clearly shows that the 88%, 84%, 76%, 70%, and 66% datasets computed by Hybrid GRG-GA approach, GRG approach, Camenen (2007); Wu and Wang (2006); and Jiménez and Madsen (2003), respectively lies under the 15% error. Similarly, 98%, 92%, 90%, 86% and 84% datapoints lie under the 25% error using Hybrid GRG-GA approach, GRG approach, Camenen (2007); Wu and Wang (2006); and Jiménez and Madsen (2003), respectively. It can be stated that the Hybrid GRG-GA and GRG approaches predict settling velocity with least error, as can be seen in Figs. (3.4-3.6).

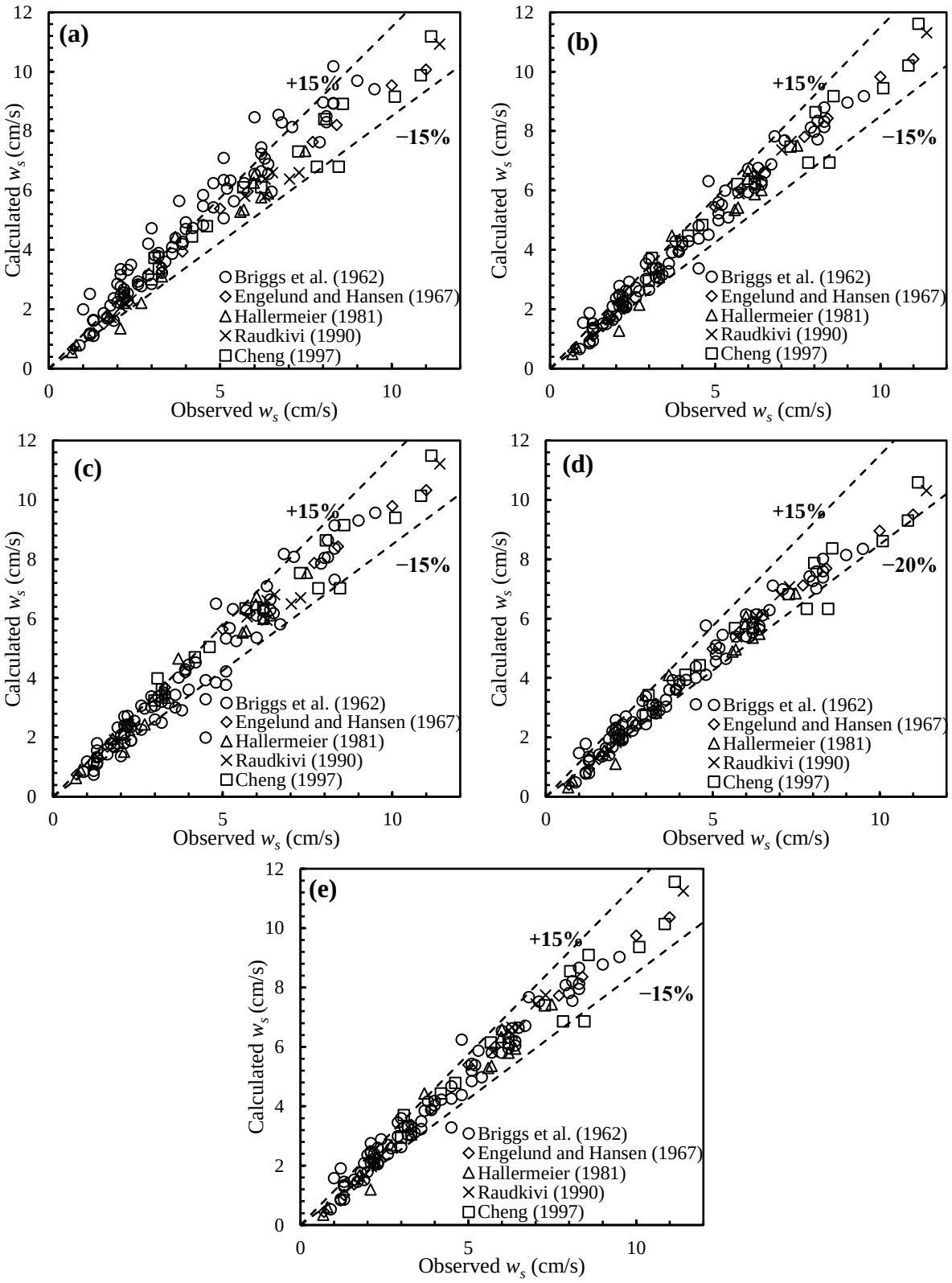

Figure 3. 4 Observed and calculated settling velocity using training datasets as per; (a) Jiménez and Madsen (2003), (b) Wu and Wang (2006), (c) Camenen (2007), (d) GRG approach, and (e) Hybrid GRG-GA approach

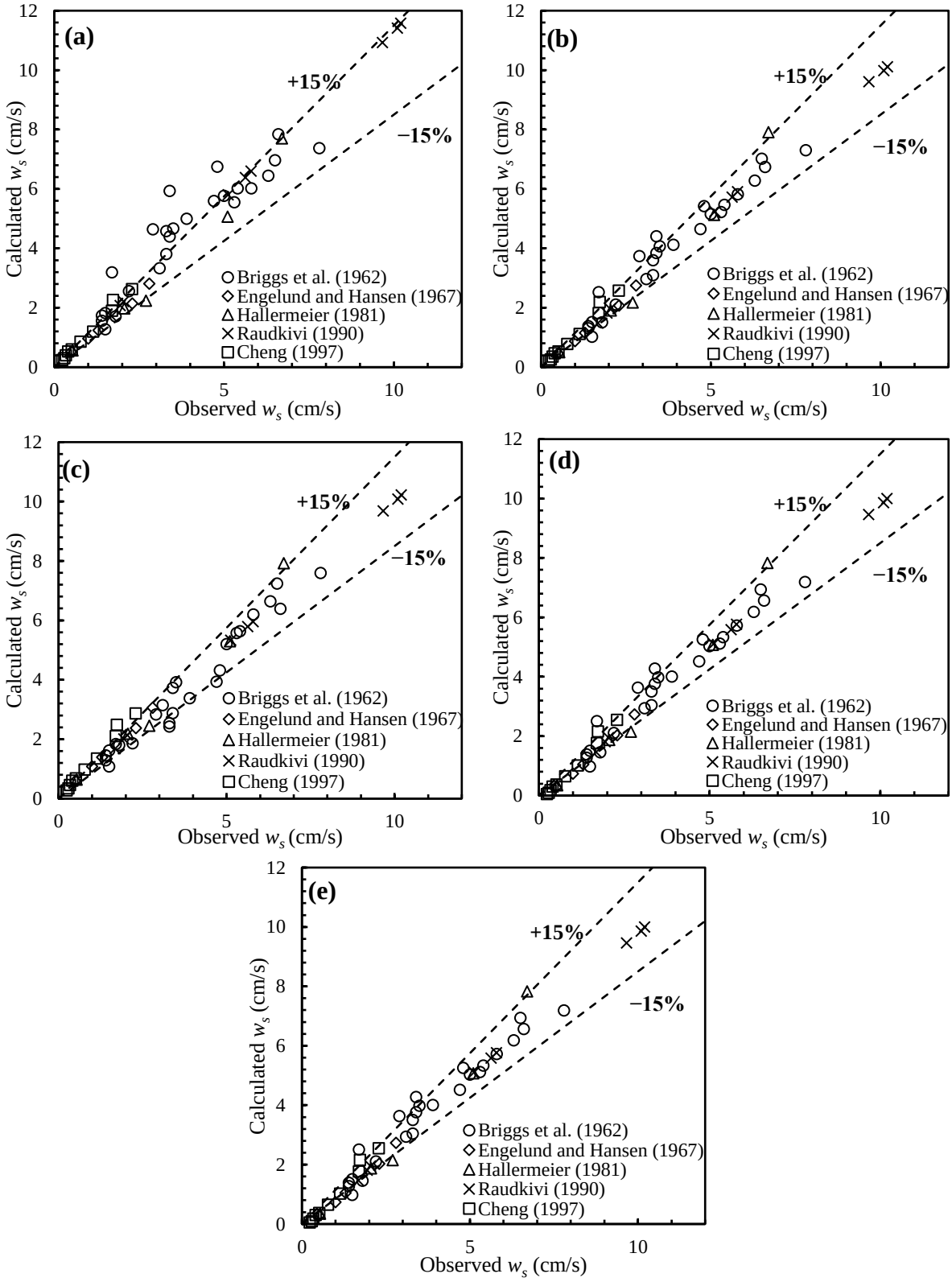

Figure 3. 5 Observed and calculated settling velocity using validation datasets as per; (a) Jiménez and Madsen (2003), (b) Wu and Wang (2006), (c) Camenen (2007), (d) GRG approach, and(e) Hybrid GRG-GA approach

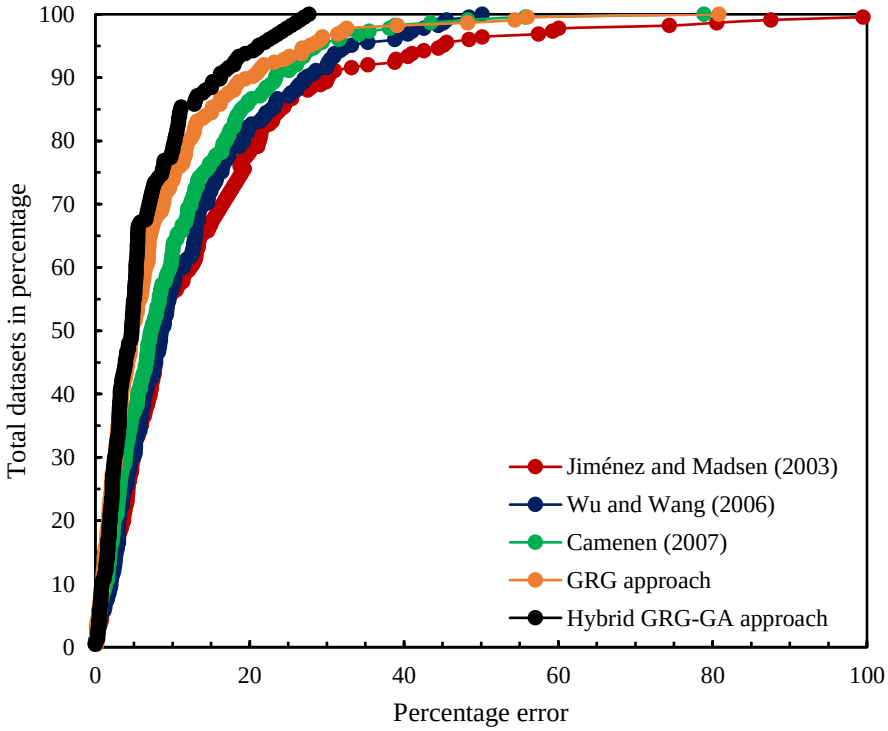

Figure 3. 6 Percentage error vs percentage datasets using Jiménez and Madsen (2003); Wu and Wang (2006); Camenen (2007); GRG approach, and Hybrid GRG-GA approach.

The performance of Hybrid GRG-GA approach and GRG approaches and previously proposed equations was assessed statistically and qualitatively. For statistically assessment NSE, KGE, PBIAS, MAE and R^2 were used. These different indices were explained and formulae were mentioned in the 3.1.4 section of this chapter (i.e., Eqs. 3.12 - 3.16).

The values of performance indices obtained from present work (GRG and hybrid GRG-GA) and previous researchers are shown in Table 3.3. Statistically, equations given by Camenen (2007) shows better agreements than Jiménez and Madsen (2003) and Wu and Wang (2006), as can be seen in Table (3.3) and Fig. (3.6). It may be observed that estimates obtained from Jiménez and Madsen (2003) for settling velocity showed maximum departure from the observed data while the Hybrid GRG-GA provided the most accurate estimates of fall velocity during calibration as well as validation. Among the three equations of fall velocity proposed by previous researchers Wu and Wang (2006) provided the most accurate estimate of the fall velocity. Among the algorithms proposed in the present work Hybrid GRG-GA provided the better estimates as compared to GRG. This shows that application of hybrid optimization techniques can provide more accurate results and can be applied to various problems in water resource engineering and specifically to the complex equations of fluvial mechanics.

Table 3. 3 Values of performance evaluation criteria for different methods

Researcher	Calibration					Validation				
	NSE	KGE	PBIAS	MAE	R^2	NSE	KGE	PBIAS	MAE	R^2
Jimenez and Madsen (2003)	0.954	0.916	11.212	0.727	0.958	0.904	0.805	14.282	0.544	0.962
Wu and Wang (2006)	0.979	0.984	0.083	0.416	0.975	0.981	0.967	2.251	0.282	0.983
Camenen (2007)	0.959	0.958	-2.276	0.608	0.960	0.979	0.974	1.820	0.345	0.970
Present Work (GRG)	0.976	0.869	-8.478	0.673	0.981	0.970	0.908	-7.334	0.365	0.982
Present Work (GRG-GA)	0.995	0.997	-0.159	0.340	0.995	0.982	0.979	-0.403	0.249	0.983

3.3.4 Conclusions

The present study describes the settling velocity phenomenon and deals with the methods for its estimation. Hybrid GRG-GA has been proposed to estimate the fall velocity in the present study. The accuracy of three previously proposed settling velocity equations were also checked in this study both qualitatively and quantitatively based on historical datapoints. The datapoints were divided into training (75%) and testing (25%) to determine the reliability of the obtained results. The NSE, KGE, PBIAS, MAE, R^2 and ± 15% error line were used to compare the settling velocity estimations generated from various approaches. The study's main noteworthy findings are listed below.

- The accuracy of GRG and hybrid GRG-GA based settling velocities, as well as three previously proposed settling velocity equations were analyzed both quantitatively and qualitatively.
- The NSE, KGE, PBIAS, MAE, R^2 and ± 15% error line were used to compare the settling velocity estimations generated from various approaches.

- The hybrid GRG-GA-based settling velocity estimates were more precise than previous empirical equations as well as those obtained through GRG algorithm stand-alone.
- This study highlights that the hybrid approaches have the capability to significantly improve the accuracy of stand-alone algorithms.
- To be more specific, gradient-based and evolutionary algorithms can be hybridized to overcome the problem of obtaining local optimum solution and computation expense involved in the evolutionary algorithms.
- Such combinations of hybrid algorithms can be very useful for modelling various phenomenon associated with water resource engineering and other fields of engineering.

CHAPTER 4

COMPUTATIONAL FLUID DYNAMICS MODEL THEORY

4.1 General

A multiphase flow (two-phase), water (secondary phase) and air (primary phase), were considered in this study. Multiphase flow is the sequential movement of materials in various states or phases. It is a flow of substances with various chemical properties that are still in the same state or phase. In multiphase model concept, there are different types of phases like separated phase, mixed phase and dispersed phase. One or more immiscible fluids in a continuous phase are separated by an interface to form a separated phase, according to the definition. In mixed phase one or more fluid substances (separated and dispersed phases) mixed together. The dispersed phase is defined as the large number of particles are spread in a continuous phase. However, in the multiphase model the flow regimes are classified as bubble flow (bubble flow is defined as the flow of discrete bubbles in continuous fluid flow), slug flow, churn flow, annular flow and dispersed flow (it is defined as two phase flow in which one phase is dispersed into another continuous phase). In ANSYS Fluent, there are four different Euler–Euler based multiphase models available: (1) Volume of Fluid (VOF) model, (2) Mixture model, and (3) Eulerian model (4) Wet steam model. The VOF multiphase model along with stochastic Discrete Phase Models (DPM) were employed in this investigation. This chapter relies on the ANSYS Fluent documentation (ANSYS, 2021).

4.2 Assumptions of the Model

(i) To use coupled stochastic DPM and the VOF model, a sediment concentration of under 10% is assumed (by volume). Controlling the rate of sediment input through the regulator allowed for the incorporation of this assumption into the experiment as well.

(ii) The sediment particles behave independently and do not interfere with one another.

(iii) Although there are sub-models, the second phase is by default thought to be made up of spherical particles.

(iv) The particle diameter is smaller than the grid cell size.

(v) The secondary phase (air) has no density.

(vi) At the free surface and above of it, there is no gauge pressure (assumed as Atmospheric pressure).

4.3 CFD Model for Multiphase Flow

A multiphase flow (two-phase), water (secondary phase) and air (primary phase), were considered in this study. There are currently two methods for computationally predicting multiphase flows in ANSYS Fluent:

(a) The Euler–Lagrange approach (which has been detailed in DPM section), and

(b) the Euler–Euler approach.

The VOF model of the Euler-Euler technique has been used in the present research and is detailed in more depth below.

4.4 Euler–Euler Approach

In the Euler–Euler approach, the distinct phases are treated numerically as no interpenetrating continua. The concept of phasic volume fraction is introduced because the volume of the primary (one) phase cannot be occupied by the secondary phases, and vice versa. These phasic volume fractions are treated as continuous functions of space and time, and their total as 1. Conservation equations for every phase are acquired to obtain a set of equations with identical arrangements for all phases. These equations are solved by incorporating constitutive relations, which are derived from empirical equations or, in the case of particle flows, via the use of kinetic theory.

In ANSYS Fluent, there are four different Euler–Euler based multiphase models available: (1) Volume of Fluid (VOF) model, (2) Mixture model, and (3) Eulerian model (4) Wet steam model.

4.4.1 Volume of Fluid (VOF) Model

A fixed Eulerian mesh is used to monitor the free surface in a VOF multiphase model. The VOF multiphase model is intended to assess the position of the interface between two or more immiscible fluids. Using this technique, the volume fraction of each fluid in each cell throughout the domain can be tracked, and a single set of momentum equations is only shared by the phases. This model can be used to simulate stratified flows, free surface flows/gravity-driven flows/open channel flows, the flow of large bubbles in a liquid, the flow of water after a dam breach, jet breakup modeling, and the steady or transient prediction of any liquid gas interface. This technique only works with pressure-based solvers. The mixture and Eulerian multiphase models are appropriate for flows in which phases mix or separate and discrete phase volume portions exceed 10% by volume in a cell.

The DPM model was chosen to explore the sediment trapping phenomenon of the invert trap because the sediment content in the current study was kept low (i.e., less than 10% by volume). Because the invert trap is used in an open channel with gravity flow (also known as free surface flow), the VOF model was employed in CFD modeling. The open channel flow was modelled using a methodology for the numerical assessment of trap efficiency that was later developed.

The discrete particle trajectories that represent the sediment's movement over time in the invert trap and channel can be tracked using the DPM. In the present study, a VOF model coupled with a DPM that has been explained further is used to simulate sediment movement in an open channel. A 2D CFD analysis has been done to predict the sediment retention ability of an invert trap constructed in an open sewer system using a VOF multiphase model of ANSYS Fluent 2021. Primarily, the effect of size and shape of invert trap on trap efficiency has been evaluated with different flow parameters. The calculated sediment trap efficiency has been related to the laboratory investigations of Mohsin and Kaushal (2017b). In the present study, 2D CFD model results have been validated and compared with the published experimental data of Mohsin and Kaushal (2017b). The geometry of the invert trap having a rectangular chamber with trapezoidal bottom was used to validate the 2D numerical model, which can be used to simulate other invert trap geometries.

The VOF model, along with stochastic DPM, was used in this study and is described in detail as follows:

The VOF model is applicable for multiple immiscible fluids (water and air) when the position of the interface between the fluids, as well as the flow field, is of interest. In the computational cell, a parameter known as the volume fraction of the phase is employed in each phase. The volume fractions of water (secondary phase) and air (primary phase) in CFD (VOF Model) is sum to one in each control volume (cell). The phases share the fields for all variables and properties, which represent volume-averaged values. As a result, depending on the volume fraction values, the variables and properties in a given cell are either representative of water or air, or of a mixture of water and air. In the flow system, the free surface is existing between the flowing water and atmospheric air. The forces of gravity and inertia govern the flow in an open channel. Water and air share a single set of momentum equations in this case, and the volume fraction of water and air in each computational cell is tracked throughout the domain. Figure 4.1 represents the proposed CFD model approach used in the present study.

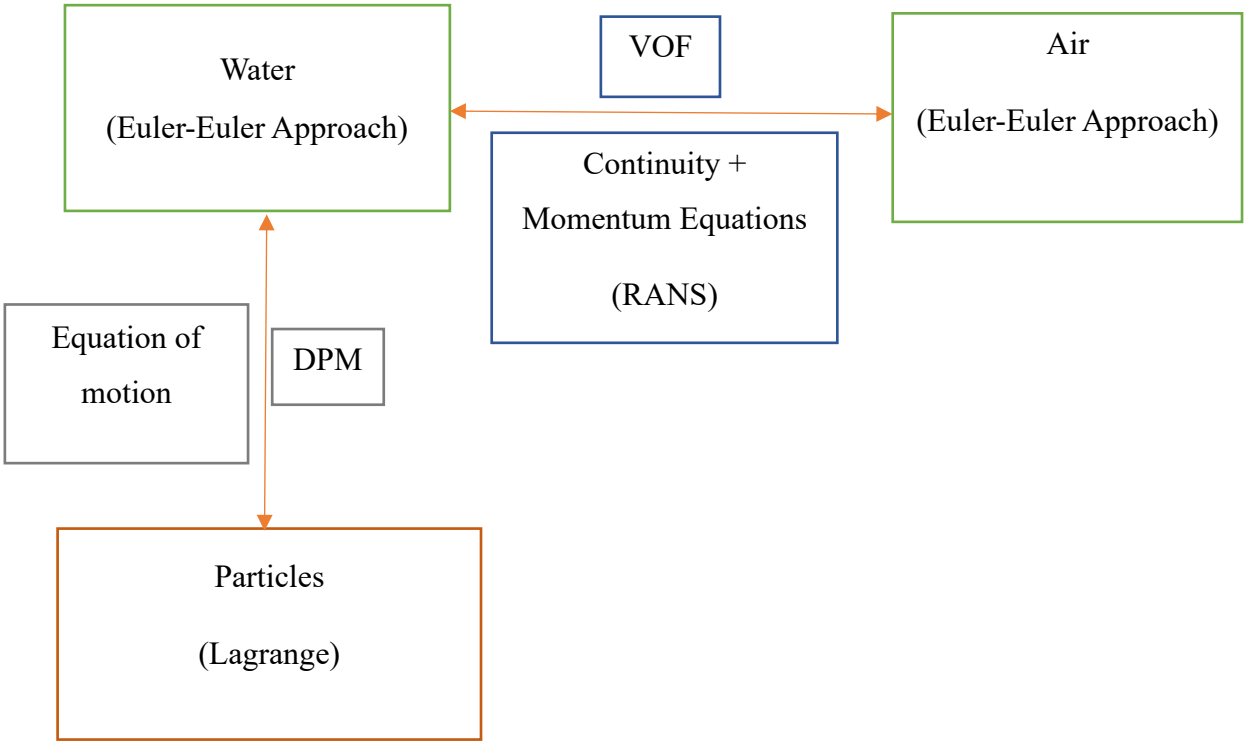

Figure 4. 1 Schematic diagram of the present CFD model approach.

Following are the governing equations (volume fraction and momentum) used in VOF modeling for unsteady open channel flow.

4.4.2 Volume Fraction Equation

The interface between different immiscible fluids is tracked involving continuity equation by monitoring the volume fraction. In computational cells, the secondary phase (water) volume fraction is defined mathematically as

$$\alpha_{2\,=}\ \frac{Volume\ of\ secondary\ phase\ (water)\ in\ the\ cell}{Volume\ of\ the\ cell}$$

Therefore, if

$\alpha_2 = 1$ cell is filled with water

$\alpha_2 = 0$ cell is empty

$0 < \alpha_2 < 1$ cell contains a free surface

Solving the continuity equation for the volume fraction of one phase identifies the interface between phases. This equation has the following form for the water phase;

$$\frac{1}{\rho_p}\left[\frac{\partial}{\partial t}\left(\alpha_p\rho_p\right) + \nabla.\left(\alpha_p\rho_p\vec{u}_p\right) = S_{\alpha_p} + \sum_{s=1}^{n}\left(\dot{m}_{sp} - \dot{m}_{ps}\right)\right] \qquad (3.1)$$

Where $\dot{m}_{sp}$ = mass transfer from phase *p* to phase *s*; $\dot{m}_{ps}$ = mass transfer from phase *s* to phase *p*; and S_{α_2}= source term.

For the primary phase, the volume fraction equation is not solved; instead, it is derived from the following equation.

$$\alpha_1 = 1 - \alpha_2$$

The volume fraction equation can be solved either implicitly or explicitly through time and space discretization.

Implicit scheme

The implicit scheme is suitable for both steady and unsteady simulations. The implicit scheme formula is as follows:

$$\frac{{\alpha_p}^{n+1}{\rho_p}^{n+1}-{\alpha_p}^{n}{\rho_p}^{n}}{\Delta t}V+\sum_f\left({\alpha_{p,f}}^{n+1}U_f^{n+1}{\rho_p}^{n+1}\right)=\left[S_{\alpha_p}+\sum_{s=1}^{n}\left(\dot{m}_{sp}-\dot{m}_{ps}\right)\right]V \quad (3.2)$$

Explicit scheme

For time-sensitive problems, an explicit scheme is used. The volume fraction values in this method are obtained from the previous time step. The explicit scheme formula is as follows:

$$\frac{{\alpha_p}^{n+1}{\rho_p}^{n+1}-{\alpha_p}^{n}{\rho_p}^{n}}{\Delta t}V+\sum_f\left({\alpha_{p,f}}^{n}U_f^{n}{\rho_p}\right)=\left[S_{\alpha_p}+\sum_{s=1}^{n}\left(\dot{m}_{sp}-\dot{m}_{ps}\right)\right]V \quad (3.3)$$

Where,

$n+1$ = index for new (current) time step

n = index for previous time step

$\alpha_{p,f}$ = face value of the p[th] volume fraction, computed from the first or second-order upwind, QUICK, modified HRIC, or CICSAM scheme

V = volume of cell

U_f = volume flux through the face, based on normal velocity

4.4.3 Momentum Equation

The momentum equation, as shown below, is affected by the volume fractions of all phases via the properties like density (ρ) and viscosity (μ).

$$\frac{\partial(\rho u)}{\partial t}+\nabla.(\rho \boldsymbol{uu})=-\nabla p+\rho g+[\mu(\nabla u+\nabla u^T)] \quad (4.4)$$

Where, *p* is the pressure, *u* is the velocity vector, *g* is the acceleration vector due to gravity.

The Reynolds-averaged Navier-Stokes (RANS) equation can be used to transform Eq. 4.4.

The Reynolds- Averaged Navier-Stokes (RANS) equation is solved throughout the domain and the velocity field is shared among the different phases in proportion to their volume fractions.

$$\frac{\partial(\rho u_i)}{\partial t}+\frac{\partial\left(\rho u_i u_j\right)}{\partial x_j}=-\frac{\partial p}{\partial x_i}+\rho g_i+\mu\frac{\partial^2 u_i}{\partial x_j \partial x_j}-\frac{\partial\rho\left(\overline{u_i' u_j'}\right)}{\partial x_j} \quad (4.5)$$

Where p= pressure; u= average velocity; and i and j = 1, 2, and 3. The term $\rho\left(\overline{u_i' u_j'}\right)$ is called Reynolds stresses can be estimated using any turbulence model, such as the Reynolds Stress Model (RSM), the k-ε turbulence model, k-ω turbulence model, and so on.

The presence of the constituent phases in each control volume determines the properties appearing in the transport equations. The volume fraction-averaged density of a two-phase system (water and air) is as follows:

$$\rho = \alpha_w \rho_w + \alpha_a \rho_a$$

4.4.4 Open Channel Flow

Using the VOF model formulation and the open channel boundary condition, ANSYS Fluent 2021 can model open channel flow (e.g., rivers, dams, etc.). These flows are characterised by the presence of a free surface between the flowing fluid and the fluid above it (typically, the atmosphere air). Wave propagation and free surface behaviour become important in such cases. The forces of gravity and inertia govern the flow in general. The flow of drainage systems can be modelled by using the above-mentioned features. The dimensionless parameter known as the Froude Number (F_r) characterises open channel flows and is stated to be the ratio of inertia force to gravitational force.

$$F_r = \frac{U}{\sqrt{gy}} \tag{4.6}$$

Where, U = Average velocity magnitude, g = Acceleration due to gravitational force

y = Characteristic length scale (in this case, the depth of flow)

Eq. 4.6's denominator is the wave's propagation speed. As seen by a fixed observer, the wave speed is defined as

$$U_W = U \pm \sqrt{gy}$$

Open channel flows can be categorized into three distinct groups depending on the Froude number (F_r):

(i) When $F_r < 1$, the flow is said to be 'sub-critical' meaning that disturbances can travel both upstream and downstream. In this case, the flow upstream may be influenced by downstream conditions.

(ii) When $F_r = 1$, the flow is said to be 'critical' meaning that upstream propagating waves remain stationary.

(iii) When $F_r > 1$, the flow is said to be 'super-critical' meaning that disturbances cannot travel upstream. The flow upstream is unaffected by downstream conditions in this case.

4.5 Discrete Phase Model (DPM)

The fluid phase is treated as a continuum while solving the Navier-Stokes equations, whereas the dispersion phase is determined by tracking a large number of particles through the predicted flow field.

4.5.1 Particle Tracking

In the DPM, integrating the differential equations of force balance on the particle yields particle trajectories. The equation for the force balance is as follows:

$$\frac{\partial(u_p)}{\partial t} = F_D(u - u_p) + \frac{g_x(\rho_p - \rho)}{\rho_p} + \frac{1}{2}\frac{\rho}{\rho_p}\frac{\partial(u - u_p)}{\partial t} + u_p\left(\frac{\rho}{\rho_p}\right)\frac{\partial u}{\partial x} \tag{4.7}$$

$$F_D = \frac{18\mu}{\rho_p d_p^2}\frac{C_D Re_p}{24} \tag{4.8}$$

$$Re_p = \frac{\rho d_p|(u - u_p)|}{\mu} \tag{4.9}$$

Where,

$g_x =$ Gravity term, F_D= drag force term

u_p, ρ_p, d_p and Re_p= velocity, density, diameter, and Reynolds number of the particle, respectively

C_D= drag coefficient

4.5.2 Drag Coefficient of Sphere (C_D)

The drag coefficient of a sphere is affected by the flow regime. The below equation gives the drag coefficient for particles with low Reynolds numbers (Re_p < 0.1).

$$C_D = \frac{24}{Re_p} \tag{4.20}$$

The relationship between C_D and Reynolds number is more complicated for $0.1 < Re_p < 50{,}000$. However, for this flow situation Morsi and Alexander (1972) proposed the relationship through Eq. 4.11. The constants α_1, α_2, and α_3 depend on the particle Reynolds number.

$$C_D = \alpha_1 + \frac{\alpha_2}{Re_p} + \frac{\alpha_3}{{Re_p}^2} \tag{4.11}$$

Two of the drag laws available are relevant to this work. The drag-laws are spherical and non-spherical. Because the particle tracking routine in FLUENT implies spherical particles by default, the drag-law of sphere was applied. In the current study, using micro solid spheres, adapting the drag law from spherical to non-spherical had no significant effect on trap efficiency.

4.5.3 Particle Trajectories

Particle trajectories are indeed the calculated paths that a particle takes in a fluid. Eq. (4.7) integration by time yields the particle velocity, u_p, but the u_p can also be expressed as;

$$\frac{\partial x}{\partial t} = u_p \tag{4.12}$$

A pair of ordinary differential Eqs. (4.7) and (4.12) are coupled and Eq. (4.7) can be expressed in the following way:

$$\frac{\partial(u_p)}{\partial t} = \frac{1}{\tau_p}(u - u_p) + a \tag{4.13}$$

Where,

τ_p= particle relaxation time; except for the drag force, the term "a" refers to accelerations caused by all other forces. Therefore, Eqs. (4.12) and (4.13) are solved to predict the particle trajectories.

Continuous phase variables such as velocity, pressure, and stream function can be used to represent the particle trajectory, as can particle variables such as particle residence time, particle ID (i.e., Particulate number), particle velocity, particle sizes, density, particle mass, particle temperature, Re_p, and so on. The particle ID in this study shows that particles near the bed are mostly trapped, while those near the top surface escape.

4.6 CFD Model Setup

In the present study, pressure-based solver has been used with steady-state conditions. The open channel flow was driven by gravity force which results in gravity being enabled in the solution set up; the Operating pressure and density were taken as 101325 Pascals and 1.225 kg/m^3 of air, respectively.

In the numerical modeling, the inlet and outlet boundary conditions were assigned as pressure inlet and pressure outlet, respectively. The top of the channel was given as symmetry boundary, while all the other boundaries were chosen to be a wall and no-slip boundary condition was adapted. The model setup walls were made of Perspex which has a roughness of 0.0000015 m. In the simulation, the initial values of flow velocities were given for different flow depths, as mentioned in Table 3. The coupled scheme was selected for the pressure-velocity coupling with the pseudo-transient formulation. Pressure, Volume fraction and momentum discretization scheme were chosen as PRESTO! And modified HRIC, second-order upwind, respectively. In the present case, most of the flow happened away from the wall boundary. Taking this into consideration, a well-accepted realizable k-ε turbulence model with a scalable wall function was chosen due to its flexibility. The steady-state VOF model with Open-Channel sub-model was chosen for computational modeling along with implicit body force volume fraction scheme. The turbulent intensity and viscosity ratio were taken as 5% and 100 at the inlet and outlet boundary of the channel.

A Discrete phase model (DPM) was used to simulate the trap efficiency of the invert trap by injecting the sediment particles into the flowing water. 100 particles were injected by group injection type at 0.5 m from the inlet of channel and 0.15 m from the top of the channel. Saffman lift force, pressure gradient force and accretion/erosion models were enabled in the solution setup to include the forces acting on the particle. In an actual sense, sediment particles enter into the invert trap and escape from the outlet. The particles that had entered into the invert trap will reach the invert trap bottom and gets deposited there; whereas some of the particles will re-enter the flow and escape from the outlet. DPM offers different boundary conditions,

like reflect, escape, and trap, to reproduce the particle movement in the channel and invert trap. For DPM, inlet of the channel was assigned as reflect boundary condition, whereas outlet as escape boundary condition. The discrete Random Walk Model was selected with ten stochastic tries in the DPM calculation. The particle trap efficiency of the selected geometries has been calculated by Eq. 1.1.

4.6.1 Two-way Coupling

Because the continuous phase influences the dispersed phase and vice - versa, the dispersed phase's influence on the continuous phase is included as well. This two-way coupling is accomplished in ANSYS FLUENT by solving the dispersed phase and continuous phase equations alternately until the solutions in those phases stop changing. When a particle's trajectory is computed, Fluent keeps track of the mass and momentum gained or lost by the particle stream that tries to follow that trajectory, and all these quantities are used in the CFD (VOF Model) Theory's subsequent continuous phase calculations. As a result, a two-way coupling strategy between the continuous and dispersed phases was used in this study.

4.6.2 Turbulence Models

Realizable *k*-*ε* Turbulence Model

Usually, the flow nature in an open channel flow is turbulent. Hence a turbulent modeling has been chosen for the simulation. Reynolds-average approach to turbulence modeling requires that the Reynolds stresses in equations are appropriately modelled to obtain average velocity and pressure field. There are three available models in *k*-*ε* turbulence modeling (standard, renormalized grouped method and realizable *k*-*ε* models). The realizable *k*-*ε* turbulence model has been opted as it is well proven for its superior performance (Mohsin and Kaushal, 2017a, b).

The turbulence kinetic energy, *k*, and its rate of dissipation, *ε*, are obtained from the following transport equations.

$$\frac{\partial(\rho k)}{\partial t}+\frac{\partial(\rho k u_i)}{\partial x_i}=\frac{\partial}{\partial x_j}\left[\left(\mu+\frac{\mu_t}{\sigma_k}\right)\frac{\partial k}{\partial x_j}\right]+G_k+G_b-\rho\varepsilon-Y_M+S_k \qquad (4.14)$$

And

$$\frac{\partial(\rho\varepsilon)}{\partial t}+\frac{\partial(\rho\varepsilon u_i)}{\partial x_i} = \frac{\partial}{\partial x_j}\left[\left(\mu+\frac{\mu_t}{\sigma_\varepsilon}\right)\frac{\partial\varepsilon}{\partial x_j}\right]+\rho C_1 S_\varepsilon+C_{1\varepsilon}\frac{\varepsilon}{k}-C_{3\varepsilon}G_b-\rho C_2\frac{\varepsilon^2}{k+\sqrt{\upsilon\varepsilon}}+S_\varepsilon \quad (4.15)$$

In these equations,

G_k = turbulence kinetic energy generation related to mean velocity gradients, G_b = turbulence kinetic energy generation related to buoyancy, Y_M = contribution of the fluctuating dilatation in compressible turbulence to the overall dissipation rate, $C_{1\varepsilon}, C_{2\varepsilon}\ and\ C_{3\varepsilon}$ are the model constants and σ_k, σ_ε are the Prandtl numbers for k and ε respectively, S_k, S_ε are source terms(=0 in this case), $C_1 = max(0.43, \eta/(\eta+5))$;η=Sk/$\varepsilon$; $S = \sqrt{2S_{ij}S_{ij}}$

Turbulent (eddy) viscosity, $\mu_t = \rho C_\mu \frac{k^2}{\varepsilon}$ (4.16)

4.6.3 Near Wall Treatment

The existence of walls has a notable effect on turbulent flows. It's apparent that the no-slip condition at the wall influences the average velocity field. Yet, the wall's presence causes substantial changes in turbulence. The turbulence near the wall is decreased due to viscous damping of tangential velocity fluctuations and kinematic blocking of normal fluctuations. However, as you move away from the wall's near-edge region, the turbulence rapidly increases because of the growth of turbulence kinetic energy caused by significant mean velocity gradients.

Near-wall modeling plays a crucial role in the accuracy of numerical solutions because walls are the primary cause of mean vorticity and turbulence. Since the solution variables have significant gradients in the near-wall area and the momentum and scalar transports are most intense there, the faithful representation of flow in this region determines the accuracy of predictions for wall-bounded turbulent flow.

There have traditionally been two approaches to modeling the near-wall region can be shown in Fig. 4.2. The approaches are, 1) Wall functions and 2) near-wall modeling. The viscosity-affected inner region (viscous sublayer and buffer layer) is not resolved in one approach. To bridge the viscosity-affected region between the wall and the fully turbulent region, semi-empirical formulas known as "wall functions" are used. The use of wall functions eliminates the need to modify turbulence models to account for the wall's presence. In near wall modeling approach, the modeling techniques are enhanced so that the viscosity-affected region, including the viscous sublayer, can be resolved with a mesh all the way to the wall.

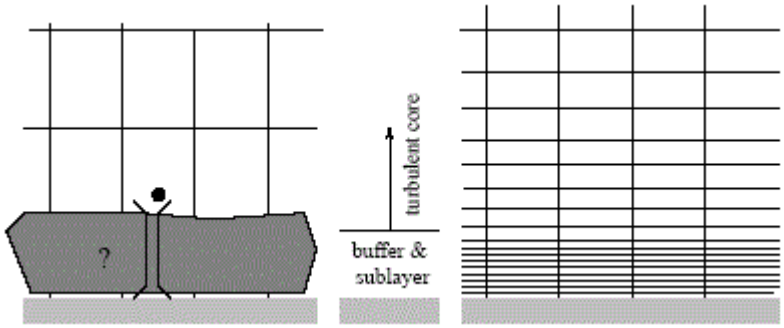

Figure 4. 2 Schematic diagram of Wall function and Near wall modeling approaches.

Scalable Wall Function

Scalable Wall Functions are a type of wall treatment used in the Ansys Fluent computational fluid dynamics (CFD) software to accurately model turbulent flows near walls. This wall treatment is based on the logarithmic wall function, which is an analytical solution used to model turbulent flows near walls. The Scalable Wall Functions allow for a more accurate and efficient computation of turbulent flows, making them an important component of CFD simulations.

The Scalable Wall Functions are based on the assumption that the velocity profile in the near-wall region can be expressed as a logarithmic function with a variable coefficient. This coefficient is determined by the local Reynolds number, which is a measure of the ratio of inertial to viscous forces in the flow. The Scalable Wall Functions also account for variations in the wall-normal direction to provide a more accurate representation of the velocity profile near the wall. The Scalable Wall Functions allow for a more efficient and accurate computation of turbulent flows, making them a popular choice for CFD simulations.

The standard wall functions in ANSYS Fluent are in line with the work of Launder and Spalding and are most often utilized in industrial flows. The basic logarithmic law for mean velocity is stated as

$$U^* = \frac{1}{K}\ln(Ey^*) \tag{4.17}$$

Where, U^* is the dimensionless velocity.

$$U^* = \frac{U_M C_\mu^{1/4} k_M^{1/2}}{\tau_w/\rho} \tag{4.18}$$

$$y^* = \frac{\rho C_\mu^{1/4} k_M^{1/2} y_M}{\mu} \tag{4.19}$$

y^* is the dimensionless distance from the wall boundary.

and

K = von Kármán constant (= 0.4187),

E = empirical constant (= 9.793),

U_M = mean velocity of the fluid at the wall-adjacent cell centroid, M

k_M = turbulence kinetic energy at the wall-adjacent cell centroid, M

y_M = distance from the centroid of the wall-adjacent cell to the wall,

μ = dynamic viscosity of the fluid.

Scalable wall functions prevent standard wall functions from deteriorating under grid refinement below $y^* < 11$. These wall functions yield consistent results for grids of any refinement level. The standard wall functions are identical for grids coarser than $y^* > 11$. Scalable wall functions are intended to force the use of the log law in connection with the standard wall functions approach. This is accomplished by inserting a limiter into the y* calculations such that

$$\widetilde{y^*} = \max\ (y^*, y^*_{limit}) \tag{4.20}$$

Where y^*_{limit} =11.225. The application of Eq. 4.20 in the context of the model of scalable wall functions is reasonable: the y* equation employed in any standard wall function formula is replaced by $\widetilde{y^*}$.

4.6.4 Surface Tension and Wall Adhesion

The effects of surface tension along the interface between each pair of phases can also be included in the VOF model. The model can be improved by specifying the contact angles between the phases and walls. The significance of surface tension effects is determined by two dimensionless quantities: the Reynolds number, *Re*, and the capillary number, *Ca*; or the Reynolds number, *Re*, and the Weber number, *We*.

For $Re \ll 1$, the quantity of interest is the capillary number: $Ca = \frac{\mu U}{\sigma}$ and for $Re \gg 1$, the quantity of interest is the Weber number: $We = \frac{\rho L U^2}{\sigma}$. Where U is the free-stream velocity. Surface tension effects can be neglected if $Ca \gg 1$ or $We \gg 1$. In this study, *Re* is greater than one, and *We* is also greater than one. As a result, the surface tension effect was ignored. Other parameters were set to their default values.

4.6.5 Grid Generation

The generation of grids has a significant impact on model accuracy. When creating high-quality CFD grids, many factors must be taken into account. A structured mesh in the wall-normal direction is strongly advisable for wall-bounded flows. To avoid limiting the growth of the boundary layer, the structured portion of the mesh should cover the whole boundary layer and enhance beyond the boundary layer thickness. However, these are not specific requirements for wall boundary layer simulations, but rather guidelines for wall boundary layer simulations.

In fact, it's more essential to make sure that the boundary layer is sufficiently covered with cells than to meet a specific y* criterion. When using wall functions, it is critical to avoid meshes with y*. values less than 30, as the wall shear stress and heat transfer may suffer significantly under such conditions.

4.6.6 Grid Quality

The orthogonal quality, aspect ratio, and skewness of the grid all have a major influence on the precision of the CFD results.

(a) Orthogonal quality

To determine a cell's quality, you can compute various vectors such as the distance from the cell's center to each of its faces, the area vector of each face, and the distance from the cell's center to the centers of neighboring cells. A cell's orthogonality can be evaluated using a metric where values closer to 1 indicate better quality, and values closer to 0 indicate poorer quality. It is generally recommended that all cell types have an orthogonal quality greater than 0.01.

(b) Aspect ratio

It is a measurement of the cell's stretching. In general, it is best to avoid abrupt and substantial changes in cell aspect ratios in regions that have significant changes or strong gradients in the flow field.

(c) Skewness

This refers to the difference in form between a cell and an equilateral cell that holds the same volume. If a cell is extremely distorted, it can negatively affect precision and hinder the resolution process. For instance, quadrilateral meshes should ideally have angles at their vertices near 90 degrees, while triangular meshes ought to have angles near 60 degrees, and all angles should be less than 90 degrees.

CHAPTER 5

TWO DIMENSIONAL CFD MODELING AND SIMULATIONS

5.1 General

It has been observed from the literature, the extensive experimental analysis was performed to determine the trap efficiency of the invert trap for varying flow, slot size, and particle parameters. Because the primary objective of this study is to replace experimentation with a desirable CFD model to perform simulation studies to evaluate the efficiency of a proposed invert trap in the future without performing experimentation. The current chapter includes a 2D CFD (Coupled VOF and DPM model) simulation of flow in an open rectangular channel placed with an invert trap at the bottom of the channel and its validation with experimental results (Mohsin and Kaushal 2017b). Chapter 3 outlined the fundamental principles of CFD modeling.

Computational fluid dynamics (CFD) is a branch of fluid mechanics that uses numerical analysis and data structures to analyse and solve problems that involve fluid flows. Computers are used to perform the calculations required to simulate the interaction of liquids and gases with surfaces defined by boundary conditions. With high-speed supercomputers, better solutions can be achieved. There are various commercial CFD software tools available today, and they all utilise the same fundamental fluid flow mathematics. Most commercial CFD tools include several broad turbulence models, as well as advanced grid generation and data visualisation facilities. The CFD software, ANSYS Fluent 2021 Student version, was used in this study.

The sediment transport and trap efficiency aspects of the simulation methodology was aimed to be accomplished using the particle tracking approach available in ANSYS FLUENT. The particle tracking technique requires a modelled flow field as input data. The flow field is simulated by using the VOF multi-phase model and the discrete phase model (DPM) predicts the sediment movement in the channel as well as in the invert trap by taking a calculated flow field as input.

Commercial CFD software is now used to address an ever-expanding range of engineering applications. There is no guarantee, however, that the simulation results will be

precise or meaningful. This is determined by a number of interconnected factors, including grid consideration, turbulence analysis options, and the way the model boundaries are characterized in 2D CFD (VOF) Modeling. As a result, the modeling approach used for each unique application must be validated and customized. Turbulence modeling and mesh density were deemed to be critical considerations in the case of the invert trap.

5.2 Source of Data

5.2.1 Experimental Setup

In the present study, CFD model results have been validated and compared with the published experimental data of Mohsin and Kaushal (2017b). The geometry of the invert trap having a rectangular chamber with trapezoidal bottom was used to validate the numerical model, which can be used to simulate the other invert trap geometries. The experimental setup and invert trap geometry of Mohsin and Kaushal (2017b) have been shown in Fig. 5.1 and 5.2.

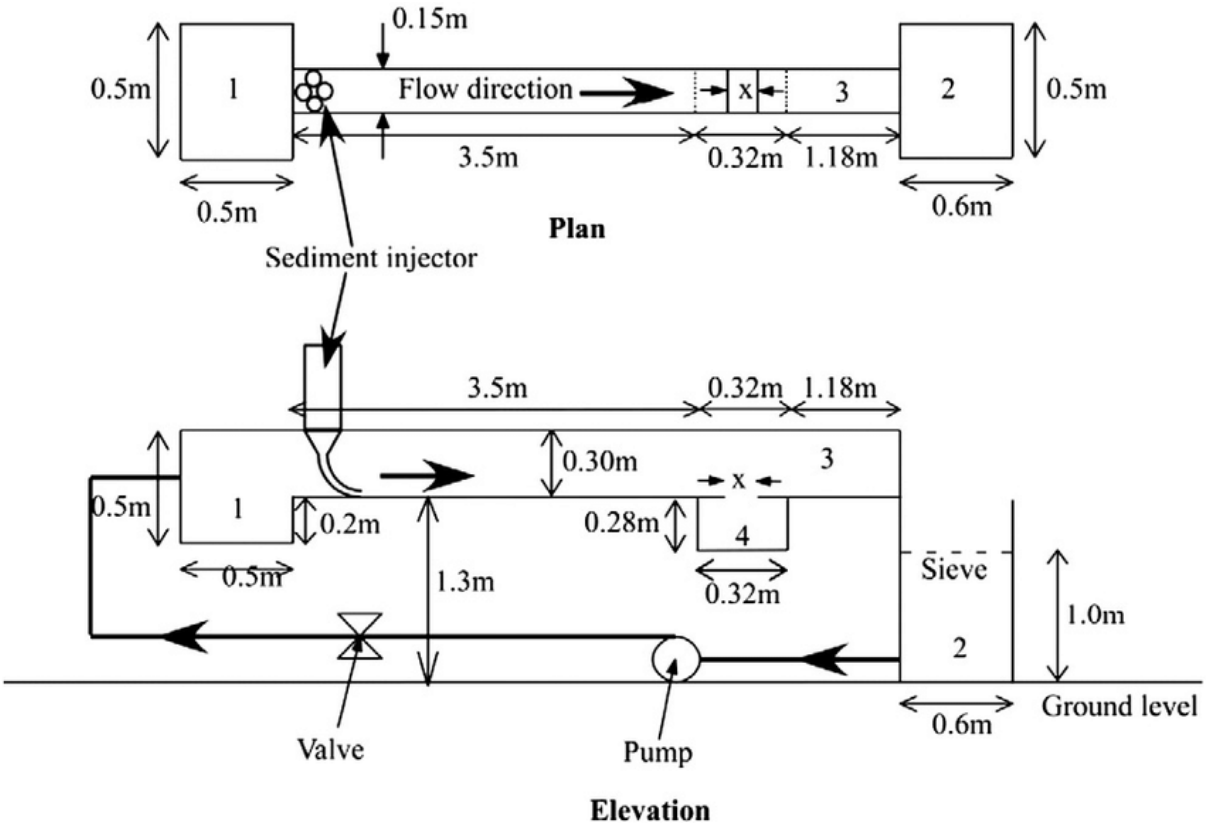

Figure 5. 1 Schematic diagram of plan and elevation of experimental setup

(Source: Mohsin and Kaushal, 2017b)

5.2.2 Dimensions of Laboratory Channel

A rectangular chamber with a trapezoidal base has been used for this study as the most efficient geometry of the invert trap (Kaushal et al., 2012). Figure 5.1 illustrates the sketch view of experimental setup with invert trap that has been taken from the Mohsin and Kaushal, 2017b. The dimension of the channel was 5.0 m long,0.15 m wide, and 0.20 m deep, respectively. The invert trap was placed at 3.5 m from the inlet of the channel. This invert trap had a top and bottom length of 0.32 m and 0.16m, respectively. Trapezoidal and rectangular sections of the invert trap were 0.08 m and 0.2 m high, respectively.

5.2.3 Particle Trap Efficiency

For given characteristics of the sediment particle, the particle trap efficiency (η) is defined as

$$\eta(\%) = \frac{N_T}{N_I} \times 100 \tag{5.3}$$

where N_T is the total number or mass of the sediments that are retained inside the invert trap chamber, and N_I is the total number or mass of the sediments that are injected into the channel (sediments are fed into the channel). The total number of sediment particles injected in this investigation was 100, with a 10 stochastic trail. As a result, sediment trap efficiency (percentage) equals the number of trapped sediment particles divided by ten.

5.2.4 Sedimentation Parameter

Two different approaches mainly classify sediments; one is the source of sediment particles and another mode of transport of sediment particles. Based on the first approach, sediments are classified as wash load and bed material load; according to the next approach, sediments are classified as suspended load, saltation and bed load. Raudkivi (1990) recommended a non-dimensional parameter known as sedimentation parameter (SP) for anticipating the kind of transport of sediments in a channel by including the particle, channel, and flow properties.

$$\text{Sedimentation parameter (SP)} = \frac{w_s}{k\vartheta^*} \tag{5.4}$$

Where, w_s is the particle settling velocity (m/s), ϑ^* is the bed shear velocity and k is the Von-Karman's constant (= 0.4)

The channel's bed shear velocity can be calculated as:

$$\vartheta^* = \sqrt{gRS_o} \tag{5.5}$$

Where,

g = gravitational acceleration, R = hydraulic radius, and S_o = channel bed slope ($6*10^{-3}$).

In chapter 4, different existing equations for settling velocity of particles were examined and new equations were also developed using optimization algorithms. However, the particle settling velocity is an essential parameter to analyse the invert trap efficiency (η). In this present study, the particle settling velocities (w_s) have been calculated using Hybrid GRG-GA based expression (Eq. 4.18). After getting the bed shear velocity (ϑ^*) and particle settling velocity (w_s), the SP can be calculated by using Eq. 5.2 to find out the mode of sediment transport in the channel setup. Classification of sediment transport mode as per the SP given by Raudkivi (1990) is mentioned in Table 5.1.

Table 5. 1 Sedimentation parameter (SP)-based classification of sediment transport modes.

Mode of sediment transport	Sedimentation parameter, SP
Bedload	5-15
Saltation	1.5-5
Suspended load	0-1.5

5.2.5 Materials and Properties

The flow and sediment properties are also taken from Mohsin and Kaushal (2017b) for water. Four flow depths (0.02 m, 0.03 m, 0.04 m, and 0.05 m) were chosen for the current study. In the present numerical modeling, the materials adopted and their properties are discussed in this section.

Flow Properties

The flow and sediment properties are also taken from Mohsin and Kaushal (2017b) for water. Four flow depths (0.02 m, 0.03 m, 0.04 m, and 0.05 m) were chosen for the current study; selection of flow depths based on the wet and dry weather situations of stormwater channels. Table 5.2 contains the flow parameters used for the numerical modeling. Outcomes of the present CFD model for different geometries are validated using Mohsin and Kaushal's (2017b) experimental data.

Table 5. 2 Inlet flow properties for CFD model (b = 1m and S_o= 0.006) (from Mohsin and Kaushal, 2017b).

Flow depth (y) (m)	Flow velocity (U) (m/s)	Mass flow rate ($\boldsymbol{\rho Q = \rho AU}$) (kg/s)	Area ($\boldsymbol{A = by}$)	Wetted Perimeter ($\boldsymbol{P = b + 2y}$) (m)	Hydraulic Radius ($R=A/P$) (m)	$F_r = U/\sqrt{\boldsymbol{gy}}$	Re = $4UR/\boldsymbol{\vartheta}$	Flow regime
0.02	0.622	12.4167	0.02	1.04	0.01923	1.40	47614	Supercritical Turbulent
0.03	0.879	26.3225	0.03	1.06	0.02830	1.62	99033	Supercritical Turbulent
0.04	0.992	39.6086	0.04	1.08	0.03703	1.58	146,260	Supercritical Turbulent
0.05	1.100	54.9010	0.05	1.1	0.04545	1.57	199,043	Supercritical Turbulent

Sediment Properties

Two types of natural sewer solid (NSS) particle properties were directly taken from the literature, but only NSS1 sediment properties were used in the present study. These sediment properties are given in Table 5.3. The sediment density (ρ_p) was determined using the density bottle method, and the diameter of the sediment particles (d_p) was obtained using sieve analysis.

Table 5. 3 Physical properties of the sediment particles.

Sediment material type	Terminology	Diameter range ($\boldsymbol{d_p}$) (mm)	Density ($\boldsymbol{\rho_p}$) (kg/$\boldsymbol{m^3}$)	Settling velocity ($\boldsymbol{w_s}$) (mm/s)	Mean Sedimentation parameter range (SP)
Natural sewer solids	NSS1	0.15-0.30	2,679	14.58-42.26	0.941-2.728
	NSS2	0.30-0.425	2,679	42.26-65.61	2.728-4.235

5.3 Methodology

A CFD analysis has been done to predict the sediment retention ability of an invert trap constructed in an open sewer system using VOF multi-phase model of ANSYS Fluent 2021.

Mainly the effect of size and shape of invert trap on trap efficiency has been evaluated with different flow parameters. The calculated sediment trap efficiency has been related to the laboratory investigations of Mohsin and Kaushal (2017b). In the present study, CFD model results have been validated and compared with the published experimental data of Mohsin and Kaushal (2017b). The geometry of the invert trap having a rectangular chamber with trapezoidal bottom was used to validate the numerical model, which can be used to simulate the other invert trap geometries. The methodology has been mentioned in the Fig. 5.2.

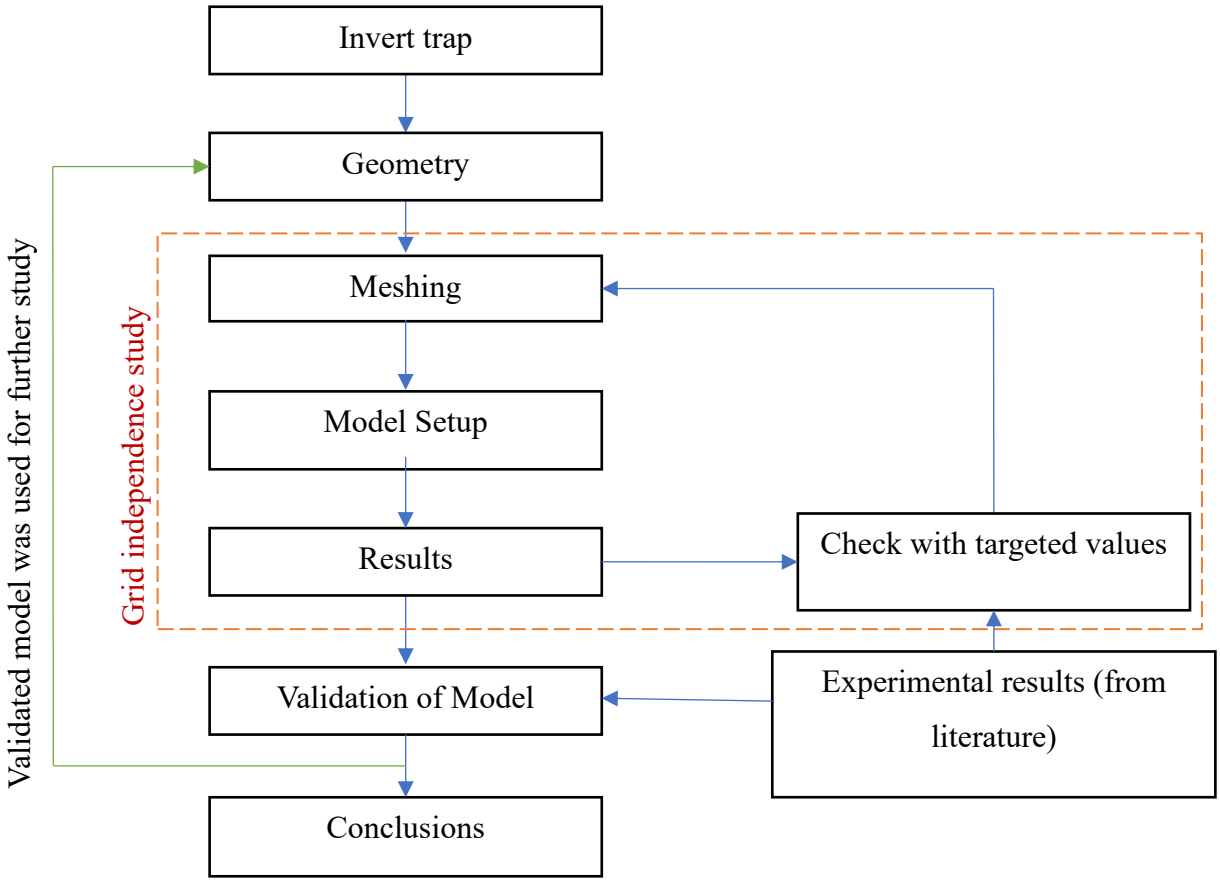

Figure 5. 2 Flow chart for CFD model validation and evaluation of Invert trap geometry.

5.3.1 CFD Model Geometry

This research is made use of a rectangular open channel, which was shown in Fig. 5.3. The length of open channel is 5 m, width is 0.15 m and depth is 0.2 m. Two different slot openings (0.09 m, 0.15 m) are provided at the bottom of the open channel at 3.5m from the inlet of the channel to allow the water into the chamber called invert trap. The invert trap consists of a rectangular top and different shaped bottom, as mentioned above. Initially, the depth of the rectangular portion and bottom portion is 0.2 m, 0.08 m, respectively. There is no change in

length i.e., 0.32 m and width i.e., 0.15 m of the invert trap. The dimensions of open channel and Invert trap were mentioned in the Table 5.4.

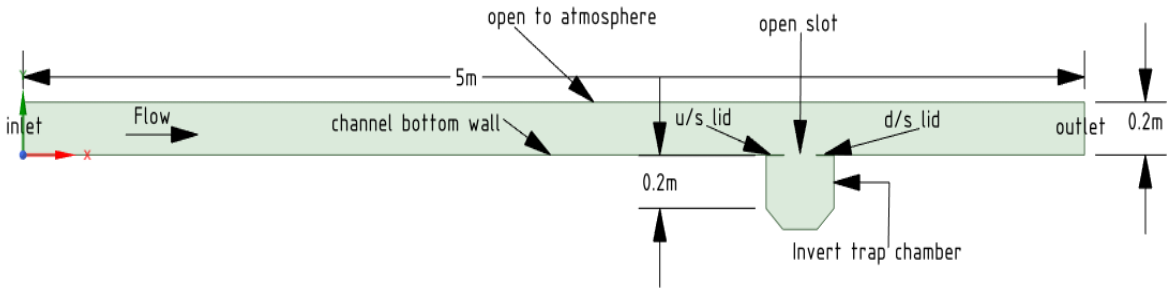

Figure 5. 3 Two-Dimensional geometry of an open channel and an invert trap for CFD study.

Table 5. 4 Physical parameters of open channel and invert trap geometry.

	Open channel parameters	Trap parameters
Length, L (m)	5.0	0.32
Width, W (m)	0.15	0.15
Depth, H (m)	0.2	0.28
Bed slope, S_0	0.006	0.006
Slot openings, Δx (m)	-	0.09 and 0.15

5.3.2 Invert Traps

Figure 5.1 shows the schematic view of used experimental setup. The 2D geometry of this case study has been developed using SpaceClaim of ANSYS Fluent 2021. Different geometries were considered to evaluate the efficiency of settled sediments and shown in Fig. 5.4. A rectangular chamber with a base geometry (BG) of trapezoidal bottom was used to validate the model. Then the shape of invert trap base was changed from trapezoidal to arc shape passing through three points with the same depth (G1). The second geometry was considered as an isosceles triangular base (G2). The last geometry was selected as right triangle with the same depth (G3).

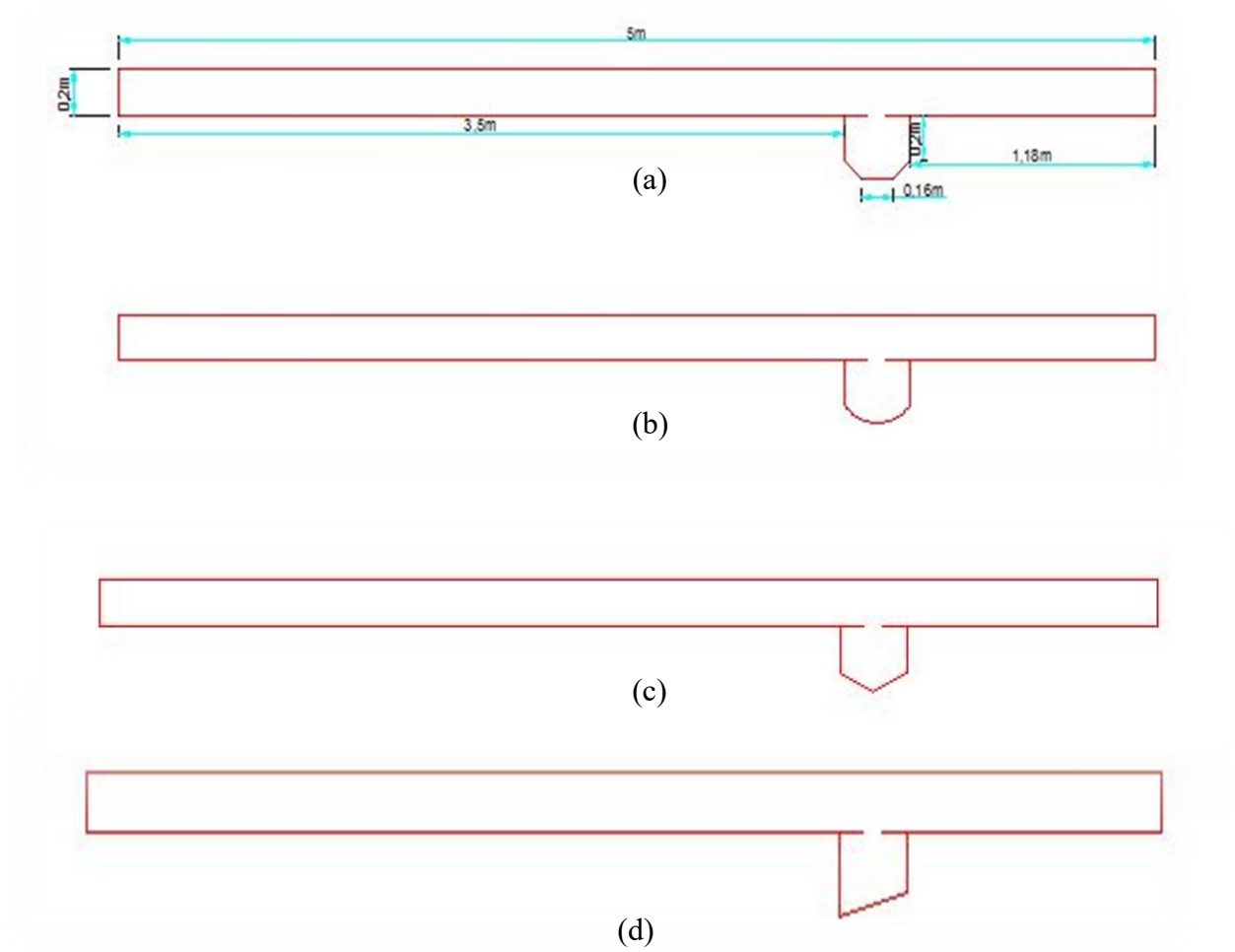

Figure 5. 4 (a-d) Line diagram of proposed Invert trap geometries: (a) Invert trap of rectangular chamber with a base geometry (BG) of trapezoidal bottom; (b) Invert trap of rectangular chamber with a base of arc shape passing through three points (G1); and (c) Invert trap of rectangular chamber with an isosceles triangular base (G2); (d) Invert trap of rectangular chamber with a right triangle base (G3).

The 2D geometry of the chosen channel was divided into small grids using ANSYS Meshing tool in ANSYS Fluent 2021 software. The adaptive structured meshing was chosen to discretize the domain with a quadrilateral cell shape for a better computational efficiency and accuracy. The grid generation of open channel along with Invert trap chamber was shown in Fig. 5.5. For Y^+ = 70 first cell height was determined as 0.0012 m at flow depth of 0.05 m. A grid independence test was also done to optimize the grid size by aiming the mass flow rate at the inlet of the channel; in this case, the grid size has been calculated to be 0.002 m. To resolve the flow field near to the boundary, three inflation layers have been incorporated with the first cell height of 0.0012 m. Table 5.5 is illustrates the quality of mesh adopted for the numerical simulation of flow and sediment deposition in an open channel.

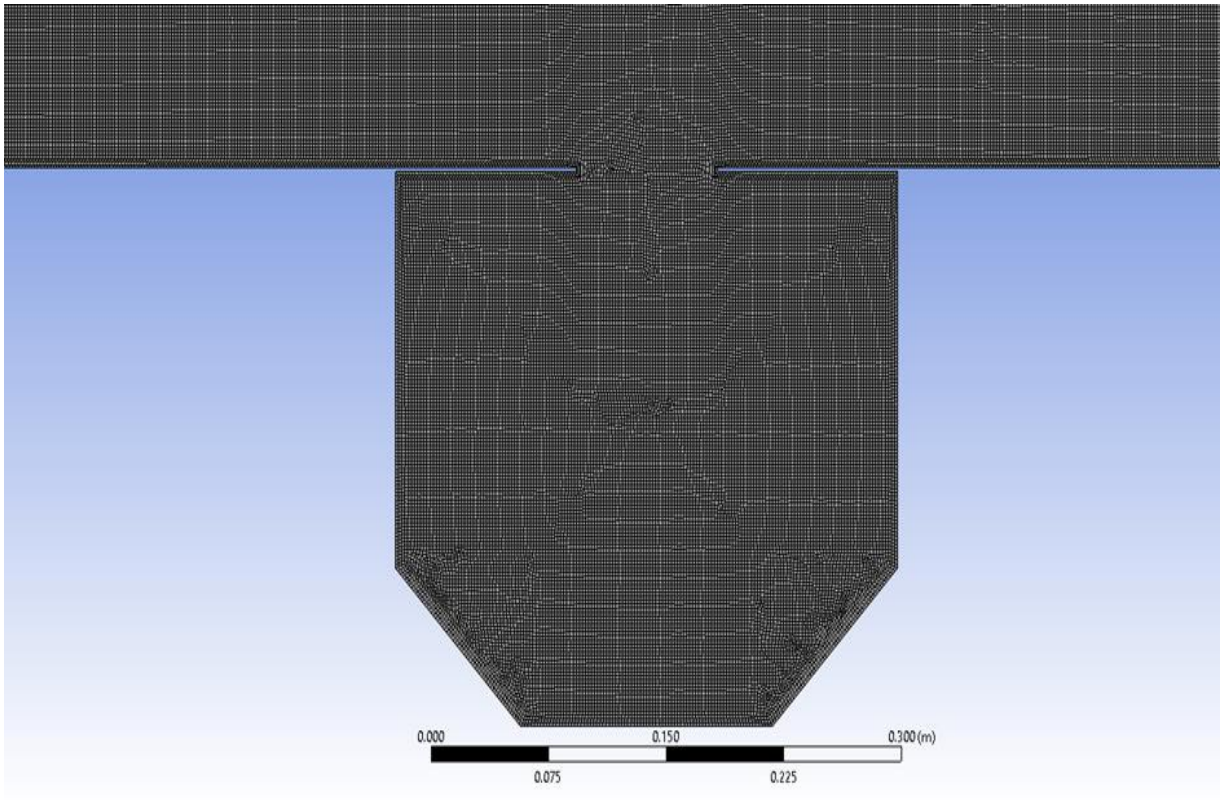

Figure 5. 5 Generation of Mesh of Invert Trap and Channel.

Open channel flow is a gravity driven flow. In the present study, sloped channel (S_o = 0.006) has been taken in the analysis of sediment trap efficiency of invert trap. The gravity term has been resolved into components with respect to slope of the channel. For CFD modeling, to incorporate the gravity, firstly, the gravity should be enabled and the x and y components of gravitational acceleration have been entered in the model setup.

Table 5. 5 Two-dimensional mesh quality details

Mesh Details		
Element shape	Quadrilaterals, Triangles	
Element size	0.002m	
Mesh Quality	Mesh Metric - Orthogonal Quality	
	Min.	0.680
	Max.	1
	Avg.	0.999
No. of Elements	274224	

5.4 CFD Model Setup

The 2D geometry of this case study has been developed using SpaceClaim of ANSYS Fluent 2021. The 2D geometry of the chosen channel was divided into small grids using ANSYS Meshing tool in ANSYS Fluent 2021 software. In the present study, pressure-based solver has been used with steady-state conditions. In the numerical modeling, the inlet and outlet boundary conditions were assigned as pressure inlet and pressure outlet, respectively. The top of the channel was given as symmetry boundary, while all the other boundaries were chosen to be a wall and no-slip boundary condition was adapted. The steady-state VOF model with Open-Channel sub-model was chosen for computational modeling along with implicit body force volume fraction scheme. A Discrete phase model (DPM) was used to simulate the trap efficiency of the invert trap by injecting the sediment particles into the flowing water. 100 particles were injected by group injection type at 0.5 m from the inlet of channel and 0.15 m from the top of the channel. Saffman lift force, pressure gradient force and accretion/erosion models were enabled in the solution setup to include the forces acting on the particle. In the open channel flow, solution convergence can be monitored by observing the residual of the variables. In the present study, along with residual monitoring, significant parameter monitoring has been done, i.e., the difference in mass flow rate at inlet and outlet of the channel.

5.4.1 Boundary Conditions

In the present study, pressure-based solver has been used with steady-state conditions. The open channel flow was driven by gravity force which results in gravity being enabled in the solution set up; the Operating pressure and density were taken as 101325 Pascals and 1.225 kg/m^3 of air, respectively.

In the numerical modeling, the inlet and outlet boundary conditions were assigned as pressure inlet and pressure outlet, respectively. The top of the channel was given as symmetry boundary, while all the other boundaries were chosen to be a wall and no-slip boundary condition was adapted. The model setup walls were made of Perspex which has a roughness of 0.0000015m. In the simulation, the initial values of flow velocities were given for different flow depths, as mentioned in Table 3. The coupled scheme was selected for the pressure-velocity coupling with the pseudo-transient formulation. Pressure, Volume fraction and momentum discretization scheme were chosen as PRESTO! And modified HRIC, second-order upwind, respectively. In the present case, most of the flow happened away from the wall boundary. Taking this into consideration, a well-accepted realizable k-ϵ turbulence model with a scalable wall function was chosen due to its flexibility. The steady-state VOF model with Open-Channel sub-model was chosen for computational modeling along with implicit body force volume fraction scheme. The turbulent intensity and viscosity ratio were taken as 5% and 100 at the inlet and outlet boundary of the channel.

A Discrete phase model (DPM) was used to simulate the trap efficiency of the invert trap by injecting the sediment particles into the flowing water. 100 particles were injected by group injection type at 0.5 m from the inlet of channel and 0.15m from the top of the channel. Saffman lift force, pressure gradient force and accretion/erosion models were enabled in the solution setup to include the forces acting on the particle. In an actual sense, sediment particles enter into the invert trap and escape from the outlet. The particles that had entered into the invert trap will reach the invert trap bottom and gets deposited there; whereas some of the particles will re-enter the flow and escape from the outlet. DPM offers different boundary conditions, like reflect, escape, and trap, to reproduce the particle movement in the channel and invert trap. For DPM, inlet of the channel was assigned as reflect boundary condition, whereas outlet as escape boundary condition. The discrete Random Walk Model was selected with ten stochastic tries in the DPM calculation. The particle trap efficiency of the selected geometries has been calculated by Eq. 5.1.

5.4.2 Convergence Criterion

Setting up a convergence criterion for a VOF model in an open-channel simulation is critical. In the open channel flow, solution convergence can be monitored by observing the residual of the variables. In the present study, along with residual monitoring, significant parameter monitoring has been done, i.e., the difference in mass flow rate at inlet and outlet of the channel. The model calculations were stopped automatically when the difference in mass flow rate is approximately zero. To avoid early convergence of the solution, the *y* velocity residual monitor was set as 10^{-7} and others were set as default values (ANSYS Fluent, 2021). The mass balance of water at solution convergence with flow depth 5 cm was shown in Table 5.6. The water volume fraction of channel flow at solution convergence was shown in Fig. 5.6.

Table 5. 6 Mass Balance of water at Convergence (for y = 5cm and Δx = 9cm)

Item	Mass flow rate(kg/s) at		Net
	Channel Inlet	Channel Outlet	
2D-VOF	54.99487	-54.99390	0.00097
Theoretical	54.9010	-	-

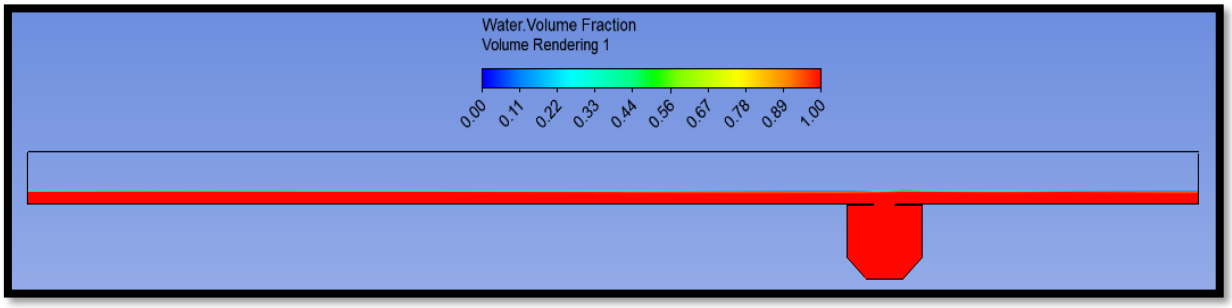

Figure 5. 6 Volume fraction of water in the channel after convergence.

5.5 Results and Discussion

In the present study, a VOF multiphase model with realizable *k-ε* turbulence and DPM models were utilized to simulate trap efficiency, flow tracking, particle trajectory, pressure and velocity contours, and formation of vortex zones inside the invert trap geometry, as explained in the following sub-sections.

5.5.1 Validation of 2D CFD Model

The validation of model was done with 2D CFD results of base geometry and experimental results of Mohsin and Kaushal (2017b). Sediment trap efficiency of base geometry was predicted with VOF multiphase model along with the DPM model. In this case, four different flow depths (2 cm, 3 cm, 4 cm, and 5 cm) and two different slot openings (9 cm and15 cm) were used for the numerical modeling. The velocity contours and particle trajectory of invert trap with base geometry were shown in Fig. 5.8 and Fig. 5.14, respectively. Sediment retention efficiency was predicted by CFD model and validated with laboratory investigation of Mohsin and Kaushal (2017b). It was observed that numerical model shows good agreements with experimental data with less than 10% error. The comparison of results is shown in Table 5.7.

Table 5. 7 Validation of 2D CFD model with experimental (Mohsin and Kaushal 2017b) results for NSS1 particles.

Geometry	y (cm)	U (m/s)	Δx (cm)	Mohsin and Kaushal (2017) Exp. η (%)	Mohsin and Kaushal (2017) 2D CFD η (%)	Present study 2D CFD η (%)	Error (%)
Base Geometry	2	0.622	9	85.35	78.06	82.1	3.25
			15	89.35	88.48	87.3	2.05
	3	0.879	9	70.9	69.48	73.6	-2.7
			15	79.05	73.4	78	1.05
	4	0.992	9	62.35	64.86	64.7	-2.35
			15	66.9	68.88	68.4	-1.5
	5	1.1	9	59.25	61.86	61.5	-2.25
			15	61.6	64.5	63.1	-1.5
						MAPE	2.94

(a) **(b)** **(c)**

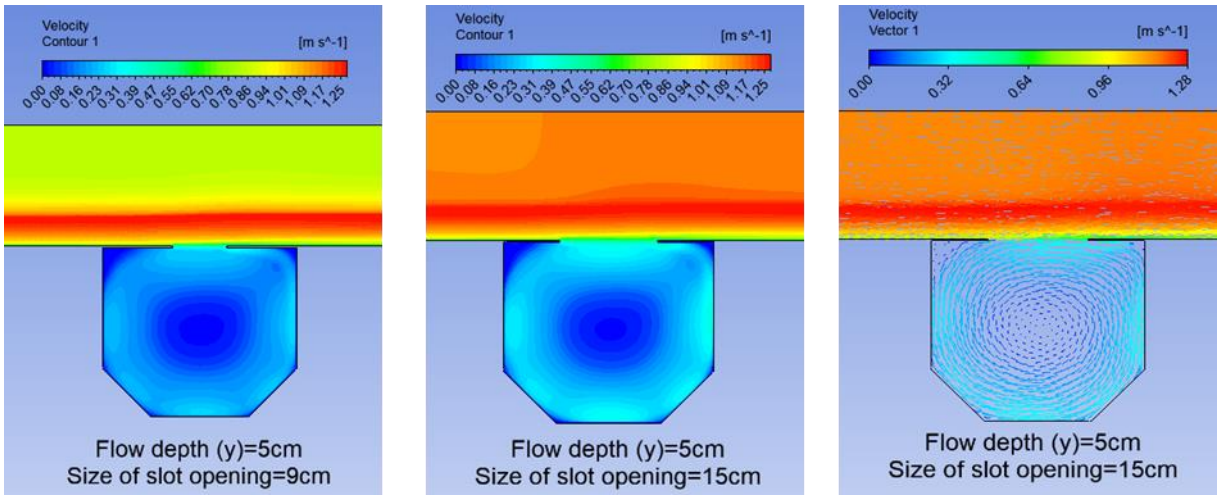

Figure 5. 7 2D predicted velocity contours and velocity vector of base geometry (BG) coloured by velocity magnitude for a flow depth of 5 cm: (a) 2D velocity contours of base geometry (BG) with slot opening, Δx = 9 cm; (b) 2D velocity contours of base geometry (BG) with slot opening, Δx = 15 cm; and (c) 2D velocity vector of base geometry (BG) with slot opening, Δx =15 cm.

The scatter plot has been made to observe the validation of 2D-CFD model predicted results with the experimental results as shown in Figure 5.8. The present 2D-CFD model has been well validated with experimental results with the coefficient of determination (R^2) of 0.99.

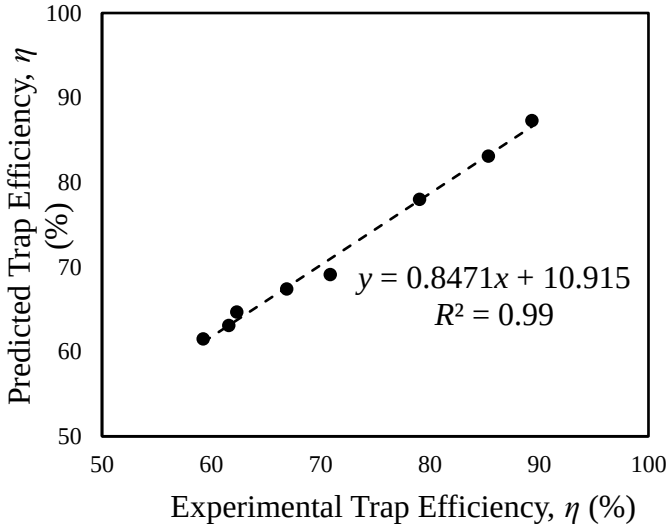

Figure 5. 8 Validation of 2D CFD model using Mohsin and Kaushal (2017b) experimental data.

5.5.2 Analysis of the Effect of Invert Trap Geometry on Sediment Retention Efficiency

(i) Velocity distribution in an Invert trap

The velocity contours for varying flow depths were simulated using VOF Model of ANSYS Fluent 2021. The velocity contours of the simulation had low-velocity zones at the centre of any geometry of Invert trap. These low-velocity zones were responsible for the settlement of sediments in trap chambers. It was observed that the low velocity zone increases with the decrease in flow depth. From the velocity contours, it has been noticed that the increase in the slot opening size of the Invert trap decreases the low-velocity zone. The geometry of the trap determines the change in velocity.

In general, the velocity loss for the curved surfaces is less as compared to the wedged surfaces. The simulation resulted in higher velocity contour for G1 (curved) as seen in Fig. 5.9, where the wedge-shaped trap (BG, G2 and G3) had relatively low-velocity contour profiles. 2D predicted velocity contours and velocity vector of Geometry (G2) coloured by velocity magnitude for a flow depth of 5 cm is shown in Fig. (5.10). The G3 in Figs. (5.11-5.12) shows low-velocity zone at the corner, which is efficient in trapping the sediment. The velocity vector for this geometry infers the same results as velocity contours.

(ii) Influence of depth of flow on trap efficiency

From this present study, the trap efficiency of the invert trap decreases with the increase in flow depth for all the numerically estimated geometries. It was observed that an increase in flow depth increases the flow velocity causing more turbulence. The increased turbulence initiates re-entrainment of the settled particles lifted above the channel bed, travels with the flow, and escapes from the outlet. However, only the heavier particles settle in the Invert trap. The influence of the depth of flow and trap efficiency for various geometries is shown in Table 5.8.

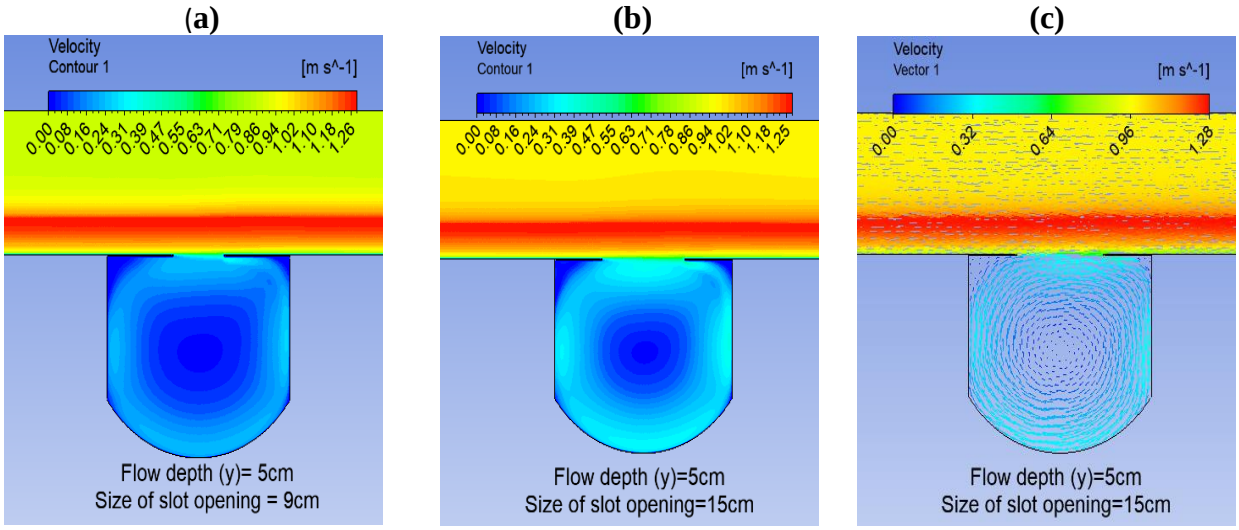

Figure 5. 9 2D predicted velocity contours and velocity vector of Geometry 1 (G1) coloured by velocity magnitude for a flow depth of 5 cm: (a) 2D velocity contours of G1 with slot opening, Δx = 9 cm; (b) 2D velocity contours of G1 with slot opening, Δx =15 cm; and (c) 2D velocity vector of G1 with slot opening, Δx =15 cm.

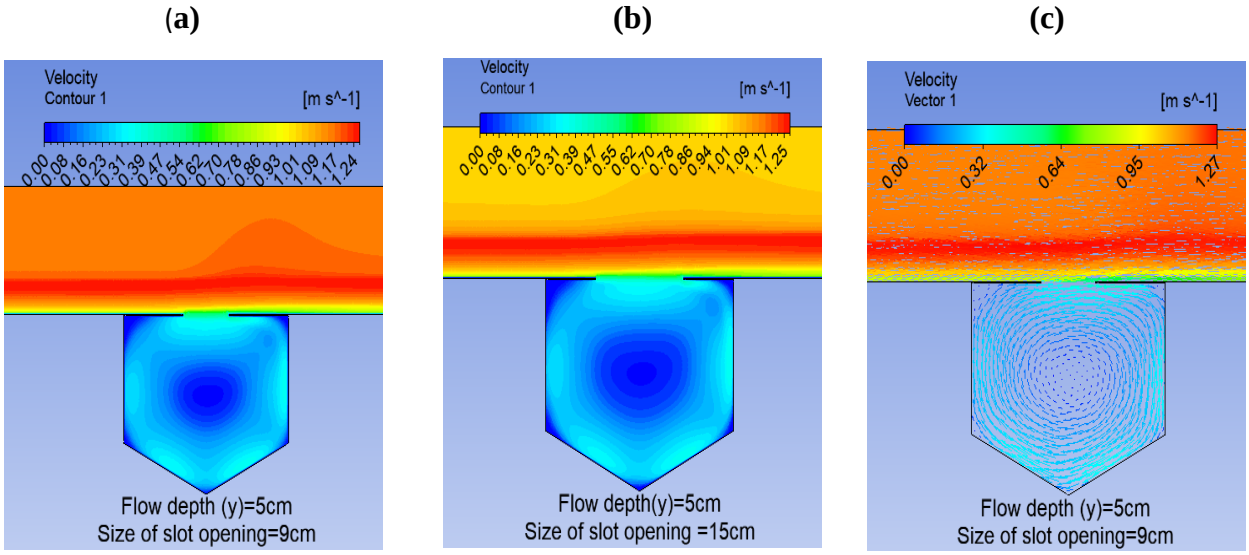

Figure 5. 10 2D predicted velocity contours and velocity vector of Geometry 2 (G2) coloured by velocity magnitude for a flow depth of 5 cm: (a) 2D velocity contours of G2 with slot opening, Δx = 9 cm; (b) 2D velocity contours of G2 with slot opening, Δx =15 cm; and (c) 2D velocity vector of G2 with slot opening, Δx = 9 cm.

(iii) Variation of Trap Efficiency with slot size

The slot opening size of the trap influences the settling of the particles. The large opening of the slot, traps more sediment with good efficiency for all flow depths. The horizontal movement of the sediments is reduced for small opening of the slots resulting in decrease in trap efficiency. This study resulted in variation in the trap efficiencies for different slot opening sizes (0.09 m and 0.15 m) and geometry of the traps. From Table 5.8 the trap efficiency for BG, G2 and G3 increases for 0.15 m slot size. In turn for G1 the trap efficiency decreases for 0.15 m slot opening. The reduction in the trap efficiency for G1 is due to the base geometry being curved causing the re-entrainment of the settled particles with the flow, as shown in Fig. (5.10). In the G1, the re-entrainment of sediment particles has caused due to the smooth vortex flow and higher velocity gradients which made the particles to lift and escape from the invert trap chamber with the flow.

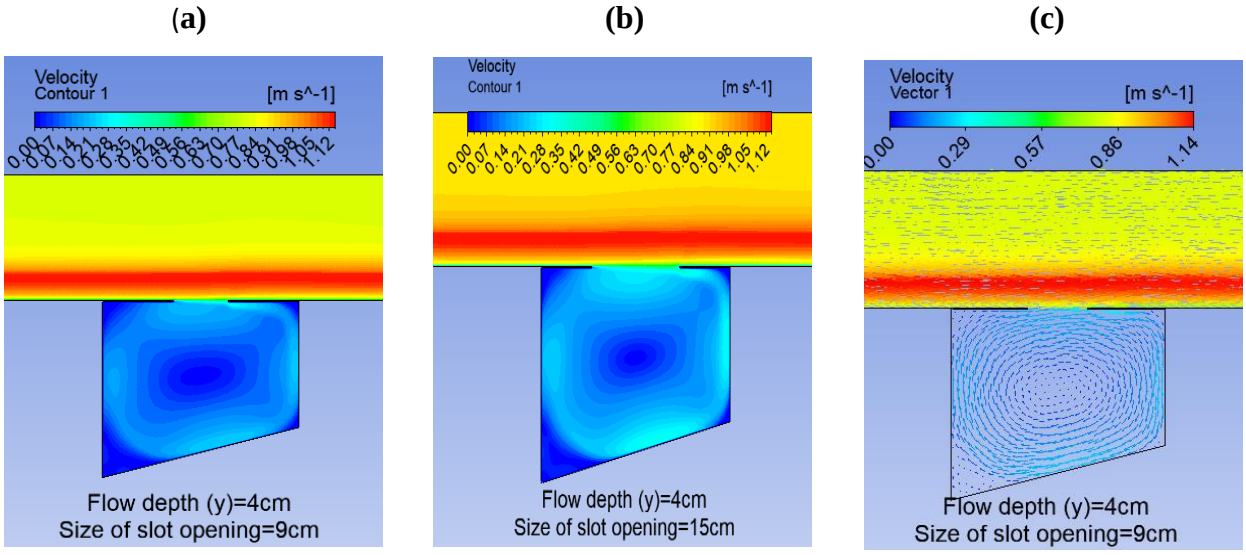

Figure 5. 11 2D predicted velocity contours and velocity vector of Geometry 3 (G3) colored by velocity magnitude for a flow depth of 4 cm: (a) 2D velocity contours of G3 with slot opening, Δx = 9 cm; (b) 2D velocity contours of G3 with slot opening, Δx =15 cm; and (c) 2D velocity vector of G3 with slot opening, Δx = 9 cm.

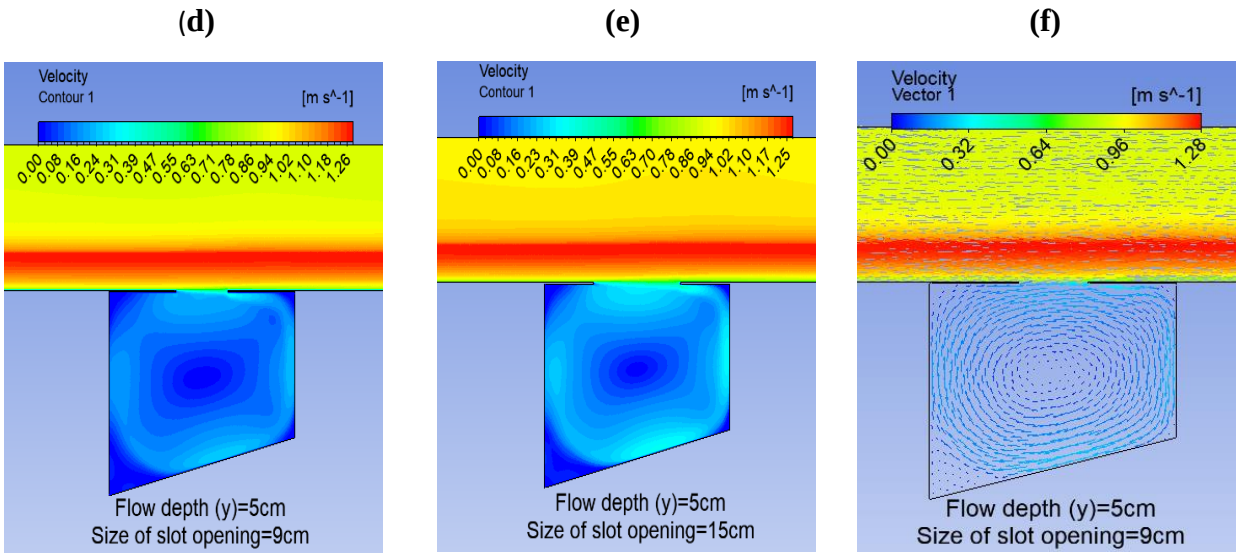

Figure 5. 12 2D predicted velocity contours and velocity vector of Geometry 3 (G3) colored by velocity magnitude for a flow depth of 5 cm: (a) 2D velocity contours of G3 with slot opening, Δx = 9 cm; (b) 2D velocity contours of G3 with slot opening, Δx =15 cm; and (c) 2D velocity vector of G3 with slot opening, Δx = 9 cm.

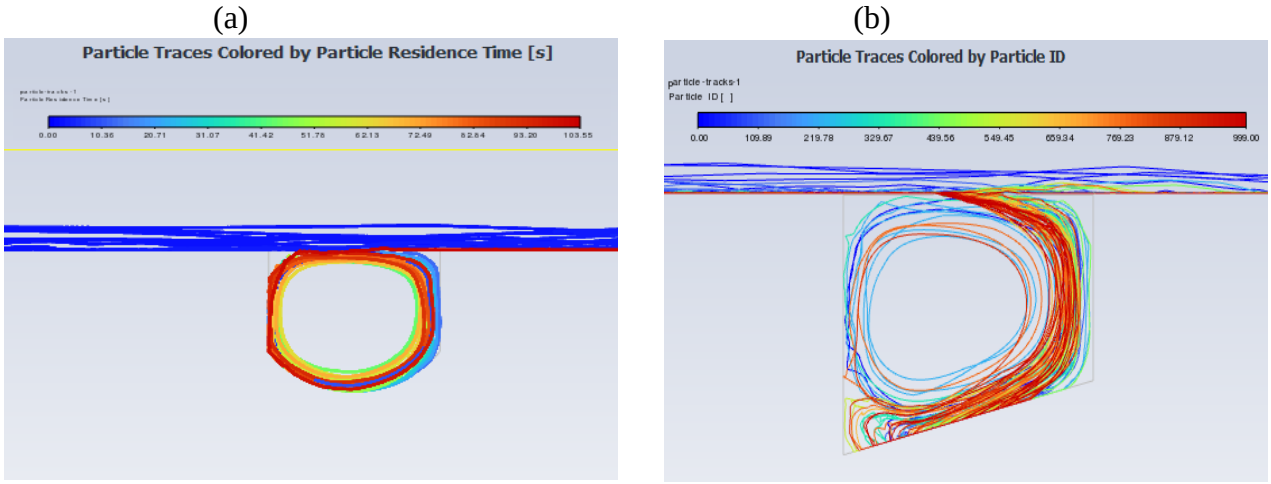

Figure 5. 13 Particle trajectories inside the G1 and G3 invert trap for slot size of Δx = 9 cm: (a) particle trajectories inside the G1 for a flow depth of 5 cm; and (b) particle trajectories inside the G3 for a flow depth of 4 cm.

Table 5. 8 Predicted trap efficiency for different geometries using NSS1.

Flow depth y (cm)	U (m/s)	Δx (cm)	Trap efficiency, η (%)			
			Experimental Mohsin and Kaushal (2017b)	2D CFD-VOF-DPM model		
			Base Geometry	G1	G2	G3
2	0.622	9	82.1	83.1	75.8	86.3
		15	87.3	89	83.5	91.2
3	0.879	9	73.6	77.3	71.3	81.2
		15	78	80.3	80	84.1
4	0.992	9	64.7	66.4	63.9	77.3
		15	68.4	67.7	72.5	78.6
5	1.1	9	61.5	60.1	58.4	74.1
		15	63.1	60.4	70.6	76

(iv) Influence of various geometry on Trap efficiency

The geometry has a considerable impact on the trap efficiency. The G1 showed a maximum trap efficiency percentage of 89 at a flow depth of 2 cm for slot opening of 0.15 m. In case of G2, the peak trap efficiency of 83.5 percent was observed for the flow depth of 2 cm for the slot opening 0.15 m. G3 showed the highest efficiency of 91.2 percent for slot opening 0.15 m when the flow depth is 2 cm. G3 was consistently observed to perform with a better trap efficiency for any given depth, it also noted by Fig. 5.13 of the particle trajectories inside the trap geometry. For all the flow depths and geometries (BG, G2, G3), there was an increase in the trap efficiency with increase in the slot opening. In contrast, in case of G1 for flow depths of 4 cm and 5 cm there was a decrease in the trap efficiency with an increase in the slot opening. This was due to the peculiar geometry of an arc passing through three points that induced free vortex motion to the particle entering with higher velocities. Thus, for a given slot opening, in case of a decrease in the flow depth, there was a scenario of increase in the trap efficiency, this observation is given in Table 5.8 and the same is shown in Figure 5.14.

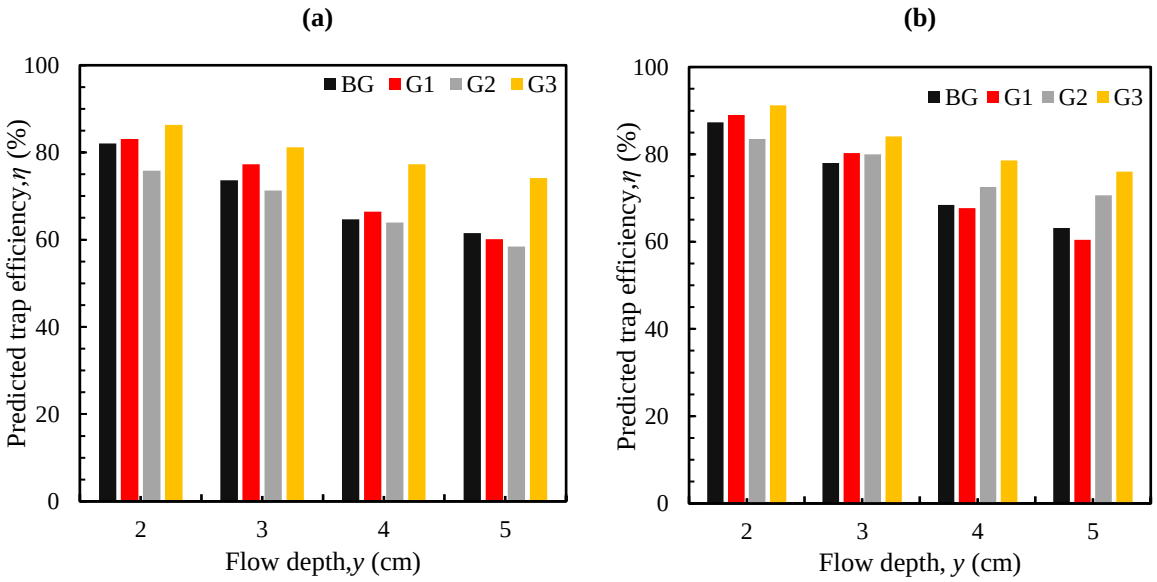

Figure 5. 14 Predicted trap efficiency with the different flow depths for two slot size; (a) Δx = 9 cm, and (b) Δx =15 cm.

5.5.3 Analysis of the Effect of Invert Trap Depth on Sediment Retention Efficiency

In the present study, 6 trap depths have been taken along with four different flow depths and two slot openings to further optimize the invert trap geometry (G3), the same was shown in Fig. 5.16. For numerical calculation, the above-mentioned methodology has been employed to evaluate the effect of depth of invert trap on sediment retention efficiency for the optimized invert trap geometry.

The VOF Model in ANSYS Fluent 2021 was employed to simulate the velocity contours for different trap depths. These contours revealed the presence of low-velocity zones at the center of any Invert trap geometry, which caused the sediment to settle in the trap chambers. It was noted that as the trap depth increases, the extent of the low-velocity zone increased for a given slot opening and it was shown in Fig. 5.15. Furthermore, the analysis of velocity contours indicated that the size of the slot opening in the Invert trap is inversely proportional to the low-velocity zone.

Table 5. 9 Predicted trap efficiency for different invert trap depth using NSS1

Trap efficiency, η (%)								
y (cm)	U (m/s)	Δx (cm)	Trap depth (m)					
			0.24	0.28	0.35	0.45	0.55	0.65
2	0.622	9	81.7	86.3	87.1	86.8	**86.6**	85.5
		15	83.3	91.2	93.5	94.9	**96.2**	96.8
3	0.879	9	77.1	81.2	82.4	80.9	**80.6**	80.4
		15	76.0	84.1	86.1	88.2	**88.9**	89.4
4	0.992	9	74.3	77.3	79.5	81.2	**78.6**	76
		15	73.0	78.6	80.6	82.8	**83.6**	84.3
5	1.1	9	71.7	74.1	68.2	74.9	**74.7**	75.4
		15	70.1	76	78.7	79.3	**81.7**	81.2

In the present study, it has been observed that the depth of an Invert trap has a considerable impact on the sediment trap efficiency. The G3 with a trap depth 0.55 m showed a maximum trap efficiency percentage of 96.2 at a flow depth of 2 cm for slot opening of 0.15 m. In case of G3 with a trap depth 0.45 m, the peak trap efficiency of 94.9 percent was observed for the flow depth of 2 cm for the slot opening 0.15 m. G3 with a trap depth 0.65 m showed the efficiency of 96.8 percent for slot opening 0.15 m when the flow depth is 2 cm. For all trap depths, smaller flow depth shows more or less the same trap efficiency irrespective of trap depths. The observation says that with the increase in trap depth, the trap efficiency increases and it was shown in Table 5.9 and in Fig. 5.16. Till 0.55 m trap depth, there is a considerable increase in trapping efficiency, but as we move towards the greater depth which is 0.65 m, the rate of increment of the trap efficiency decreases.

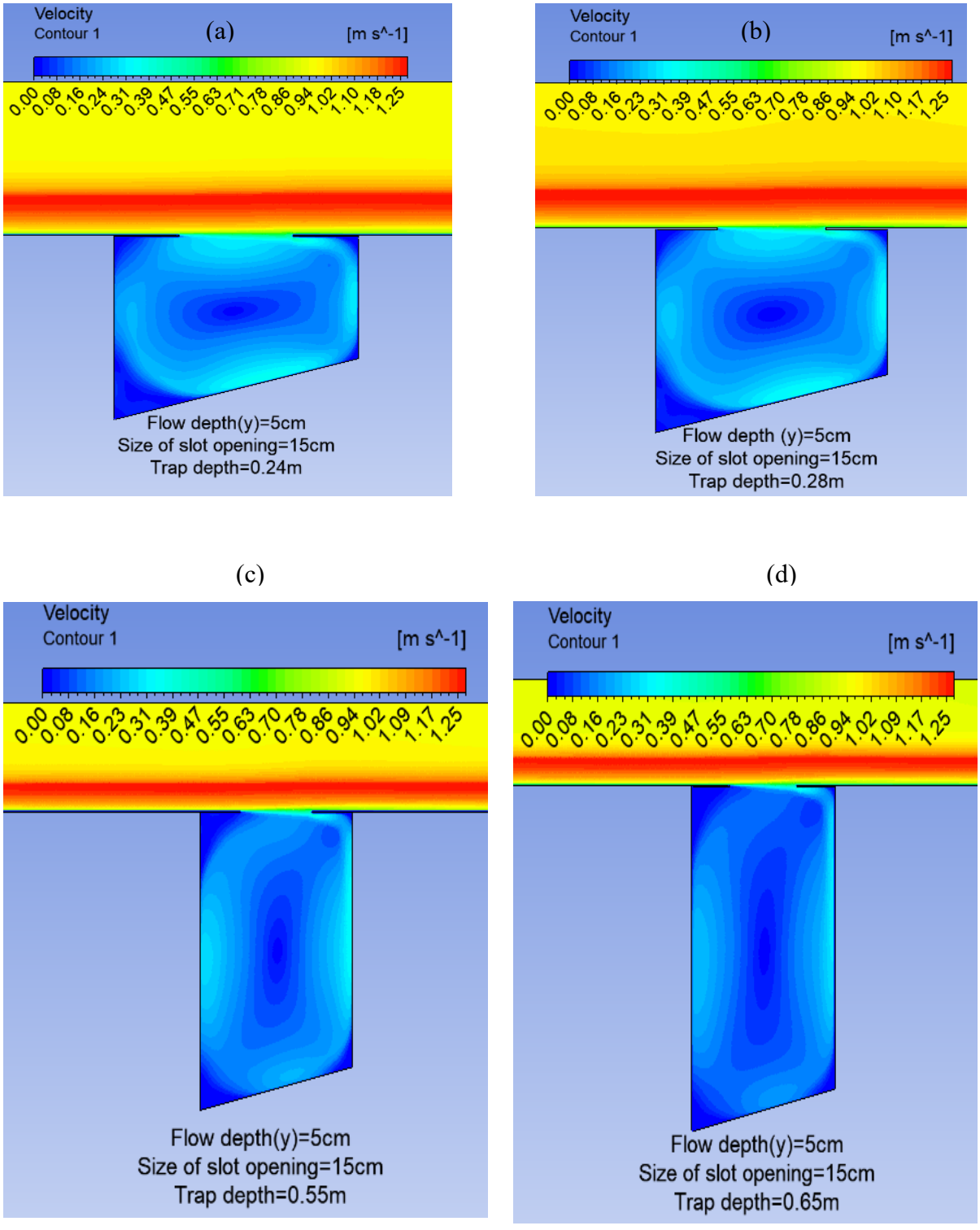

Figure 5. 15 (a-d) Numerically simulated velocity distribution inside right angular (G3) invert trap at depth of flow (Y) = 0.05 m and average velocity (U) = 1.1 m/s with slot opening size (Δx) = 0.15 m.

(a)

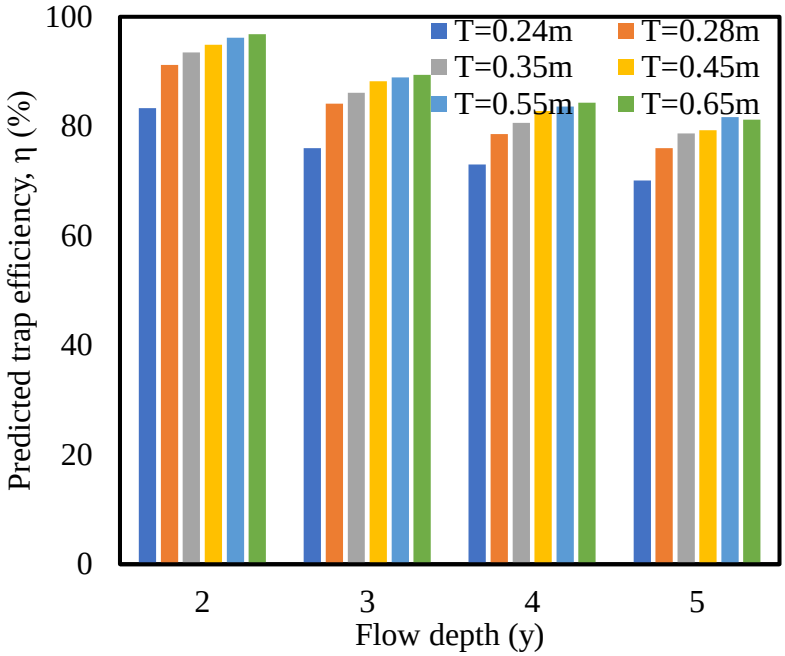

(b)

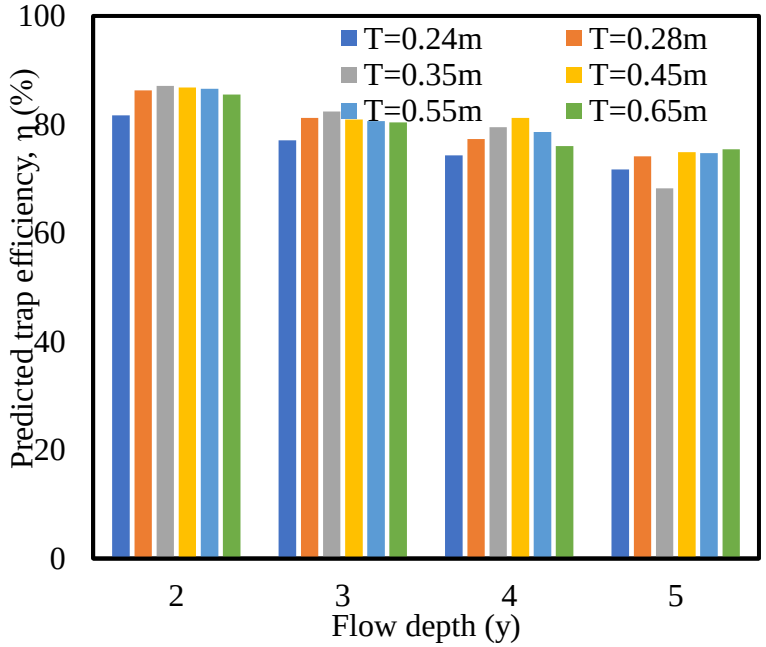

Figure 5. 16 Predicted trap efficiency with the different flow depths for two slot size; (a) Δx =15 cm, and (b) Δx = 9cm.

5.6 Conclusions

The flow velocity distribution (velocity contours and velocity vectors) and direction, water pressure distribution (pressure contours), and sediment particle trajectories (particle tracking) in a rectangular open channel placed with an invert trap were modelled and analysed for varying parameters (flow, particle and trap geometry) using 2D CFD (coupled VOF and DPM) model. The following are the study's most notable findings:

- The 2D CFD (coupled VOF and DPM) model validates Mohsin and Kaushal (2017b) experimental trap efficiencies for NSS1.
- The trap efficiency varies with flow depth, slot opening, and geometry of the invert trap.
- The observed variations were due to changes in the flow field when any of the considered parameters are varied.
- For the slot opening case, an increment in the opening size increases the efficiency.
- In the case of G1, for lower flow depths (3 cm and 2 cm), the trap efficiency decreases with an increase in the slot opening; this is due to the base geometry resulting in the free vortex motion of particles being settled.
- The geometry of base in an invert trap is often given less importance, which shows a significant increase in the trap efficiency when the change has been brought in base geometry.
- The right triangle base geometry (G3) offers maximum trap efficiency out of the three trial geometries. There is also a competitive advantage in emptying the invert trap as all the particles settle on only one side of the base. In other base geometries, the settlement is widely distributed.
- Trap efficiencies were shown to be improved with a slot opening of 0.15 m compared to 0.09 m for natural sediments (NSS1).
- The simulated trap efficiency results are used to analyze the variation in trap efficiency with the depth of invert trap.
- The observation says that with the increase in trap depth, the trap efficiency increases. Till 0.55 m trap depth , there is a considerable increase in trapping efficiency, but as we move towards the greater depth which is 0.65 m, the rate of increment of the trap efficiency decreases.
- For all trap depths, smaller flow depth shows more or less the same trap efficiency irrespective of trap depths.

- The overall observations clearly show that 0.55 m invert trap depth is the optimum invert trap depth for all flow depth and slot openings, under the given sediment parameter.

CHAPTER 6

FINANCIAL VIABILITY OF INVERT TRAP

6.1 General

In the Telangana state, government has implemented several projects to address the issue of flooding in the state, including the introduction of open drainage channels. Open drainage channels are essentially channels that are constructed to carry rainwater and wastewater away from populated areas and into nearby water bodies such as rivers, lakes, or the sea. These channels can be either concrete or earthen and are typically constructed along the sides of roads or in low-lying areas.

The introduction of open drainage channels in Telangana has been aimed at preventing flooding in urban and rural areas, particularly during the monsoon season. The state government has undertaken several projects to construct open drainage channels in various cities and towns across Telangana. In addition to preventing flooding, the introduction of open drainage channels has also helped in improving the overall sanitation and hygiene of the state. By diverting wastewater away from populated areas, open drainage channels have helped in reducing the incidence of waterborne diseases in Telangana.

Overall, the introduction of open drainage channels has been a significant step towards ensuring the safety and well-being of the people of Telangana, particularly during the monsoon season. The state government is committed to continuing its efforts to improve the infrastructure and amenities in the state to make Telangana a more liveable and prosperous place for all its citizens.

However, sediments such as natural sediment particles, construction debris and particles that come from industrial and domestic waste enter into drainages and sewers from the surrounding areas and create several problems like reduced hydraulic efficiency, which leads to overflow, clogging problems, and hinders the pumping of sewer treatment plants, and to overcome this, many excluding or sediment trapping devices have been proposed and are being used practically at appropriate locations along the length of the channel to reduce the sediment concentration and to make sure the smooth and best possible functioning of the drainage system.

According to the numerical analysis in Chapter 5, the Invert Trap with rectangular chamber and right triangular base has the highest trap efficiency. This type of invert trap could be used practically to solve sediment-related issues were mentioned above.

6.2 Methodology

In this study, the cost comparative analysis of conventional drainage channel and hypothetical drainage channel with Invert Trap, as well as the financial viability of Invert Trap, was performed by collecting all necessary data from the Panchayat Raj Department of Telangana State, India. The proposed methodology for cost comparison and financial viability of invert trap to be used in the Indian scenario is shown in Fig. 6.1.

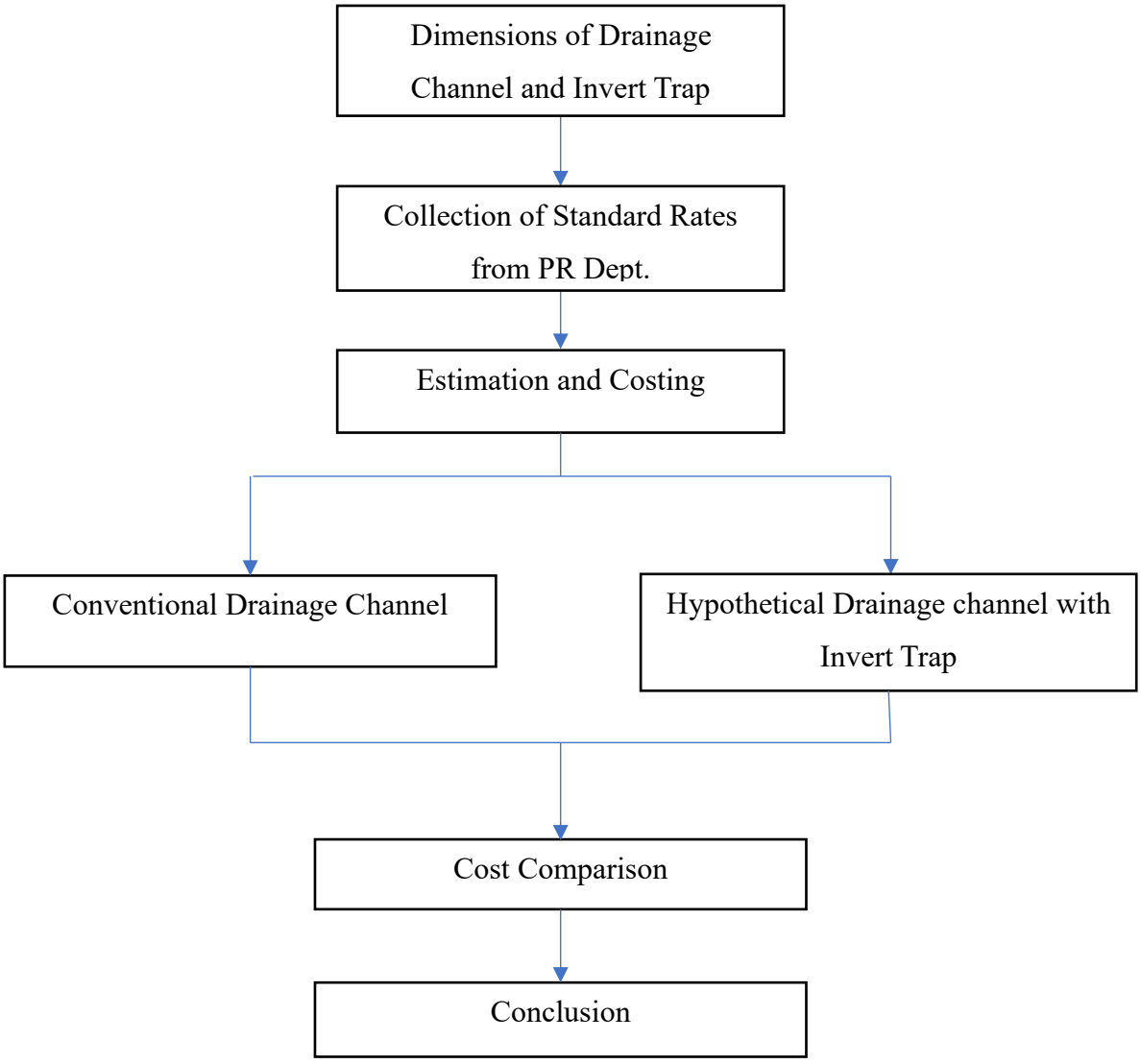

Figure 6. 1 Flow chart of Methodology

6.3 Location and Dimensions of Drainage Channel

The ongoing drainage channel construction project in Bollaram (village), Nagireddypet (mandal), Telangana, India, has been considered to analyse the financial viability of optimised sediment invert trap design for rural applications. In this study, the cost estimation was done for a 1 km stretch of the drainage channel, which includes earth work and PCC works.

The cost comparison study was conducted by comparing two different drainage channels: conventional drainage channel and hypothetical drainage channel with invert trap. A rectangular channel has been adopted for open drainage at Bollaram village. The dimension of the channel was 1000.0 m long (estimation was done per unit length of the channel),0.45 m wide, and 0.45 m deep, respectively. In the hypothetical channel, invert trap was placed at every 20 m span of the conventional channel. This invert trap measured 0.6 m in length and 1.0m in depth, as shown in Table 6.1. Figure 6.2 shows the preparation of open drainage channel formwork, and Fig. 6.3 and 6.4 illustrates the placing of concrete and completed open drainage channel, respectively.

Table 6. 1 Parameters of open drainage channel and invert trap geometry.

	Conventional channel	Hypothetical channel	
	Drainage channel	Drainage channel	Invert Trap
Length, *L* (m)	1000.0	1000.0	0.6
Width, *W* (m)	0.45	0.45	0.45
Depth, *H* (m)	0.45	0.45	1

Figure 6. 2 Preparation of formwork to construction open drainage channel by TS Panchayat Raj Dept. at Bollaram village.

Figure 6. 3 Conventional drainage channel construction by TS Panchayat Raj Dept. at Bollaram village.

Figure 6. 4 Placing of concrete while construction of open drainage channel at Bollaram village.

Figure 6. 5 Photo view of under construction open drainage channel.

6.4 Standard Rates

Table 6. 2 Standard rates for earth and PCC work from P.R department

Description	Rate per 1cum
Cost estimation of earth work will be included: Earthworks for structures as per design and technical requirements, including setting out, propping and girding construction, stump elimination and disposal up to a lead of 50 m, dressing of sides walls and bottom, and filling the gaps in trenches with excavated suitable material after construction of drainage channel.	Rs.178.36/-
Cost estimation of PCC will be included: To make M15 grade Plain Cement Concrete (PCC) with Nominal mix of 40, 20, and 10 mm sized coarse aggregates, mechanical mixing, place PCC in foundation, and compacted by vibration, including 14 days curing complete according to drawings and technical specifications.	Rs.5546.56/-
GST Labour cess QC	12% 1% 0.5%

Table 6.2 summarised all Standard rates per unit quantity for earth and PCC work, including labour charges for earth work, material purchases (cement, 40 mm, 20 mm, 10 mm coarse aggregates, coarse sand, and water), labour charges for PCC work, Machinery (mechanical concrete mixer, generator), Formwork, and so on.

6.5 Estimation and Costing

6.5.1 Cost Estimation for Conventional Drainage Channel

In this study, the cost estimation was done for a 1 km stretch of the drainage channel, which included earth work and PCC works. By considering these standard rates (Table 6.2) from the P. R department, the estimation and costing for a conventional drainage channel for a stretch of 1 km has been calculated and mentioned in Table 6. 3.

Table 6. 3 Estimation and costing for conventional drainage channel for stretch of 1 km

Description		L(m)	B(m)	D(m)	No	Quantity (cum)	Rate per 1cum	amount
Earth work		1000	1.20	0.60	1	720.00	178.36	1,28,419.00
PCC work	bed	1000	1.05	0.1	1	105.00	5546.56	17,30,527.00
	Side walls	1000	0.23	0.45	2	207.00		
Total						312.00		18,58,946.00
						GST	12%	2,23,074.00
						Labour cess	1%	18,590.00
						QC	0.5%	9,295.00
							Grand Total	**21,09,905.00**

6.5.2 Cost Estimation for Hypothetical Drainage Channel

The optimised invert trap design from Chapter 5 was hypothetically installed in a standard drainage channel with one invert trap at a span of 20 m. Using the P. R department's standard rates (Table 6.2), the estimating and costing for a hypothetical drainage channel with a length of 1 km has been determined and is shown in Table 6. 4.

Table 6. 4 Estimation and costing for drainage channel including invert trap for stretch of 1 km

Description		L(m)	B(m)	D(m)	No	Quantity (cum)	Rate per 1cum	amount
Earth work	Channel	1000	1.20	0.60	1	720.00	178.36	144900.00
	Invert trap	1.4	1.20	1.1	50	92.4		
	Total					812.4		
PCC work	Channel bed	1000	1.05	0.1	1	105.00	5546.56	1826482.00
	Channel side walls	1000	0.23	0.45	2	207.00		
	Invert trap walls (2)	1.06	0.23	1	50	12.13		
	Invert trap Side walls (2)	0.45	0.23	1	50	5.175		
Total						329.30		1971382.00
						GST	12%	2,36,566.00
						Labour cess	1%	19,714.00
						QC	0.5%	9,857.00
							Grand Total	**22,37,519.00**

6.6 Cost Comparison

A conventional drainage channel and a hypothetical drainage channel for a 1 km stretch are predicted to cost Rs. 21,09,905 and Rs. 22,37,519, respectively. There is around 6.04% increase in the initial capital cost if the invert traps are included in the channel design at centre-to-centre distance of 20 m between the invert traps. Based on the predicted initial capital cost, the invert trap can be easily implemented to reduce sediment-related problems. Therefore, manpower and work hour both will get reduced that leads to less maintenance cost.

6.7 Conclusions

The cost comparative analysis of conventional drainage channel and hypothetical drainage channel with Invert Trap, as well as the financial viability of Invert Trap, were undertaken in this study by collecting all essential data from Telangana State's Panchayat Raj Department. The following are the study's most notable findings:

- Open drainage channels are essentially channels that are constructed to carry rainwater and wastewater away from populated areas (i.e., Rural) and into nearby water bodies such as rivers, lakes, or the sea.
- With the maximum sediment trap efficiency, an invert trap with a rectangular chamber and a right triangle base could be employed practically to tackle sediment-related problems in drainage channels.
- There is around 6.04% increase in the initial capital cost if the invert traps are included in the channel design at centre-to-centre distance of 20m between the invert traps.
- Manpower and work hours will both be reduced, which will lead to lower maintenance costs.

CHAPTER 7

CONCLUSIONS AND SCOPE FOR FUTURE WORK

7.1 Conclusions

In the present research, the 2D CFD (Coupled VOF & DPM) model was validated with experimental data (Mohsin and Kaushal, 2017b) for the performance analysis of the invert trap using two slot sizes of the invert trap with a given sediment type and varying flow conditions. Previous researchers did not compare the sediment particle settling velocity equations, which will be fed into a CFD model to assess the sediment trap efficiency of an invert trap. The study's main objective was to analyse different invert trap geometries in sewer solid management to trap the most sediments that entered the drainage channel.

The following are the study's most notable findings:

1. The settling velocity of particles must be calculated with more precision in order to define the sediment mode of transit with the flow.
2. After graphical and statistical analysis, it was discovered that the Wu and Wang (2006) equation calculates the settling velocity of sediment particles with better accuracy and reliability.
3. The hybrid GRG-GA-based settling velocity estimates were more precise than previous empirical equations as well as those obtained through GRG algorithm stand-alone.
4. This study highlights that the hybrid approaches have the capability to significantly improve the accuracy of stand-alone algorithms.
5. To be more specific, gradient-based and evolutionary algorithms can be hybridized to overcome the problem of obtaining local optimum solution and computation expense involved in the evolutionary algorithms.
6. The 2D CFD (coupled VOF and DPM) model validates Mohsin and Kaushal (2017b) experimental trap efficiencies for NSS1.
7. The trap efficiency varies with flow depth, slot opening, and geometry of the invert trap.
8. For the slot opening case, an increment in the opening size increases the efficiency.

9. The geometry of base in an invert trap is often given less importance, which shows a significant increase in the trap efficiency when the change has been brought in base geometry.
10. In the case of G1 (Invert trap of rectangular chamber with a arc shaped base), for lower flow depths (3 cm & 2cm), the trap efficiency decreases with an increase in the slot opening; this is due to the base geometry resulting in the free vortex motion of particles being settled.
11. The right triangle base geometry (G3) offers maximum trap efficiency out of the three trial geometries. There is also a competitive advantage in emptying the invert trap as all the particles settle on only one side of the base. In other base geometries, the settlement is widely distributed.
12. Trap efficiencies were shown to be improved with a slot opening of 0.15 m compared to 0.09 m for natural sediments (NSS1).
13. The simulated trap efficiency results are used to analyze the variation in trap efficiency with the depth of invert trap.
14. The observation says that with the increase in trap depth, the trap efficiency increases. Till 0.55 m trap depth , there is a considerable increase in trapping efficiency, but as we move towards the greater depth which is 0.65 m , the rate of increment of the trap efficiency decreases.
15. For all trap depths, smaller flow depth shows more or less the same trap efficiency irrespective of trap depths.
16. The overall observations clearly show that 0.55 m invert trap depth is the optimum invert trap depth which shows minimum re-entrainment of the sediment particles for all flow depth and slot openings, under the given sediment parameter.
17. With the maximum sediment trap efficiency, an invert trap with a rectangular chamber and a right triangle base could be employed practically to tackle sediment-related problems in drainage channels.
18. There is around 6.04% increase in the initial capital cost if the invert traps are included in the channel design at centre-to-centre distance of 20 m between the invert traps.
19. Both manpower and work hours will be reduced, which will lead to lower maintenance costs.

7.2 Scope for Future Work

1. In the present study, only 2D CFD model has been used to analyse the Invert Trap geometries with various flow and slot opening parameters. Therefore, 3D numerical simulation studies can be performed and validated with experimental results to ensure that the proposed geometry has maximum trap efficiency.
2. Previous research had not addressed the use of optimised sediment invert trap design for rural applications. To achieve this, the present work can be implemented experimentally in the field through a pilot scale research project.
3. Because of time constraints, the influence of other turbulence models, % of turbulent kinetic energy, and so on could not be investigated in this study. As a result, it is also advised to numerically investigate the effect of these parameters and compare the simulated results with the presented experimental results.

Appendix-I

Publications from Present Research Work

(1) **Shankar, M. S**., Pandey, M., & Shukla, A. K. (2021). Analysis of Existing Equations for Calculating the Settling Velocity. *Water (Switzerland)*, *13*(14), 1–12. [https://doi.org/10.3390/w13141987]. SCI, I.F.: 3.1

(2) **Shivashankar, M.,** Pandey, M., & Zakwan, M. (2022). Estimation of Settling Velocity Using Generalized Reduced Gradient (GRG) and Hybrid Generalized Reduced Gradient–Genetic Algorithm (Hybrid GRG-GA). *Acta Geophysica*, 0123456789.
[https://doi.org/10.1007/s11600-021-00706-2]. SCI, I.F.: 2.1

(3) **Shivashankar, M**., Pandey, M., & Shukla, A. K. (2022). Numerical investigation on evaluation of the sediment retention efficiency of the invert traps in an open rectangular combined sewer channel. *Journal of Hazardous, Toxic, and Radioactive Waste* (ASCE), Volume 27(1), 2022.
[DOI:10.1061/(ASCE)HZ.2153-5515.0000733]. SCI, I.F.: 1.44

Communicated

(1) **Shivashankar, M**., Pandey, M., & Shukla, A. K. (2022). The effect of invert-trap depth on sediment trap efficiency in an open rectangular drainage channel using CFD model. Water Supply (IWA). (Submitted, WS-0062). SCI, I.F.: 1.2.

Appendix-II

List of symbols

A	Cross-sectional area of flow (m^2)
b	Width of the channel (m)
Ca	Capillary Number
d_p	Mean diameter of sediment (mm)
ρ_p	Sediment density
U	Average flow velocity
y	Flow depth
F_D	Drag force
F_G	Gravitational force
η	Sediment Trap Efficiency
N_T	Total number or mass of the sediments that are retained inside the invert trap
N_I	Total number or mass of the sediments that are injected into the invert trap
w_s	Settling velocity of a solid particle
τ_{oc}	Critical bed shear stress
k	Turbulent kinetic energy
ε	Turbulent kinetic energy dissipation
C_d	Coefficient of Drag
ρ	Density of water
g	Gravitational acceleration
d	Nominal diameter of particle
$\emptyset$	Angle of repose under water
d	Mean diameter of sediment (mm),
S	Relative density of sediment in water,
r	Mean ratio of longest and shortest diameters,
k	a constant (=0.6)
q_B	Bed load (N/s/m)
τ_c	Critical shear stress
τ_0	Bed shear stress
$\emptyset_B$	Bed load function

τ'_*	Dimensionless grain shear stress
R	Hydraulic radius of the channel
γ	Unit weight of water
γ_s	Unit weight of sediment particles
n	Manning's coefficient for the whole channel
n_s	Manning's coefficient of the particle roughness
R'	Hydraulic roughness corresponding to grain roughness
S_0	Longitudinal slope of the channel
C	Concentration of sediment, by weight
ε_s	Mass diffusion coefficient
C_a	Sediment concentration at any height *a* above the bed
q_s	Suspended sediment load
S	Specific gravity of particle
ϑ	Kinematic viscosity of water, (cm^2/s)
CSF	Corey Shape Factor
D_{gr}	Dimensionless particle size
S_f	Shape Factor
P	Particle roundness
R^2	Coefficient of determination
σ_p	Standard deviation of predicted data
σ_m	Standard deviation of observed data
μ_p	Mean of predicted data
μ_m	Mean of observed data
$\alpha_{2\,=}$	Secondary phase (water) volume fraction
$\dot{m}_{sp}$	Rate of mass transfer from phase *p* to phase *s*
$\dot{m}_{ps}$	Rate of mass transfer from phase *s* to phase *p*
U_f	Volume flux through the face
p	Intensity of pressure
F_r	Froude Number
Re_p	Reynolds number of the particle
τ_p	Particle relaxation time
G_k	Turbulence kinetic energy generation related to mean velocity gradients

G_b	Turbulence kinetic energy generation related to buoyancy
μ_t	Turbulent (eddy) viscosity
U^*	Dimensionless velocity
y^*	Dimensionless distance from the wall boundary
K	Von Kármán constant
U_M	Mean velocity of the fluid at the wall-adjacent cell centroid, M
k_M	Turbulence kinetic energy at the wall-adjacent cell centroid, M
y_M	Distance from the centroid of the wall-adjacent cell to the wall
μ	Dynamic viscosity of the fluid
Re	Reynolds number
We	Weber number
SP	Sedimentation Parameter
$\boldsymbol{Q}$	Flow discharge, m^3/s
Δx	Size of slot opening
L	Length of the channel
W	Width of the channel
H	Depth of the channel

References

(1) Ansys Inc. (2013). ANSYS fluent user's guide. *Ansys Fluent*, *15317*, 2498.

(2) Ansys, Inc. (2011). ANSYS FLUENT theory guide. *Canonsburg, Pa* 794.

(3) Aryanfar, A., Bejestan, M. S., Khosrojerdi, A., and Badazadeh, H. (2014). Laboratory Investigation on Changes in the Angles of the Invert Traps in Order to Increase the Trapping. *Journal of Ecology, Environment and Conservation*, *20*(2), 439–449.

(4) Ashley, R. M., Krajewski, J.L.B., Jacobsen, T. H. and Verbanck, M. (2004). Solids in Sewers: Characteristics, Effects and Control of Sewer Solids and Associated Pollutants. *Scientific and Technical Report No.* 14, IWA Publishing, U. K.

(5) Ashley, R. M., Fraser, A., Burrows, R., and Blanksby, J. (2000). The Management of Sediment in Combined Sewers. Elsevier *Urban Water*, *2*(4), 263–275.

(6) Ashley, R. M., Tait, S. J., Stovin, V. R., Burrows, R., Fraser, A., Buxton, A. P., Blackwood, D. J., Saul, A. J., and Blanksby, J. R. (2003). The Utilisation of Engineered Invert Traps in the Management of Near Bed Solids in Sewer Networks. *Water Science and Technology*, *47*(4), 137–148.

(7) Aslam, M. T. (2013). Settling of Solids in Raw Wastewater-Primary Settling Tanks and Storm Water Tanks. *Ph.D. Thesis*, Technical University Graz.

(8) Atkinson, E. (1992). The Design of Sluiced Settling Basins: A numerical modelling approach. *Rep. OD* 124, Overseas Development Unit, *HR Wallingford, U.K*.

(9) Azamathulla, H. M., and Ahmad, Z. (2012). Gene-Expression Programming for Transverse Mixing Coefficient. *Journal of Hydrology*, *434–435*, 142–148. [https://doi.org/10.1016/j.jhydrol.2012.02.018]

(10) Azamathulla, H. M., Chang, C. K., Ab. Ghani, A., Ariffin, J., Zakaria, N. A., and Abu Hasan, Z. (2009). An ANFIS-Based Approach for Predicting the Bed Load for Moderately Sized Rivers. *Journal of Hydro-Environment Research*, *3*(1), 35–44.
[https://doi.org/10.1016/j.jher.2008.10.003]

(11) Azamathulla, H. M., and Zahiri, A. (2012). Flow Discharge Prediction in Compound Channels Using Linear Genetic Programming. *Journal of Hydrology*, *454–455*, 203–207.
[https://doi.org/10.1016/j.jhydrol.2012.05.065]

(12) Bachoc, A. (1992). Location and General Characteristics of Sediment Deposits into Man-Entry Combined Sewers. *25*(8), 47–55.

(13) Barati, R. (2013). Application ff Excel Solver for Parameter Estimation of The Nonlinear Muskingum Models. *KSCE Journal of Civil Engineering*, *17*(5), 1139–1148. [https://doi.org/10.1007/s12205-013-0037-2]

(14) Bhattacharya, B., Price; R K, and Solomatine, D. P. (2007). Machine Learning Approach to Modeling Sediment Transport. *Journal of Hydraulic Engineering*, Vol. 133. [https://doi.org/10.1061/ASCE0733-94292007133:4440]

(15) Bizimana, H., and Altunkaynak, A. (2021). Investigating the Effects of Bed Roughness on Incipient Motion in Rigid Boundary Channels with Developed Hybrid Geno-Fuzzy versus Neuro-Fuzzy Models. *Geotechnical and Geological Engineering*, *39*(4), 3171–3191. [https://doi.org/10.1007/s10706-021-01686-2]

(16) Bowden, G. J., Maier, H. R., and Dandy, G. C. (2012). Real-Time Deployment of Artificial Neural Network Forecasting Models: Understanding the Range of Applicability. *Water Resources Research*, *48*(10). https://doi.org/10.1029/2012WR011984

(17) Briggs, L. I., McCulloch, D. S., and Moser, F. (1962). The Hydraulic Shape of Sand Particles. *Journal of Sedimentary Research*, *Vol. 32*(4), 645–656. [https://doi.org/10.1306/74d70d44-2b21-11d7-8648000102c1865d]

(18) Buxton, A. P., Tait, S., Stovin, V., and Saul, A. (2002). Developments in a Methodology for the Design of Engineered Invert Traps in Combined Sewer Systems. *Water Science and Technology*, *45*(7), 133–142.

(19) Camenen, B. (2007). Simple and General Formula for the Settling Velocity of Particles. *Journal of Hydraulic Engineering*, *133*(2), 229–233. [https://doi.org/10.1061/(asce)0733-9429(2007)133:2(229)]

(20) Chebbo, G., Laplace, D., Bachoc, A., Sanchez, Y., and Le Guennec, B. (1996). Technical Solutions Envisaged in Managing Solids in Combined Sewer Networks. *Water Science and Technology*, *33*(9), 237–244.

(21) Cheng, N. S. (1997). Simplified Settling Velocity Formula for Sediment Particle. *Journal of Hydraulic Engineering*, *123*(February), 149–152.

(22) Pierre Y. Julien. (1995). Erosion and Sedimentation. *Cambridge University Press, 1995*. Elsevier.

(23) Dey, S., Ali, S. Z., and Padhi, E. (2019). Terminal fall velocity: The Legacy of Stokes from the Perspective of Fluvial Hydraulics. In *Proceedings of the Royal Society A: Mathematical, Physical and Engineering Sciences* (Vol. 475, Issue 2228).
[https://doi.org/10.1098/rspa.2019.0277]

(24) Engelund, F., and Hansen, E. (1390). A Monograph on Sediment Transport in Alluvial Streams. *3rd Ed., Technical Press, Copenhagen, Denmark*, 99-117.

(25) Faram, M. G., and Harwood, R. (2000). CFD for the Water Industry; The Role of CFD as a Tool for the Development of Wastewater Treatment Systems. *Fluent Users' Seminar, Sheffield, UK*, 21–22.

(26) Gandhi, B. K., Verma, H. K., and Abraham, B. (2010). Investigation of Flow Profile in Open Channels using CFD. 8th International Conference on Hydraulic Efficiency Measurement, 243-251.

(27) Garde, R. J., and Raju, K. G. R. (2000). Mechanics of Sediment Transportation and Alluvial Stream Problems. *Taylor & Francis*.

(28) Gardner, W. D. (1980). Field Assessment of Sediment Traps. *J. Mar. Res*, *38*(1), 41–52.

(29) Ghani, A. A., Bong, C. H. J., and Lau, T. L. (2013). Sediment Flushing Using Tipping Flush Gate in an Open Storm Concrete Drain – A Case Study in Nibong Tebal, Penang, Malaysia. *Proceedings of 2013 IAHR World Congress.*

(30) Gibbs, R. J., Matthews, M. D., and Link, D. A. (1971). The Relationship Between Sphere Size and Settling Velocity. *Journal of Sedimentary Petrology* (Vol. 41).

(31) Goldstein, E. B., and Coco, G. (2014). A Machine Learning Approach for The Prediction of Settling Velocity. *Water Resources Research*, *50*(4), 3595–3601. [https://doi.org/10.1002/2013WR015116]

(32) Graf, W. H. (1984). Hydraulics of Sediment Transport. *Water Resources Publication*.

(33) Gupta, K., Mehta, P., Thinglas, T., Tait, S. J., and Stovin, V. (2005). Optimization of Sediment Trap Configuration Using CFD Modelling for Indian Drainage Systems. 10th Int. *Conf. on Urban Drainage. Copenhagen, Denmark*.

(34) Guy, H. P., Simons, D. B., and Richardson, E. V. (1966). Summary of Alluvial Channel Data from Flume Experiments*, 1956-61*. U.S. Government Printing Office.

(35) Hallermeier, R. J. (1981). Terminal Settling Velocity of Commonly Occurring Sand Grains. *Sedimentology*, *28*(6), 859–865. [https://doi.org/10.1111/j.1365-3091.1981.tb01948.x]

(36) Harwood, R., and Saul, A. J. (2001). Modelling the Performance of Combined-Sewer Overflow Chambers. *Water and Environment Journal*, *15*(4), 300–304.

(37) Hirt, C. W., and Nichols, B. D. (1981). Volume of Fluid (VOF) Method for the Dynamics of Free Boundaries. In *Journal of Computational Physics* (Vol. 39).

(38) Hubbell, D. W. (1964). Apparatus And Techniques for Measuring Bedload. *U.S. Geological Survey.*

(39) Hunt, J. N. (1969). On the Turbulent Transport of a Heterogeneous Sediment. http://qjmam.oxfordjournals.org

(40) Jimenez, J. A., and Madsen, O. S. (2003). A Simple Formula to Estimate Settling Velocity of Natural Sediments. *Journal of Waterway, Port, Coastal, and Ocean Engineering*, *129*(2), 70–78. [https://doi.org/10.1061/(asce)0733-950x(2003)129:2(70)]

(41) Kaushal, D. R., Thinglas, T., Tomita, Y., Kuchii, S., and Tsukamoto, H. (2012). Experimental Investigation on Optimization of Invert Trap Configuration for Sewer Solid Management. *Powder Technology*, *215*, 1–14.

(42) Khazaee, I., and Mohammadiun, M. (2012). Effect of Flow Field on Open Channel Flow Properties Using Numerical Investigation and Experimental Comparison. *International Journal of Energy and Environment (Print)*, *3*.

(43) Lipeme Kouyi, G., Bret, P., Didier, J. M., Chocat, B., and Billat, C. (2011). The Use of CFD Modelling to Optimise Measurement of Overflow Rates in a Downstream-Controlled Dual-Overflow Structure. *Water Science and Technology*, *64*(2), 521–527.

(44) Mahtabi, G., Chaplot, B., Azamathulla, H. M., and Pal, M. (2020). Classification of Hydraulic Jump in Rough Beds. *Water (Switzerland)*, *12*(8).

(45) Malalasekera, W., & Versteeg, H. K. (2007). An Introduction to Computational Fluid Dynamics. *The Finite Volume Method, Harlow: Prentice Hall*, 1995.

(46) Mohapatra, P. K., Eswaran, V., & Bhallamudi, S. M. (1999). Two-Dimensional Analysis of Dam-Break Flow in Vertical Plane. *Journal of hydraulic engineering* (Issue 183).

(47) Mohsin, M., and Kaushal, D. R. (2016). 3D CFD Validation of Invert Trap Efficiency for Sewer Solid Management Using VOF Model. *Water Science and Engineering*, *9*(2), 106–114. [https://doi.org/10.1016/j.wse.2016.06.006]

(48) Mohsin, M., and Kaushal, D. R. (2017a). A 2D-CFD (VOF Model) Analysis of Invert Trap for Bed Load Removal in an Open Rectangular Sewer Drain. *Particulate Science and Technology*, *35*(1), 54–66. [https://doi.org/10.1080/02726351.2015.1131786]

(49) Mohsin, M., and Kaushal, D. R. (2017b). Experimental and CFD Analyses Using Two-Dimensional and Three-Dimensional Models for Invert Traps in Open Rectangular Sewer Channels. *Journal of Irrigation and Drainage Engineering*, *143*(5), 1–13. [https://doi.org/10.1061/(ASCE)IR.1943-4774.0001142]

(50) Mohsin, M., and Kaushal, D. R. (2017c). Three-Dimensional Computational Fluid Dynamics (Volume of Fluid) Modelling Coupled with a Stochastic Discrete Phase Model for the Performance Analysis of an Invert Trap Experimentally Validated Using Field Sewer Solids. *Particuology*, *33*, 98–111. [https://doi.org/10.1016/j.partic.2016.09.010]

(51) Muzzammil, M., Alam, J., and Zakwan, M. (2018). A Spreadsheet Approach for Prediction of Rating Curve Parameters (pp. 525–533). [https://doi.org/10.1007/978-981-10-5801-1_36]

(52) Naser, G., Karney, ; B W, and Salehi, A. A. (2005). Two-Dimensional Simulation Model of Sediment Removal and Flow in Rectangular Sedimentation Basin. *Journal of Environmental Engineering,* ASCE,131(15),1740-1749.

(53) Nawaz, A. R., Zakwan, M., Khan, I., and Rahim, Z. A. (2020). Comparative Analysis of Variants of Muskingum Model. *Water and Energy International*, *63*(7), 64–73.

(54) Oehler, F., Coco, G., Green, M. O., & Bryan, K. R. (2012). A Data-Driven Approach to Predict Suspended-Sediment Reference Concentration Under Non-Breaking Waves. *Continental Shelf Research*, *46*, 96–106. [https://doi.org/10.1016/j.csr.2011.01.015]

(55) Pandey, M., Zakwan, M., Khan, M. A., and Bhave, S. (2020). Development of Scour Around a Circular Pier and its Modelling Using Genetic Algorithm. *Water Science and Technology: Water Supply*, *20*(8), 3358–3367. [https://doi.org/10.2166/ws.2020.244]

(56) Pandey, M., Zakwan, M., Sharma, P. K., and Ahmad, Z. (2020). Multiple Linear Regression and Genetic Algorithm Approaches to Predict Temporal Scour Depth Near Circular Pier in Non-Cohesive Sediment. *ISH Journal of Hydraulic Engineering*, *26*(1), 96–103. [https://doi.org/10.1080/09715010.2018.1457455]

(57) Poreh, M., Sagiv, A., and Seginer, I. (1970). Sediment Sampling Efficiency of Slots. *Journal of the Hydraulics Division*, *96*(10), 2065–2078.

(58) Pu, J. H. (2019). Turbulent rectangular compound open channel flow study using multi-zonal approach. *Environmental Fluid Mechanics*, *19*(3), 785–800.

(59) Pu, J. H., Wallwork, J. T., Khan, M. A., Pandey, M., Pourshahbaz, H., Satyanaga, A., Hanmaiahgari, P. R., and Gough, T. (2021). Flood Suspended Sediment Transport: Combined Modelling from Dilute to Hyper-Concentrated Flow. *Water (Switzerland)*, *13*(3). [https://doi.org/10.3390/w13030379]

(60) Raudkivi, A. J. (1990). Loose Boundary Hydraulics. *Ed*. Pergamon–UK.

(61) Riazi, A., and Türker, U. (2019). The Drag Coefficient and Settling Velocity of Natural Sediment Particles. *Computational Particle Mechanics*, *6*(3), 427–437.

(62) Rijn, L. C. V. (1984). Sediment Transport, Part II: Suspended Load Transport. *Journal of Hydraulic Engineering*, *110*(11), 1613–1641.

(63) Rubey (1933). Settling Velocities of Gravel, Sand, and Silt Particles. *American Journal of Science*, (pp. 188–192).

(64) Rushd, S., Hafsa, N., Al-Faiad, M., and Arifuzzaman, M. (2021). Modeling the Settling Velocity of a Sphere in Newtonian and Non-Newtonian Fluids with Machine-Learning Algorithms. *Symmetry*, *13*(1), 1–23. [https://doi.org/10.3390/sym13010071]

(65) Schmitt, F., Milisic, V., Bertrand-Krajewski, J.-L., Laplace, D., and Chebbo, G. (1999). Numerical Modelling of Bed Load Sediment Traps in Sewer Systems by Density Currents. *Water Science and Technology*, *39*(9), 153–160.

(66) Singh, U. K., Ahmad, Z., Kumar, A., and Pandey, M. (2019). Incipient Motion for Gravel Particles in Cohesionless Sediment Mixtures. *Iranian Journal of Science and Technology - Transactions of Civil Engineering*, *43*(2), 253–262. [https://doi.org/10.1007/s40996-018-0136-x]

(67) Soulsby, R. L. (1997). Dynamics of Marine Sands: A Manual for Practical Applications. *Oceanographic Literature Review*, *9*(44), 947.

(68) Stokes, G. G. (1851). On The Effect of The Internal Friction of Fluids on The Motion of Pendulums.

(69) Stovin, V. R., Grimm, J. P., Buxton, A. P., and Tait, S. J. (2002). Parametric Studies on CFD Models of Sewerage Structures. *Global Solutions for Urban Drainage*, 1–15.

(70) Stovin, V. R., and Saul, A. J. (1996). Efficiency Prediction for Storage Chambers Using Computational Fluid Dynamics. *Water Science and Technology*, *33*(9), 163–170.
[https://doi.org/10.1016/0273-1223(96)00383-6]

(71) Stovin, V. R., and Saul, A. J. (1998). A Computational Fluid Dynamics (CFD) Particle Tracking Approach to Efficiency Prediction. *Water Science and Technology*, *37*(1), 285–293.
[https://doi.org/10.1016/S0273-1223(97)00780-4]

(72) Subramanya, K. (2009). Flow in Open Channels. Tata McGraw-Hill.

(73) Swamee, P. K., and Ojha, C. S. P. (1991). Drag Coefficient and Fall Velocity of Nonspherical Particles. *Journal of Hydraulic Engineering*, *117*(5), 660–667.

(74) Thinglas, T., and Kaushal, D. R. (2008a). Comparison of Two and Three-Dimensional Modeling of Invert Trap for Sewer Solid Management. *Particuology*, *6*(3), 176–184.

(75) Thinglas, T., and Kaushal, D. R. (2008b). Three-Dimensional CFD Modeling for Optimization of Invert Trap Configuration to be Used in Sewer Solids Management. *Particulate Science and Technology*, *26*(5), 507–519. [https://doi.org/10.1080/02726350802367951]

(76) Wu, W., and Wang, S. S. Y. (2006). Formulas for Sediment Porosity and Settling Velocity. *Journal of Hydraulic Engineering*, *132*(8), 858–862.

(77) Yan, H. (2014). Experiments and 3D Modeling of Hydrodynamics, Sediment Transport, Settling and Resuspension Under Unsteady Conditions in Urban Stormwater Detention Basin. *Ph.D. Thesis,* INSA de Lyon*,* 1-226.

(78) Yan, H., Lipeme Kouyi, G., Gonzalez-Merchan, C., Becouze-Lareure, C., Sebastian, C., Barraud, S., and Bertrand-Krajewski, J. L. (2014). Computational Fluid Dynamics Modeling of Flow and Particulate Contaminants Sedimentation in an Urban Stormwater Detention and Settling Basin. *Environmental Science and Pollution Research*, *21*(8), 5347–5356.
[https://doi.org/10.1007/s11356-013-2455-6]

(79) Yoon, H. D., Cox, D. T., and Kim, M. (2013). Prediction of Time-Dependent Sediment Suspension in the Surf Zone using Artificial Neural Network. *Coastal Engineering*, *71*, 78–86. [https://doi.org/10.1016/j.coastaleng.2012.08.005]

(80) Zakwan, M. (2019). Comparative Analysis of the Novel Infiltration Model with Other Infiltration Models. *Water and Environment Journal*, *33*(4), 620-632.

(81) Zakwan, M., and Niazkar, M. (2021). A Comparative Analysis of Data-Driven Empirical and Artificial Intelligence Models for Estimating Infiltration Rates. *Complexity*, *2021*. [https://doi.org/10.1155/2021/9945218]

(82) Zanke, U. (1977). Berechnung der sinkgeschwindigkeiten von sedimenten. Hannover, Germany.

(83) Zhang, R. J. (1989). Sediment Dynamics Rivers. Water Resources Press (in Chinese).

(84) Zhou, Y. C., and Li, T. (2010). Optimized Operation Plan for Sewer Sediment Control. *Journal of Zhejiang University: Science A*, *11*(5), 335–341.

(85) Zhu, L. J., and Cheng, N. S. (1993). Settlement of Sediment Particles. Resp. Rep., Dept of River and Harbor Eng. *Nanjing Hydr. Res. Inst., Nanjing, China (in Chinese)*.